RUSSIAN ACADEMY OF SCIENCE
FEDERAL AGENCY ON EDUCATION OF RUSSIAN FEDERATION
RUSSIAN NATIONAL COMMISSION FOR UNESCO
COMMITTEE ON SCIENCE AND HIGHER EDUCATION OF THE GOVERNMENT OF SAINT-PETERSBURG
COUNCIL OF RECTORS OF SAINT-PETERSBURG HIGHER EDUCATION ESTABLISHMENTS
SAINT-PETERSBURG STATE UNIVERSITY OF AEROSPACE INSTRUMENTATION (SUAI)
UNESCO CHAIR "DISTANCE EDUCATION IN ENGINEERING" OF SUAI
RUSSIAN SECTION OF THE INTERNATIONAL SOCIETY OF AUTOMATION

ИЗВЕСТИЯ КАФЕДРЫ UNESCO ГУАП «ДИСТАНЦИОННОЕ ИНЖЕНЕРНОЕ ОБРАЗОВАНИЕ»

Сборник статей

Выпуск 3

BULLETIN OF THE UNESCO DEPARTMENT «DISTANCE EDUCATION IN ENGINEERING» OF THE SUAI

Collection of the papers

Issue 3

РОССИЯ, САНКТ-ПЕТЕРБУРГ 2018 SAINT-PETERSBURG, RUSSIA

УДК 378.1
ББК 74.58
И33

И33 Bulletin of the UNESCO department “Distance education in engineering” of the SUAI: Collection of the papers. St. Petersburg, Issue 3. - SPb.:SUAI, 2018. - 106 p.

ISBN 978-5-8088-1265-9

ISA District 12 (The International Society of Automation) and SUAI (Saint-Petersburg State University of Aerospace Instrumentation) have organized the Fourteenth ISA European student paper competition (ESPC-2018). Papers of professors and the best students were included into this issue of the Bulletin of the UNESCO department “Distance education in engineering” of the SUAI. Papers can be interesting for students, post-graduate students, professors and specialists.

ISBN 978-5-8088-1265-9

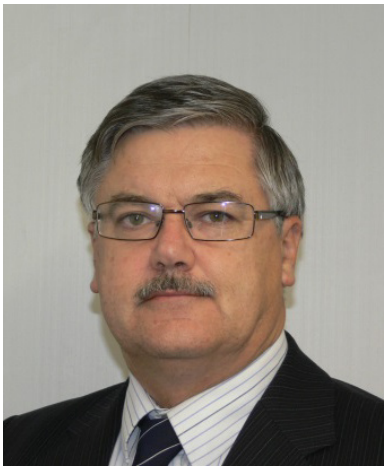

On behalf of ISA, I extend congratulations to the ISA Russia Section and the St. Petersburg State University of Aerospace Instrumentation (SUAI) on successfully completing the Fourteenth ISA European Student Paper Competition.

The papers published in this volume, selected by the advisory committee, represent the best contributions from among an excellent group of papers. The students who committed their time to prepare a paper should be very proud to be selected for this publication.

Students today are the engineers of tomorrow. We are all excited about these talented individuals who will be instrumental in "setting the standard for automation" that will enhance our lifestyle in the 21st century.

Whichever career path the students choose, we hope ISA will continue to play an important role in their continuing education and professional development.

May I extend my best wishes to all students and attendees in the 2018 ISA European Student Paper Competition.

Sincerely,

Brian J. Curtis
2018 ISA Society President

International Society of Automation
67 Alexander Drive
P.O. Box 12277
Research Triangle Park, NC 27709
PHONE (919) 549-8411
FAX (919) 549-8288
E-MAIL info@isa.org
www.isa.org

I would like to extend congratulations to the ISA Russia Section, ISA District 12, and The Saint Petersburg State University of Aerospace Instrumentation (SUAI) for successfully organizing the Fourteenth ISA International Student Paper Competition.

As an educator and a member of ISA for over 30 years, I never tire of the opportunity to share with students the amazing challenges and personal rewards that a career in automation can bring. ISA is proud to have the opportunity to nurture the next generation of automation professionals.

We look forward to continuing the close relationship we have established between ISA, the Russia Section, District 12, and the SUAI. Through distance learning classes on project management and ongoing international online forums, we are developing new understandings in the technical, cultural, and personal arenas.

Congratulations to those who developed papers for this volume and to the advisory committee who had the difficult task of making paper selections.

Sincerely,

Gerald W. Cockrell

Gerald W. Cockrell
ISA Former President

ISA
67 Alexander Drive
P.O. Box 12277
Research Triangle Park, NC 27709
PHONE (919) 549-8411
FAX (919) 549-8288
E-MAIL info@isa.org
www.isa.org

APPLICATION SCHEMATICS AND ALGORITHMS OF UWB SIGNAL PROCESSING

Isakov Viktor, Shepeta Dmitry, Makhlin Alexander

Saint-Petersburg University of Aerospace Instrumentation,
Saint-Petersburg, Russia
E-mail: dept41@aanet.ru

Annotation

Schematics and processing algorithms for pulsed ultra-wideband (UWB) signals are considered in the article. UWB signals have special features in propagation and reflection from physical objects, and consequently the receiving equipment and algorithms for analyzing reflected UWB signals differ from the equipment for receiving and processing conventional radio signals. In current work the existing engineering developments in this area are analyzed, their advantages and disadvantages are considered, prospective directions of development of corresponding technics are given.

INTRODUCTION

Ultra-wideband (UWB) signals have recently found use in various technical applications: telecommunications, radar, high-precision positioning, remote control, etc. When UWB signals are used in the abovementioned fields, the problems of generation, emission, reception, detection and processing of these signals are solved, since information about the properties of the propagation medium and the properties of physical objects which UWB-sounding signals are reflected from is included in the change in the shape and spectral characteristics of the received echo- signals.

The features of UWB signals - the absence of a carrier, the ultra-short duration (units of nanoseconds), the ultra-wide frequency band (up to 50 GHz) impose specific requirements for the equipment for generation, emission, reception, detection and analysis of such signals. This equipment is significantly different from the classical equipment used in the processing of radio signals. Accordingly, today there are no "classical" algorithms for detection and processing of UWB signals. Therefore, in this paper, we consider specific algorithms and schemes for processing UWB signals
used in practice for solving the abovementioned problems.

RECEPTION AND DETECTION OF UWB SIGNALS

The structure of the "optimal" UWB signal receiver, obtained from the receiver scheme of classical correlation processing, is described in [1]. The structure is shown in Fig. 1.

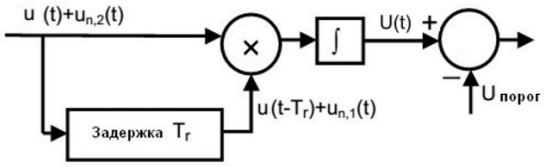

Fig. 1.

In contrast to the classical scheme, the reference signal in the of the correlation function here is not the local oscillator signal, but the received echo signal delayed for a time Tr (the repetition period of the pulses). In addition, noises are sent to both inputs of the correlator, but since they are in different repetition periods, it is considered that the noise is not correlated. The integration time T in the circuit is determined not by the duration of the radiated signal τ, but by the duration of the signal reflected from the target, where L is the physical length of the target, c is the speed of light (more precisely, the speed of propagation of electromagnetic waves in a particular physical medium), and τ is the duration of the emitted pulse. The duration of the radiated τ and the received T signals will be equal only if the target is pointwise L = 0 or, which is practically impossible to do, because τ is small. The length of the received signal is unknown a priori and can be of tens times larger than τ.

In [1], the characteristics of the detection of the considered schematic are shown, it follows that the characteristics of the proposed receiver with a probability of false alarm of the order of 10-2 are comparable with those of the optimal correlation receiver, but with a decrease in the probability of false alarm, the characteristics deteriorate. Thus, the receiver given in this paper is useful only for detecting targets of known size and is not suitable for detecting arbitrary targets. It should be noted that such a receiver is only a detector, since the information contained in the received signal is lost during

integration. In addition, the implementation of a broadband integrator and a precision delay line in practice is extremely difficult.

In work [2] the way of detection of the UWB signal by means of the superregenerative receiver which, as a matter of fact, is a hypersensitive generator is resulted. Such a generator is triggered - it generates oscillations only if a certain, even weak excitation signal appears at its input at a frequency equal to the natural frequency of the oscillator circuit of the generator. Such a receiver has a high sensitivity, however, because of this high sensitivity, the probability of false alarms can also increase. In addition, the receiver can not extract information about the target embedded in the signal, therefore it is no more than a supersensitive detector of the presence of an impulse in the UWB ether, that is, simply a "good" detector.

ANALOG-TO-DIGITAL CONVERSION OF UWB SIGNALS

In [3], the idea of digitizing an UWB signal with the help of several ADCs is described, the start of conversion in which is performed sequentially with a delay of 125 ps. The receiver circuit and the received pulse pattern are shown in Fig. 2.

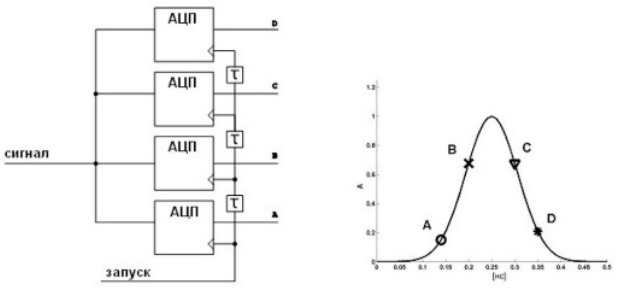

Fig. 2.

As can be seen from the figure, the samples of the signal at the outputs of the ADC appear sequentially and, when storing samples in a right order, for example, in RAM, it becomes possible to reconstruct the original signal. Such an approach allows qualitatively digitizing pulses with a duration of 500 ps, but the possibilities of an accurate analysis of signal characteristics, for example, the time of its arrival and, accordingly, the calculation of the distance to a physical object, are limited in this method and depend to a large extent on the number of ADCs in the receiver circuit. After the "collection" of the signal samples, it is possible to process this data in order to detect the UWB signal according to the algorithm described in [1]. However, upon closer examination of the scheme, it turns out that a data stream with a speed of about 8 Gbit/s will require a large DSP device and a very large amount of RAM to store the incoming signal samples from the DSP device. In addition, to reduce the requirements for this scheme, a rough search algorithm is needed, which, when detected, will trigger the process of collecting and processing the data array containing the analyzed signal. As a plus of this technical solution, it should be noted that this solution allows analyzing the frequency characteristics of the received signal.

The idea of analog-to-digital conversion of the signal described above was developed in [4]. The circuit of the receiver used is shown in Fig. 3. It consists of a microcontroller, a pulse generator, an amplifier, a sample-and-hold device, and a controlled delay line in steps of tens of picoseconds.

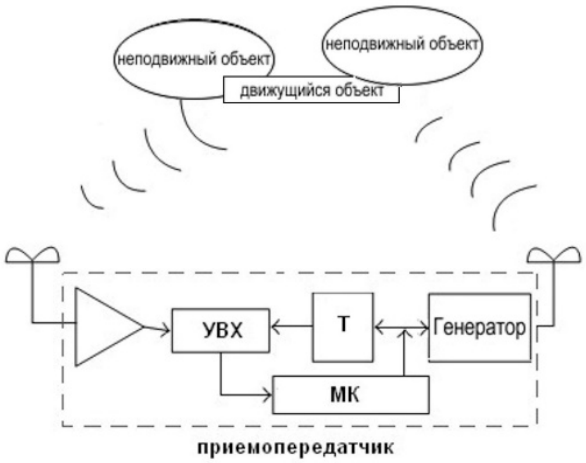

Fig. 3.

In this scheme, the signal samples also appear consecutively in time, as in the scheme shown in Fig. 2, described in [3]. The significant difference is that in this case only one ADC is used, and the variable delay line is utilized. In such a scheme, in order to obtain N samples of one pulse, a burst of N pulses is radiated, from each pulse only one sample with a shift dT is taken. It is assumed here that the propagation and reflection conditions of the probing pulses do not change throughout the whole packet, ie, the medium is stationary, and the reflected pulses in the packet are identical. This approach allows to greatly simplify the scheme (only one ADC), and, taking into account the capabilities of the modern element base, to perform analog-to-digital conversion of the signal in 23 ps steps, which is equivalent to an "unattainable" sampling frequency of about 43 GHz. Such a scheme is distinguished by the possibility, with appropriate processing, to determine distances to the target with a potential accuracy of up to 3 mm, and also to obtain an almost exact spectral composition of the echo signal in the spectrum equivalent to 23 GHz.

Thus, it turns out to be possible to calculate the pulse spectrum, which is used in [5] to "create" a time-frequency portrait of the goal, create a base of such

portraits and use this database for classification purposes. However, if the conditions of propagation are non-stationary within the pack, for example, when the target moves, that is, the pulses in the packet are not identical, then the operation of the circuit is broken. Therefore, such a scheme can be used to detect and classify only fixed targets or targets, the speed of movement of which is substantially limited.

MULTI-CHANNEL RECEIVERS OF UWB SIGNALS

In this paper [6] considered a method for receiving UWB signals using a set of bandpass filters with different center frequencies tuned to cover the entire frequency range of the UWB signal. The signal from each filter is fed to the quadratic detector and then to the integrator. In fact, such an algorithm realizes an optimal signal detection algorithm at a low signal-to-noise ratio. In view of the large width of the spectrum of the UWB signal, it falls into the passband of all filters. Accordingly, the detection output signal should appear on all outputs of the detection circuits. In the digital signal processing device, the signals of the detectors are analyzed and a decision is made about the presence of an UWB signal at the input of the circuit. The circuit of the device is shown in Fig. 4.

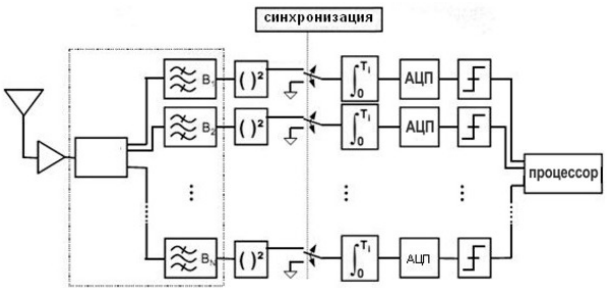

Fig. 4.

In work [7], the idea of receiving UWB signals by a multichannel superregenerative receiver given in [2] develops. In this case, the structure of the multichannel receiver consists of several channels of super-regenerative oscillators (SROs) tuned to different frequencies of the spectrum of the UWB signal. The frequencies and Q-factors of the generator circuits are chosen in the same way as in [6], namely, with such a calculation as to cover the entire spectrum of the spectrum of the UWB signal. The signal from the output of each oscillator is fed to the envelope detector, after which it goes to the synchronous D-flip-flop. In the presence of a signal, due to feedback, the gain of the SRO is reduced by means of current regulator blocks. The circuit of such a receiver is shown in Fig. 5.

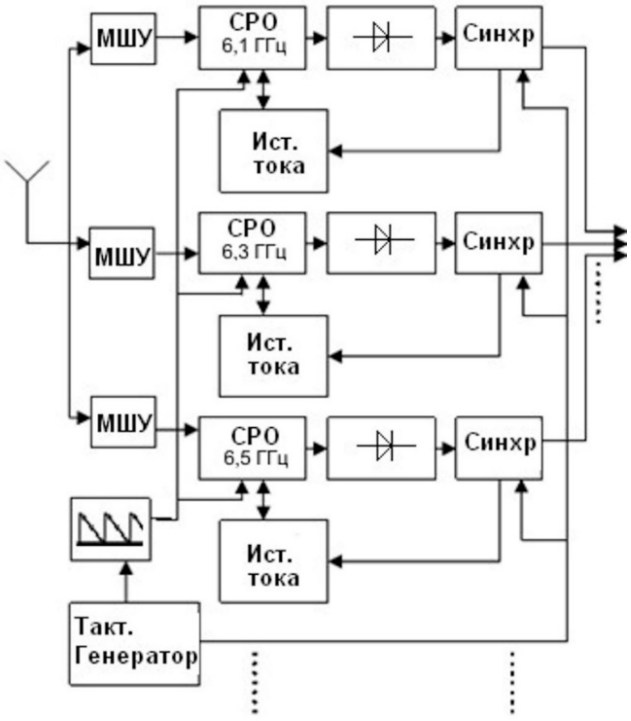

Fig. 5

If there is a signal at the input of the UWB, it comes on the inputs of each superregenerative oscillator. Each channel of the receiver generates an output signal if its resonant frequency signal is present at its input. After the output signals of super-regenerative receivers tuned to different frequencies of the spectrum of the UWB signal are converted into a stream of zeros and ones, a detection algorithm is used - "criterion k of n" [8]. The decision on the presence of a signal is accepted if k logical ones appeared on the outputs of n channels of the device. It is noted that such a UWB receiver has a high noise immunity not only to noise, but also to narrow-band interference. However, in this work it is stated that in order to ensure the reliable operation of the AGC circuit, there must be an equal number of zeros and ones in the burst, which reduces the efficiency of the digital detection algorithm "k of n".

In work [9], a receiver combining a filter bank from [6] and quadrature medium-speed converters is described. The spectrum of received pulses is concentrated in the range of 6-8 GHz. Bandpass filters are tuned to center frequencies so as to cover the entire spectrum of received signals. Since frequency converters transfer the spectrum of signals to a range of up to 300 MHz, an average-speed ADC can be used to digitize the output signals of each channel. This scheme allows to combine the possibility of spectral analysis of the signal, which is impossible in [7], while using ADC and DSP device with medium speed. In work [10] practical schemes of using the UWS for the detection and classification of physical objects located in the subsurface layer are given. In

the same place, the characteristics of such systems are given and the requirements that similar locators must satisfy are formulated.

CONCLUSIONS

Nowadays, there are no optimal algorithms for detecting and analyzing UWB signals. When UWB signals are detected with a low probability of false alarm, the algorithm of correlation processing proved to be well established. However, the most promising algorithms for detecting UWB signals are multichannel detectors based on super-regenerative receivers.

When analyzing the form of the signals reflected from UWB targets, digitization of the received signals is required, carried out by high-speed and expensive ADCs. However, due to the increase in the target observation time, with the emission of the burst, it is possible to digitize with only one ADC with an average throughput, while the modern technology allows "digitizing" the UWB pulses through an intervals up to tens of ps.

Classification of targets by the characteristics of reflected UWB signals is based on the use of frequency-time characteristics of signals. One of the promising directions in the classification of goals is the use of spatio-temporal spectrograms that allow one to distinguish fairly well the types of metal objects and distinguish them from stones similar in shape and size.

BIBLIOGRAPHY

1. Иммореев И.Я. Особенности обнаружения целей в СШП радарах / сборник «Сверхширокополосные технологии в радиолокации» под ред. Тейлора Д.Д. Изд. Бока Ратон, Лондон, Нью-Йорк, Вашингтон, 2000.

2. Pelissier M, Morcher D, Vincent P. Super regenerative architecture for UWB pulse detection: From theory to RF frontend design / IEEE Trans. Circuits and Systems – I, 56, 440-451. – 2009.

3. Matthew Bruce Blanton. An FPGA Software-Defined Ultra Wideband Transceiver / Bradley Department of Electrical and Computer Engineering Blacksburg, Virginia. – 2006.

4. Yinan Yu, Jian Yang, Tomas McKelvey, and Borys Stoew. A Compact UWB Indoor and Through-Wall Radar with Precise Ranging and Tracking / Department of Signals and Systems, Chalmers University of Technology, 41296 Gothenburg, Sweden. – 2012.

5. Celestine Twizere. Use of GPR techniques for Landmines Detection and Road monitoring / Phd thesis, The University of Rome. – 2011.

6. Martha Liliana Suárez Peñaloza. Considering a non-uniform filter bank in an UWB Multi Band On-Off Keying transceiver / Journal of Communication, Vol. 2, No 6. – 2007. –P.24-29.

7. F. Xavier Moncunill-Geniz, Pere Palà-Schönwälder, Jordi Bonet-Dalmau, Francisco del Águila-López and Rosa Giralt-Mas. Ultra Wideband Impulse Radio Superregenerative Reception / Universitat Politècnica de Catalunya, Spain, 2009.

8. . D. Shepeta, A. Makhlin, V. Nenashev. UWB Pulse Signal Detection Methods. Modern Information Society Formation – Problems, Perspectives, Innovation Approaches. XVI International Forum. 1-5 June, 2015. Saint-Petersburg, Russia.-P.16-20.

9. Moragrega A., Artiga X., Gavrincea C., Ibars C., Navarro M., Najar M., Miskovsky P., Mira F. and M. di Renzo. Ultra-Wideband Testbed for 6.0-8.5 GHz Ranging and Low Data Rate / Communication Centre Tecnologic de Telecomunicacions de Catalunya, (CTTC) Av. Canal Olimpic S/N, Castelldefels 08860, Barcelona, Spain.

10. Блаунштейн Н.Ш., Сергеев М.Б., Шепета А.П. Прикладные аспекты электродинамики. - СПб: Аграф +, 2016.- 272 с., и л.__

MODELING OF SPECTRAL EFFICIENT SIGNALS BASED ON FINITE SPLINES

A. F. Kryachko[1], M. A. Kryachko[1]

[1]Saint-Petersburg State University of Aerospace Instrumentation, 190000 St. Petersburg, Russia

Spectral efficient signals based on finite splines, which are obtained by repeated usage of discrete convolution procedure, is considered. Energy spectra of random sequence of signals is presented. Practical realization of device for generation and reception is proposed. Generation of SEPSK signals is done by matched filter with feedback line. Proposed method for reception of SEPSK signals is similar to method for reception of classical OFDM signals. High reduction rate of out-of-band emissions for random sequence of SEPSK signals is provided by proposed atomic functions.

Keywords: SEPSK, atomic functions, finite spline, out-of-band emissions.

1INTRODUCTION

Application of spectrally efficient signals with phase shift keying (SEPSK), constructed on the basis of atomic functions or finite splines [1], [2], allows to obtain efficient compression of the energy spectrum of a random sequence of signals. Application compression method based on atomic functions allows the usage of their formation and receiving simple to implementation approach based on the calculation of convolution and deconvolution of functions [1].

The objective of this paper is to study possibility of realization of device for forming and receiving SEPSK signals, obtained based on atomic functions.

2 MAIN PART

2.1 Basic properties of atomic functions

Atomic functions has properties of polynomials and splines [1]. Splines of degree γ are functions which are "piecewise" polynomials of degree γ. Reduction of out-of-band emissions for signals on the basis of finite splines of degree γ is equal to $C/\omega\gamma + 1$ (if all derivatives of the envelope of signal up to $(\gamma - 1)$-th order have no discontinuities, and γ-th derivative is everywhere finite). Distinctive features of the atomic functions are:

- analyticity;
- combination of finitely of function and high decreasing rate of Fourier transformation (faster than any power);
- connection with the derivative of functions and explicit expression for the spectrum.

Let`s consider generation of spectral efficient signals with duration T and based on application of finite splines. Repetition of convolution of basis functions is used for generation those signals. For rectangular form of envelope for PSK signals with amplitude A and centered about start of timing

$$a(t) = \begin{cases} A, & |t| \le T/2 \\ 0, & |t| > T/2 \end{cases}. \qquad (1)$$

N-fold convolution $(N + 1)$ $a(t)$ may be represented in the form of finit splines $\Theta_N(x)$ [1]. Expression (1) may be rewritten as follows:

$$\varphi(t) = \frac{A}{2\pi} \int_{-\infty}^{\infty} e^{jut} \frac{\sin(u/2)}{u/2} du . \qquad (2)$$

We obviously have for (2):

$$\varphi(t) = \mathbb{F}^{-1}\left[\nu(u)\right],$$

where $\mathbb{F}^{-1}\left[\nu(u)\right]$ – Fourier transform of function $\nu(u) = \frac{\sin(u/2)}{u/2}$. Convolution of functions can be written (using the theorem of Borel and the symmetry of the Fourier transform):

$$\varphi(t) * \varphi(t) = \mathbb{F}^{-1}\left[\nu^2(u)\right]. \qquad (3)$$

Then:

$$\varphi(t) * \varphi(t) = \frac{A^2}{2\pi} \int_{-\infty}^{+\infty} e^{jux} \left[\frac{\sin(u/2)}{u/2}\right]^2 du. \qquad (4)$$

This process may be repeated N times for obtaining more smoother function, i.e. calculation of convolution procedure functions such $\varphi(t) * \varphi(t) * \ldots * \varphi(t) * \ldots$. Thus, the result of infinite convolution is a new finite function defined on the interval $[-NT/2; NT/2]$.

2.2 Formation of spectrally effective signals on the basis of atomic functions

In general, we can write the expression for the spline $\Theta_N(t)$ for any value of N by next expression:

$$\Theta_N(t) = \frac{A^{N+1}}{2\pi} \int_{-\infty}^{\infty} e^{jut} \left(\frac{\sin(u/2)}{u/2} \right)^{N+1} du. \quad (5)$$

Let`s consider the form of the function $\Theta_N(t)$ for $N = 1 \ldots 5$. For $N = 1$:

$$\Theta_1(t) = \frac{A^2}{2\pi} \int_{-\infty}^{+\infty} e^{jut} \left[\frac{\sin(u/2)}{u/2} \right]^2 du;$$

$N = 2$:

$$\Theta_2(t) = \frac{A^3}{2\pi} \int_{-\infty}^{+\infty} e^{jut} \left[\frac{\sin(u/2)}{u/2} \right]^3 du;$$

$N = 3$:

$$\Theta_3(t) = \frac{A^4}{2\pi} \int_{-\infty}^{+\infty} e^{jut} \left[\frac{\sin(u/2)}{u/2} \right]^4 du;$$

$N = 4$:

$$\Theta_4(t) = \frac{A^5}{2\pi} \int_{-\infty}^{+\infty} e^{jut} \left[\frac{\sin(u/2)}{u/2} \right]^5 du;$$

$N = 5$:

$$\Theta_5(t) = \frac{A^6}{2\pi} \int_{-\infty}^{+\infty} e^{jut} \left[\frac{\sin(u/2)}{u/2} \right]^6 du.$$

Form of envelope $a(t)$ of SEPSK signals for each value of N is determined by function $\Theta_N(t)$. $a(t)$ for $N = 1,\ldots,5$ is shown on fig. 1. Normalized duration of SEPSK signals for $N = 1, \ldots, 5$ is increased from $T = 0.2$ to $T = 0.6$ at this figure. SEPSK signal for $N = 0$ has rectangular form of envelope (1) and duration $T = 0.1$. The degree of smoothness of the envelope of SEPSK signals with fixed energy increases with increasing of N (fig. 1).

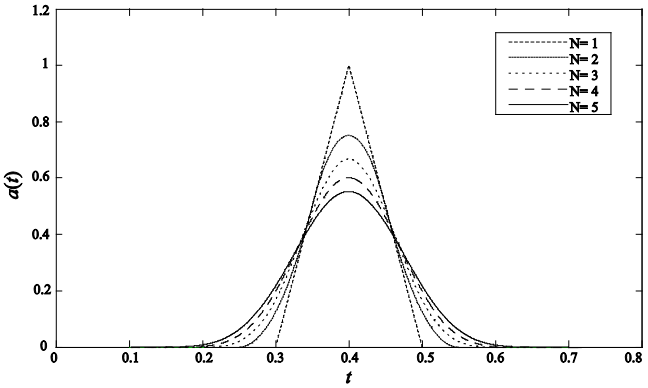

Fig. 1. *Envelope a(t) of SEPSK signals.*

Spectrum of random sequence of SEPSK signals, whose number is M, may be represented in the following form:

$$S(\omega) = A \int_0^{MT} \sum_{k=0}^{M-1} a(t - kT) d_r^{(k)} \cos\omega_0 t \cdot \exp(-i\omega t) dt = S_+(\omega) + S_-(\omega),$$

where

$$S_+(\omega) = \frac{A_0}{2} \int_0^{MT} \sum_{k=0}^{M-1} a(t - kT) d_r^{(k)} \exp(-i(\omega_0 + \omega)t) dt,$$

$$S_-(\omega) = \frac{A_0}{2} \int_0^{MT} \sum_{k=0}^{M-1} a(t - kT) \times d_r^{(k)} \exp(i(\omega_0 - \omega)t) dt$$

and values of symbols of message depends on the location of symbol in the sequence and the index $r = 1, 2$. In particular, $d_1^{(k)} = 1$ and $d_2^{(k)} = 2$; $r = 1, 2$.

After the change of variable $x = t - kT$:

$$S_+(\omega) = F_a(\omega) \sum_{k=0}^{M-1} d_r^{(k)} \exp\left[-i(\omega_0 - \omega)t\right],$$

Where $F_a(\omega) = \int_0^T a(t) \exp\left[-i(\omega_0\right]$

$F_a(\omega) = \frac{A}{2} \int_0^T a(t) \exp\left[-i(\omega - \omega_0)\right] dt$ – spectrum of envelope $a(t)$.

Energy spectrum of random sequence of signals is calculated with tendency of M to infinity:

$$G(\omega) = \lim_{M \to \infty} \frac{1}{MT} m_1 \left\{ |S(\omega)|^2 \right\}$$

and the mathematical expectation $m_1\left\{ |S(\omega)|^2 \right\}$ is determined by averaging over all possible finite sequences of symbols $d_r^{(k)}$.

Expression for energy spectrum (for narrowband signals) has the next form:

$$G(\omega) = G_+(\omega) + G_-(\omega),$$

Where $G_+(\omega) = \lim_{M \to \infty} \frac{1}{MT} m_1 \left\{ |S_+(\omega)|^2 \right\}$.

It is easy to show that:

$$m_1\left\{ \left| S_+(\omega)^2 \right| \right\} =$$

$$= |F_a(\Delta\omega)|^2 \sum_{k=0}^{M-1} \sum_{l=0}^{M-1} \exp\left[-i\Delta\omega(k-l)\right] m_1 \left\{ d_r^{(k)} d_q^{(l)} \right\},$$

where $\Delta\omega = \omega - \omega_0$.

For case of equally probable and independent symbols:

$$m_1\left\{ d_r^{(k)} d_q^{(l)} \right\} = \begin{cases} 1, & k = l, \\ 0, & k \neq l. \end{cases}$$

The final expression for calculating the power spectrum of the random sequence of SEPSK signal in area of $\omega > 0$:

$$G_+(\omega) = \lim_{M \to \infty} \frac{1}{4MT} \left\{ M |F_a(\Delta\omega)|^2 \right\} = \frac{1}{4T} |F_a(\Delta\omega)|^2.$$

Thus, energy spectrum of random sequence of SEPSK signals is determined by Fourier transform of single signals and has same frequency bandwidth.

Energy spectra for random sequences of SEPSK signals, which form of real envelope is finite splines, is shown on fig. 2. Normalized energy spectrum are presented on *Y*-axis, relative frequency ($f-f_0)T$ (where f_0 – central frequency) is shown on *X*-axis. As expected, the rate of out-of-band emissions increases with increasing of *N*.

We can see from analysis energy spectra of those signals that the reduction of out-of-band emissions is very high for large values of *N* (for example, *N* = 3-5).

The advantage of these signals is the principle of their generation and reception based on multiple repetitions of the convolution of functions.

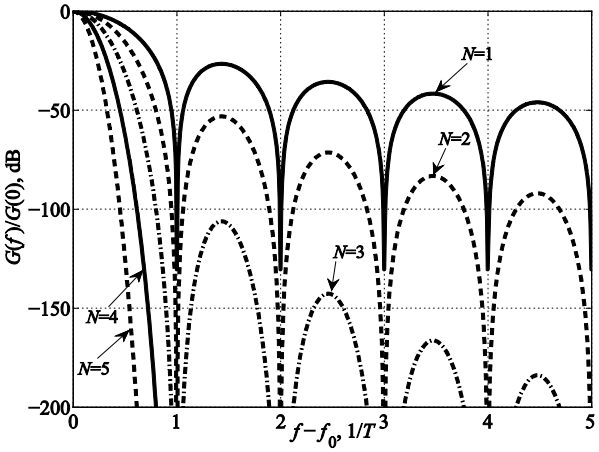

Fig. 2. Energy spectrum of SEPSK signals for N = 1,…,5.

Functional scheme of device for generation spectral effective signals based on finite splines is shown on fig. 3. This device is constructed by using matched filter with adjustable feedback. The impulse response of this filter has the envelope, which form is determined by (1). Signals from matched filter`s output come to input of delay line. Time delay of the filter response is determined by value of *N*. Delay of signal from matched filter`s output is equal to 2*T* for *N* = 2.

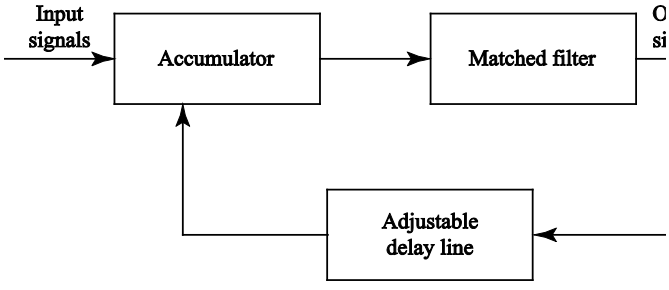

Fig. 3. Functional scheme of device for SEPSK signals generation.

Voltage from matched filter`s output is transferred to its input again after calculating first procedure of convolution. Result of calculating second procedure convolution is response of matched filter as spline $\Theta_2(t)$. This spline is the same as form of envelope $a(t)$.

Reception of SEPSK signals may be done by several stage. On first stage, input process is converted to frequency domain by Fourier transform. On next stage, reception device must do nonlinear procedure of *N*-th degree root extraction from frequency function. Conversion to time domain by Fourier inversion is done on final stage. Output result is transmitted to classic demodulation algorithm, which based on application of correlation processing of PSK signals with rectangular form of envelope.

Of course, the proposed method of reception for SEPSK signal is not optimal. However, this method is simple (especially with usage of matched filter for realization). Proposed method for reception of SEPSK signals is similar to method for reception of classical OFDM signals.

3 CONCLUSIONS.

High reduction rate of out-of-band emissions for random sequence of SEPSK signals is provided by proposed atomic functions (finite splines). In particular, reduction of out-of-band emissions is equal to $1/f^6$ for 2-3 iterations of convolution.

Generation of SEPSK signals is done by matched filter with feedback line. Reception of SEPSK signals is performed sequentially for 3 stage. On the first stage transformation of input mix of signals with additive noise to frequency domain is done. On next stage, reception device must do nonlinear procedure of *N*-th degree root extraction. Reverse operation (transformation to time domain) is performed on final stage.

REFERENCES:

[1] GulyaevYu.V., Kravchenko V.F., Pustovoit V.I. A New Class of WA-Systems of Kravchenko-Rvachev Functions // Doklady Mathematics. – 2007. – Vol. 75, No 2. – pp. 325-332

[2] Ghavami M., Michael L.B., Kohno R. Ultra Wideband Signals and Systems in Communication Engineering. – John Wiley & Sons, 2004

RESEARCH OF DATA PROCESSING METHODS IN AN OPTICAL WIRELESS DIGITAL COMMUNICATION SYSTEM

Akopyan Bella

Saint-Petersburg State University of Aerospace Instrumentation,
Saint-Petersburg, Russia
E-mail: akopyan.bella@yandex.ru

Abstract
The article considers a single-threshold method of processing a signal in a wireless optical digital communication system. A method for improving processing is proposed. The results of both methods are compared, the average error probability per bit is calculated.
Keywords: digital signal processing, digital communication, single-threshold processing, optoelectronics, decision rule, ordinary least squares, error probability per bit, regression.

INTRODUCTION

Tests of the developed prototype of the optical wireless digital communication system [1] showed that the main disadvantage of the system is the sensitivity to the overall level of external illumination, which is accompanied by a distortion of the pulse shape; this leads to errors in signal reception. Therefore, in order to solve the problem of ensuring the maximum possible reliability of the received information, it was decided to turn to the signal processing methods on the receiving device side. The task is to configure the decision rule so that it significantly reduces the average error probability per bit.

SINGLE-THRESHOLD PROCESSING

The simplest way of processing digital signals is a single-threshold processing. The principle of operation of this way is that the average value of the voltage of the i-th bit (U_i) is compared with a certain threshold value L:

$$U_i \geq L \rightarrow \text{"1"}, U_i < L \rightarrow \text{"0"}.$$

U_i is defined as the average of the voltage values:

$$U_i = \frac{1}{n}\sum_{j=1}^{n} y_j,$$

where n is the number of sample counts per bit, y_j is the voltage value of j-th sample count.

The voltage calibration values corresponding to the on (U_{in}) and off (U_{out}) state of the LED are read from the photoresistor of the receiver. the value of the correction term U_c, which depends on the calibration values should be taken as a parameter characterizing the level of the external luminosity:

$$L = \frac{U_{in} + U_{out}}{2} + U_c$$

The threshold value of the decision rule can be selected in various ways to compensate for the external luminosity. For example, in the prototype the value of the correction term U_c was chosen equal to:

$$U_c = \frac{U_{in} - U_{out}}{6}.$$

Then the threshold value is:

$$L = \frac{U_{in} + U_{out}}{2} + \frac{U_{in} - U_{out}}{6}.$$

The results of the processing are shown in Figure 1. Based on the results of the experiments, the average error probability per bit was 0.015, which is not a good enough result, since for the receiver the error probability per bit should be from 10^{-3} to 10^{-5} [1].

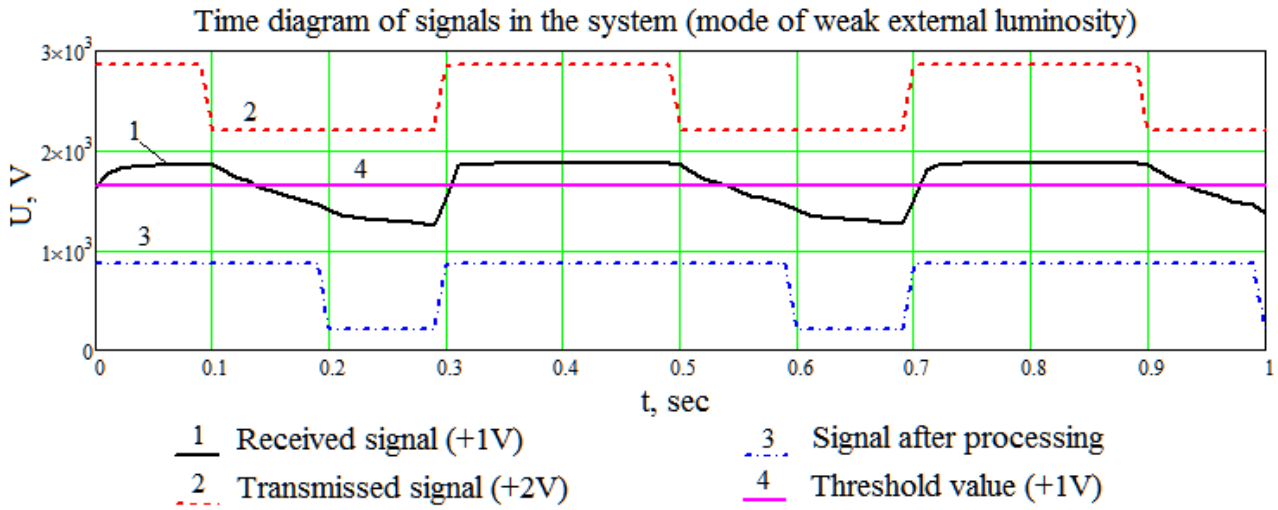

Figure 1. The result of single-threshold processing in the mode of weak external luminosity

IMPROVEMENT OF THE DECISION RULE

To compensate for the distortion of the pulse fronts, it is advisable to supplement the decision rule by processing an additional parameter that would characterize the shape of impulse. The proposed approach is to determine the slope coefficient of the regression line for the signal corresponding to each bit (regression coefficient). The most common method of approximation due to computational simplicity is the method of the ordinary least squares (OLS).

The equation of the regression line for the i-th bit is:

$$y = K_i x + b_i.$$

The coefficients of this line K and b are defined as:

$$[K_i, b_i] = \arg\min \sum_{j=1}^{n} \left(K_i x_j + b_i - y_j \right)^2,$$

where x_j is the time instant corresponding to the j-th sample count. The defining parameters of this decision rule are the absolute value and sign of the slope coefficient K_i.

The processing algorithm, as in the case of single-threshold processing, is divided into two stages: calibration of threshold values and processing of the signal according to the decision rule. Let K_{lim} be the threshold value of the regression coefficient, then if the absolute value of the regression coefficient of the bit K_i exceeds K_{lim}, then the sign of the bit regression coefficient is checked:

$$K_i > 0 \rightarrow \text{"1"}, K_i < 0 \rightarrow \text{"0"}.$$

Otherwise, the bit value is determined by a single-threshold processing.

The calibration is carried out as follows:

A test signal is sent before message. Test signal is based on the special test sequence. It is advisable to take as the such sequence with alternation of 0 and 1, since in such a test signal it is possible to trace the trends in the shape of the impulses. The test signal is processed by a single-threshold method, then it is checked for errors. If the bit was processed incorrectly, then regression line slope coefficient is determined. The regression coefficients are recorded in an array, which determinates the threshold value of the regression coefficient. It is advisable to take the minimum value of the regression coefficient of incorrectly processed test bits as the threshold value. The switching of the decision rule with this choice of the threshold value is carried out only when the single-threshold processing inevitably leads to errors.

Figure 2 shows the results of processing. The time diagrams show that the impulses, despite the distorted form, are processed correctly by switching the rules.

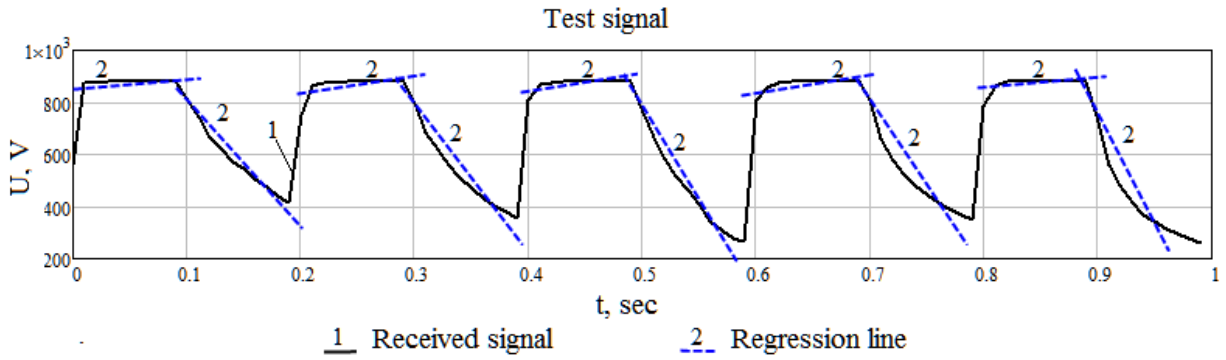

Figure 2. Time diagram of the signal of the test sequence

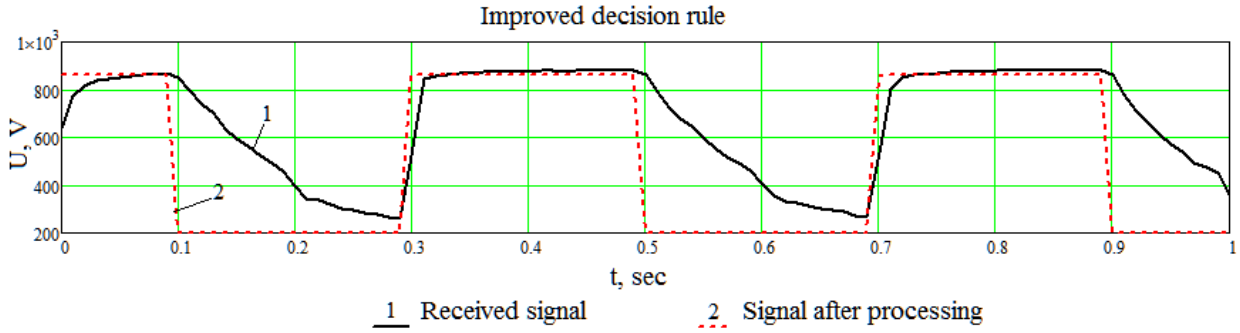

Figure 3. Time diagram of the received and processed signals in the mode of weak external luminosity

CONCLUSION

As a result of the experiments, it was found that the average error probability per bit decreased from 0.015 in the single-threshold processing to 0.0006 while using the improved decision rule. Thus, the new decision rule led to an improvement in the processing accuracy of the received signal. The received recommendations should be taken into account while developing a optical wireless digital communication system.

REFERENCES

[1] Akopyan B. K., Gorodetskaya A. V. Razrabotka maketnogo prototipa sistem tsifrovoy svyazi s peredachey po opticheskomu kanalu // Semidesyataya mezhdunarodnaya studencheskaya nauchnaya konferentsiya GUAP / [Development of a prototype of optical wireless digital communication system// The Seventieth International Student Scientific Conference of the SUAI] – SUAI, 2017 (in Russian)

[2] Sklar B. Digital Communications: Fundamentals and Applications – 2nd Edition -- University of California, Los Angeles, 2001

[3] Mironovskiy L. A., Slayev V. A. Algoritmy otsenivaniya rezul'tata trekh izmereniy [Algorithms for estimating the result of three measurements] – SPb: Professional, 2010, 192 p. (in Russian)

STUDY OF DYNAMIC CONTROL ON A REAL REGULATION LOOP.

Miguel Redondo Alonso, Alberto Justo Lobato

Industrial Engineering Faculty,
Valladolid – Spain
Email: alberto.justo@alumnos.uva.es, miguelredondo96@gmail.com

Abstract

From a process industry perspective, is very important to know different control methods, considering the specifications of the plant, the estimated time and other facts. It may not always be better to do an aggressive control of the process (or conservative) in order to achieve the desired goal. For this reason, the object of our research is to present a real regulation loop and some control techniques that are appropriated.

Key words

PI control, water level, disturbances, controlled variable, manipulated variable.

Introduction

In this project, we use one of the pilot plants from Systems Engineering Laboratory at the University of Valladolid, Spain, like the one which appears in Figure 1. We are going to expose the operation of the plant, as well as introducing control techniques for it. Typically, the kind of plants included in lab are heat interchangers, water tanks and a furnace. First, if we want to know how to do system control, we need to have good knowledge of its running. Most of mistakes in process industry are made because of uncomplete understanding of systems.

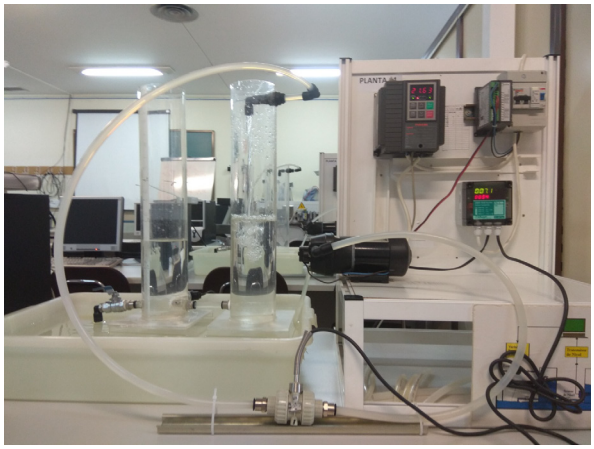

Figure 1. Plant made up of two tanks and a pipe.

In our case, we have two water tanks that interchange liquid between them, and our purpose is to know the level of the second one. The flow in the two tanks is related with the level thanks to the Bernoulli equation. Because of this, we are controlling flow and level at the same time.

Description

The main goal of this section is to explore measurement instruments of our plant. It consists in two water tanks, which are connected by a pipeline. On one hand, water is added to the first tank by a pump. On the other hand, there is a manual valve that turns out the second.

From an instrumentation point of view, we have one level transmitter and a regulator. This last device is a data acquisition system connected to a computer which makes the real control of the tanks. Furthermore, there is a flux transmitter that measures outflow water from the pump. All that is shown in Figure 2.

However, we didn´t consider it in this case because the variable, which we are interested in controlling and quantifying, is the water level in the second tank.

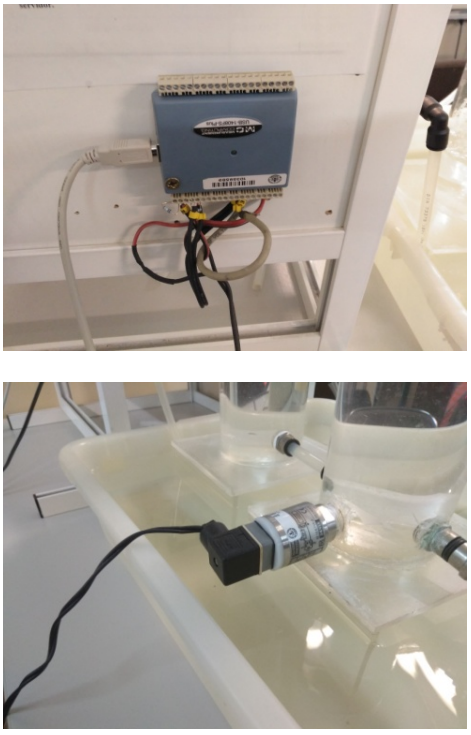

Figure 2. Data acquisition system and level regulator.

With the purpose of getting introduced with our plant control, we use the program Java-Regula. It´s a software developed by Systems Engineering Department, which provides to operate real time process control. Java-Regula let us to realize control, either water level or flow, as introducing different control methods in the system: PID, Feed-Forward, Predictive, etc. In addition, it shows graphically the response evolution, as saving obtained information in an Excel format. This can be seen in Figure 3.

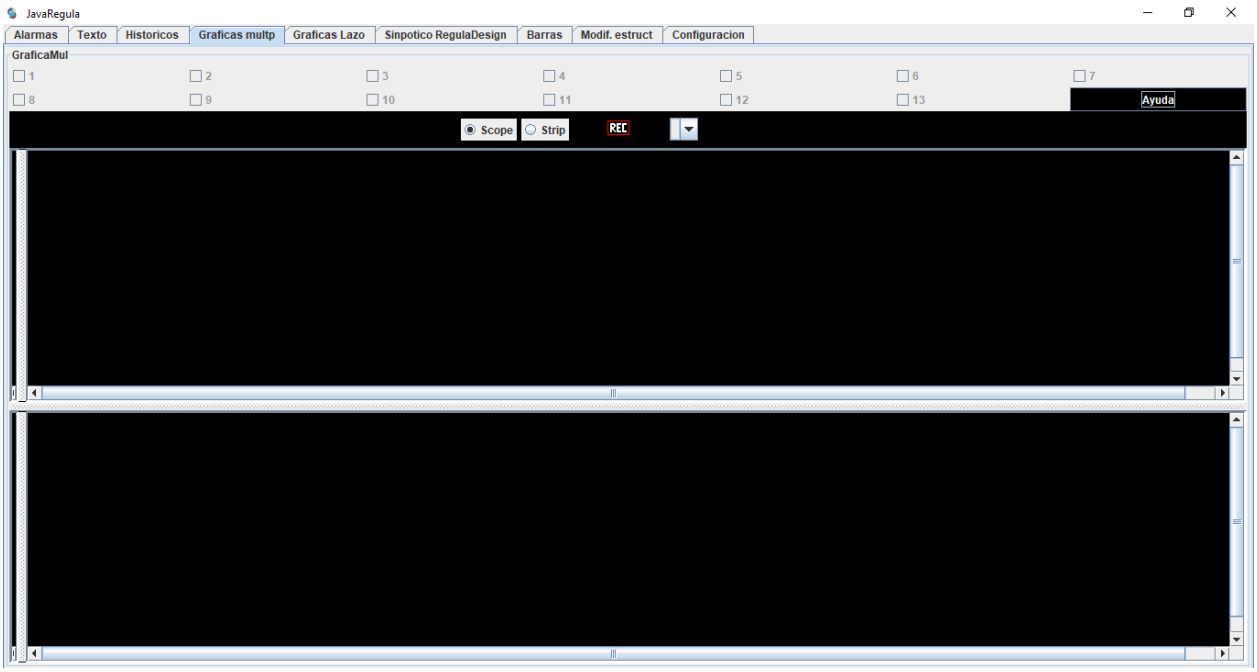

Figure 3. Java-Regula interface

When our regulators are in manual mode (in open loop), we take a look at the temporal response of the controlled variables in presence of disturbances and manipulated variables.

At this moment, our plant control begins, but first we should talk about calibration.

First, we turn on the software JAVA-REGULA and the system for the calibration. Then, we take some values of the devices (in volts) while we were comparing with the real level of water in the deposit

Calibration of real system's devices

Our system has a pressure transmitter for calculating the level of water in the deposit. We must calibrate it to get the most accurate values for the regulation process.

(in metres). Now, with the use of the linear approximation method we get the following regression line: y=22.828x-14.878.

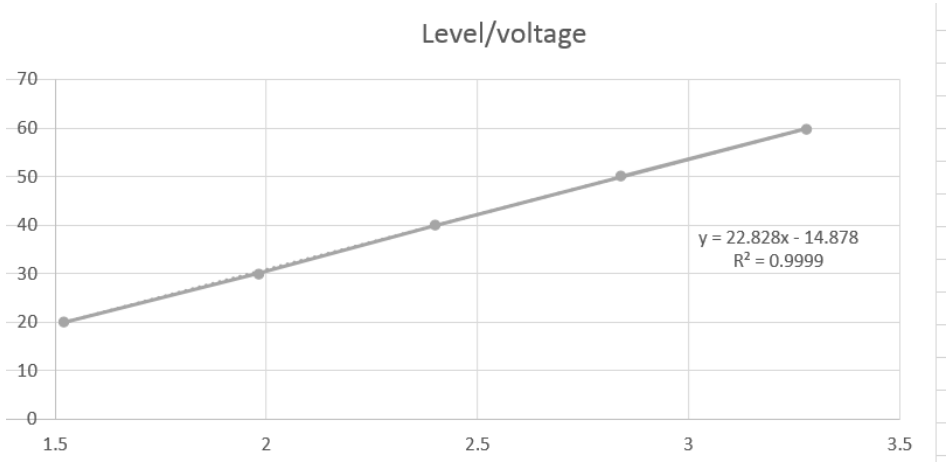

Figure 4. Calibration graphic

Study of the regulation loop elements and its dynamic behaviour.

For making the system control, we have to take in account that this is a monotonous process, in other words, it has no apparent fluctuations. For this reason, the controller will be made to follow the reference signal instead of refusing the disturbances effects, which are insignificant in our plant. Due to these, the PID tunning methods of Ziegler-Nichols, Cohen-Coon or López are ruled out because those methods are made mostly for refuse the disturbance in the system.

Now, we are going to calculate the PID parameters using the Rivera-Morari and the Rovira methods in order to make the comparison between these two methods.

Before calculating the parameters of the PID controllers, we should watch out how the system reacts to a change in the controlled variable in open loop. Then, when the system has reached stability, we can get the values of the gain, delay, settling time, etc.

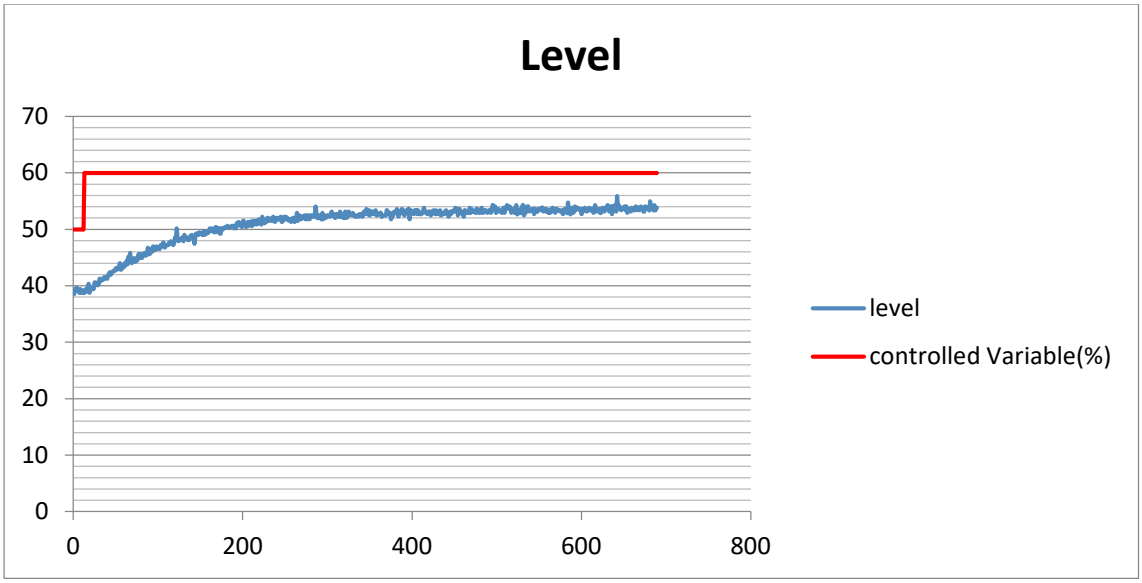

Figure 5. Water level stabilized

Rivera-Morari method has some values of λ, which corresponds with the time constant in closed loop. We chose a value of 0,8875 because it`s more interesting to have a conservative control of our system, even though the response is a bit slower, than an aggressive due to instability applicated to it with this type. Rovira method consists in some sub methods that minimize integral error by different ways, we can see them in our reference books.

Equations for the Rivera-Morari:

Tipo	K_p	T_i
PI	$\frac{\tau}{K(\lambda + d)}$	τ

	Rivera-Morari	Rovira MIAE
kp	1.075	2.88
Ti	1.775	1.81

Rivera-Morari (λ=0.8875)

On one hand, we have the Rivera-Morari method. We used a PI controller. In the experiment we made two steps in the reference signal, one positive and other negative.

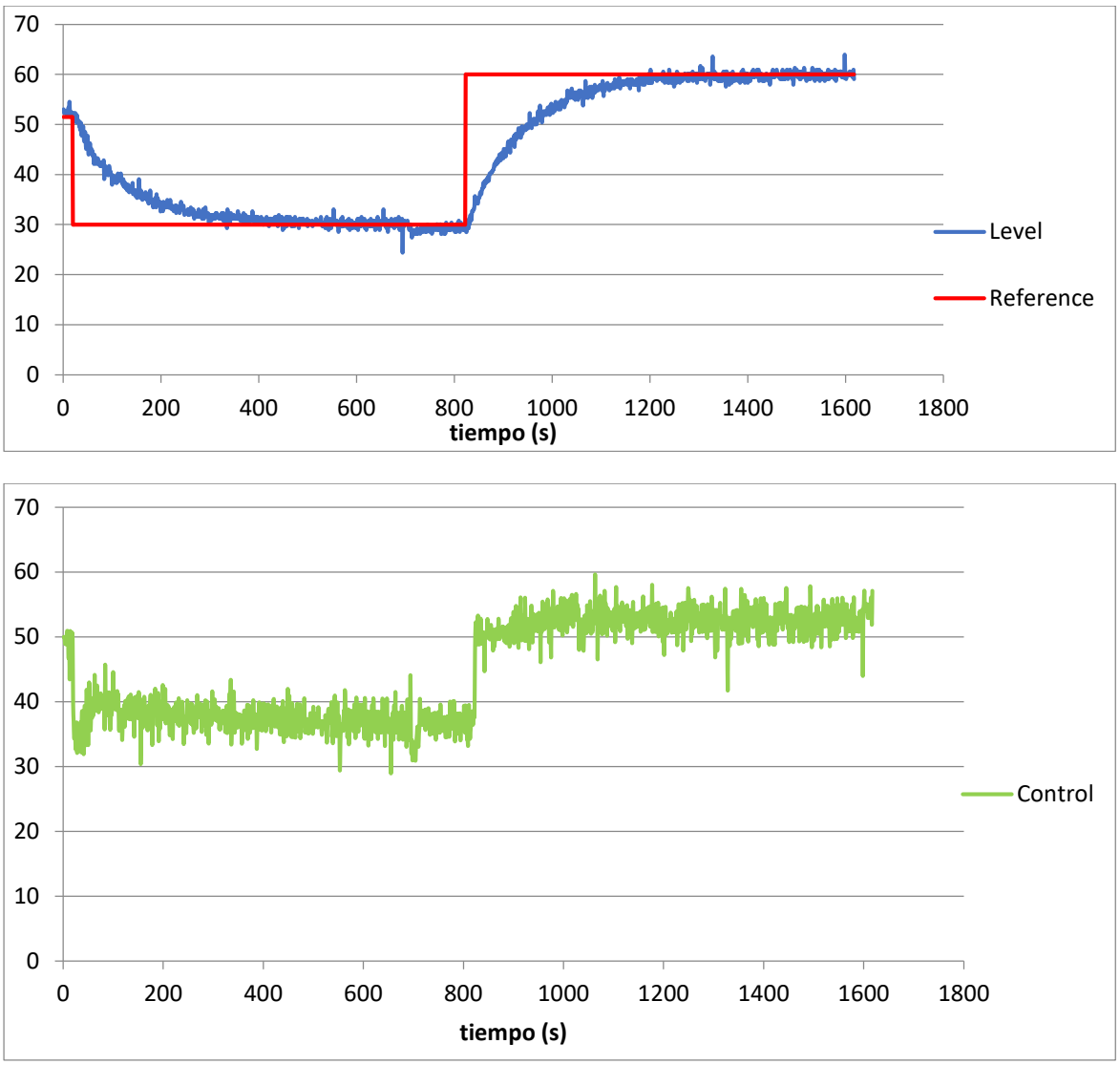

Figure 6. Rivera-Morari PI control

In this chart, we can observe that the behaviour of the system is like a First Order System Plus Delay. With this controller we can obtain a small stationary error and the system has a good reaction to a change in the reference signal. The only problem is that these reaction is quite slow, around 6.8 minutes.

Rovira

On the other hand, we have the Rovira method and a PI controller also.

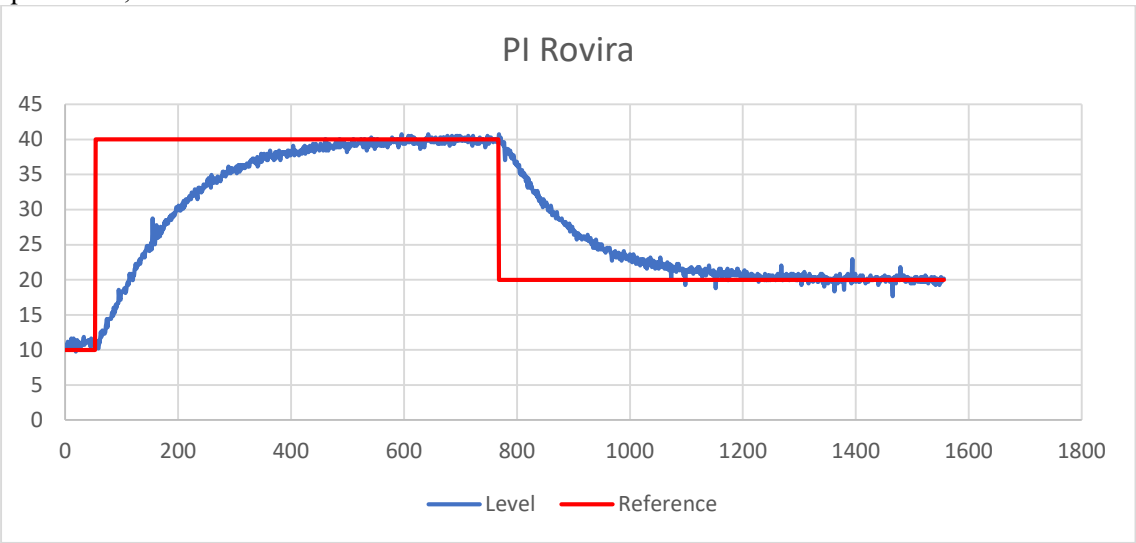

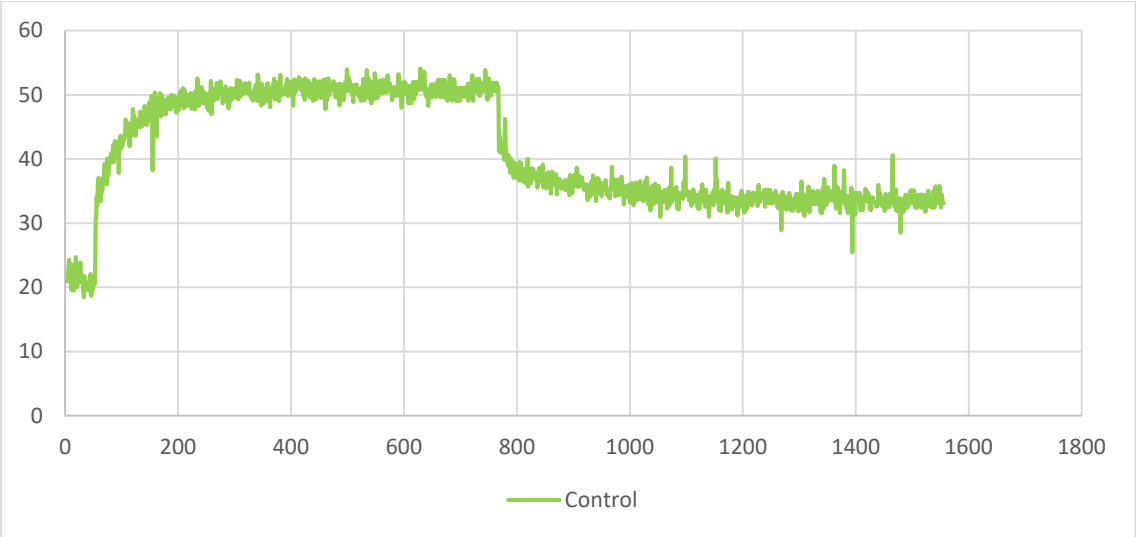

Figure 7. Rovira PI control

With this part we can see that this method is better than the Rivera-Morari one, because the reaction is faster, around 5 minutes, with more stability and accuracy regarding the reference that has been introduced. These are the main reasons why this method is the most appropriated.

References

Process Dynamics, Modeling and Control, B.A. Ogunnaike, W.H. Ray, Oxfor Univ.Press, 1994

Principles and practice of Automatic process control, Smith, Corripio, Edt. John Wiley, 3ª edc, 2006

A METHODOLOGICAL APPROACH FOR A SELF-SUFFICIENT HOUSE

Fabrizio Amico

Computer Engineering and Networks Laboratory – Kore University of Enna – Italy
Email: fabrizio.amico9@unikorestudent.it

Abstract
Nowadays it is common to read about "Smart Home," "Internet of Things" and artificial intelligence. All of them have one thing in common that is to commit one or more actions, practiced daily, directly or indirectly, by people on objects. With the technological development of electronic, electrical and information systems, there is a great need for "autonomous systems". However, the increasing of energetic waste is an issue that must be addressed. As a consequence, an extensive developing of novel solutions could be the main aim to improve the quality of life. In this paper, through a computer simulation, a methodological approach for a self-sufficient house is proposed. The goal is to show the benefit of the proposed system and its potential.

I. INTRODUCTION

A smart house can manage power consumption, activation/deactivation of lights and air-conditioners concerning their use and necessity. Its sequential and self-management working have been designed to achieve optimal conditions of temperature and humidity inside each room, to reduce energy consumption, to improve our overall quality of life and lower the risk of getting a respiratory infection associated with a domestic indoor humidity, often related to dust-mite and other bacteria dangerous to our health.

In this paper, it has been decided to adopt a centralized architecture composed of a network server with the purpose of task analysis coming from the sensors and sending commands to peripheral devices. The network of sensors exchanges serial data with the server for system commands. All communications run through the Gateway (Sensors -> Gateway -> Controller -> Gateway ->Actuator). Therefore, the topological choice of the net is point-to-point star type with the central Gateway responsible for carrying out the routing data packet.

In detail, the network of sensors, actuators, and devices is IEEE 802.11 and have a data rate assigned respectively to 5,5 and 10Mb/s. On the contrary, the network of the controller is IEEE 802.3 with a data rate of 10Mb/s. Anyhow, the Gateway can interface with both protocols. This network architecture has been chosen to develop a simple displacement of sensors and implemental devices. They are autonomous from wiring and, thanks to IEEE 802.11 technology, can interface with any similar device (such as smartphones) to obtain, in real-time, the received data. On the contrary, regarding the controller managing critical data, commands and configurations, it is necessary to achieve high efficiency (such as Ethernet) in the data transmission, avoiding any power management concerning the distance from the router. In fact, the Gateway is also the router/modem of the house serving the connection to the Internet. The devices can give commands by indoor, through a suitable IP address or DNS dynamic services. Moreover, the controller gives commands in LAN because through the static local IP addresses the devices.

In the following sections, some related works and the most used solutions in this research field will be presented. Subsequently, a novel approach for the analyzed application scenario will be introduced. Next, an evaluation of system performance will be shown.

II. RELATED WORKS

Modern automation systems, developed in a home or office, become much more critical in managing limited resources such as energy, time and workforce, as shown in [1]. The simple implementation of this kind of architecture is not sufficient to reach a high-level of comfort and energy consumption. In fact, many actions regarding setting parameters of temperature and humidity, activation of lights and power regulation (if possible) are determined by a human-labeled agent that, very often, does not take into consideration the optimal values and/or necessary or of all alternative hypothesis. Therefore, it follows the necessity to introduce a system able to be, too but not only, utterly autonomous in managing better all these parameters, to have sound values and reduced wastes, during all the day. A direct consequence is the use of soft computing techniques that allow establishing these data most efficiently.

However, in several contexts, an optimal environment regarding humidity and temperature it is not easy to realize due to connections problems and by prediction of the two measures. In these cases, it is possible to use several more or less complex techniques such as the Fuzzy logic, applied successfully also in cultural situations [2] where these values are considered critical. There are several works in this

area [3][4] and the proposed approaches often have a significant effect on applications. The goal is to achieve a limited usage by users through the artificial intelligence, automatism and machine learning. As a consequence, it is necessary to operate on automatic choices with the aim to make more proactive the domestic life.

III. THE PROPOSED APPROACH

The house taken into account in this work consists of 3 rooms all of 70 square meters. The house has a centralized air conditioning able to provide an air flow through three outlets exit for the three rooms interrupted by electric pilot valves. LED lamps supply the light. The whole system is organized as follows:

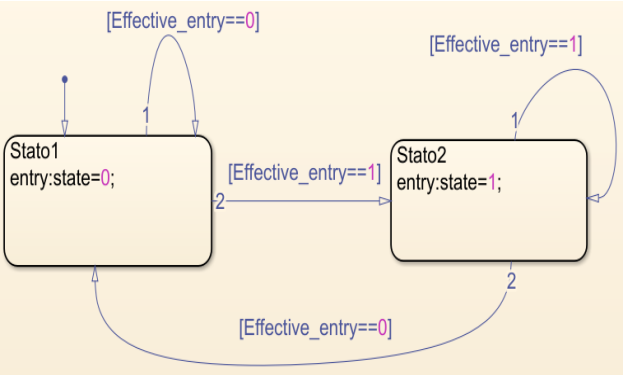

Figure 1: Diagram used to determine the state of the circuit breaker.

- 4 light sensors: 1 detects the amount of light in external lux and 3 for the indoor one;
- 4 humidity/temperature sensors: 1 for each room and 1 that records the external variations;
- 3 nodes representing clients' devices (smartphone, tablets, and so on) and that can send their preferences such as temperature and humidity;
- 3 presence sensors displaced in the rooms;
- 1 controller node (server): solves all those tasks relating to the storage, management, and evaluation of the parameters to be assigned to the devices (status, power, presence);
- 6 actuator nodes: 3 represent the electric pilot valves of the outlet's exit of each room and 3 of the lights power regulation devices;
- 1 electro-mechanical switch circuit able to reactive the circuit breaker automatically by restoring the current after an atmospheric/overload voltage event (as shown in the Fig. 2).

The topological choice of the net is point-to-point star type with the central Gateway who is responsible for carrying out the routing data packet. The transmission power is of 20 dBm, enough to reach the router in almost all rooms without, unless particular cases, excessive slowing due to objects and walls. All data periodically sent to the controller, by the sensors, first will be elaborated, and then a directive will be sent to the specific actuator. In detail, the activation and deactivation of the lights will be elaborated according to the presence sensors received value and to the light sensors through the MBSD (as shown in the Fig. 1).

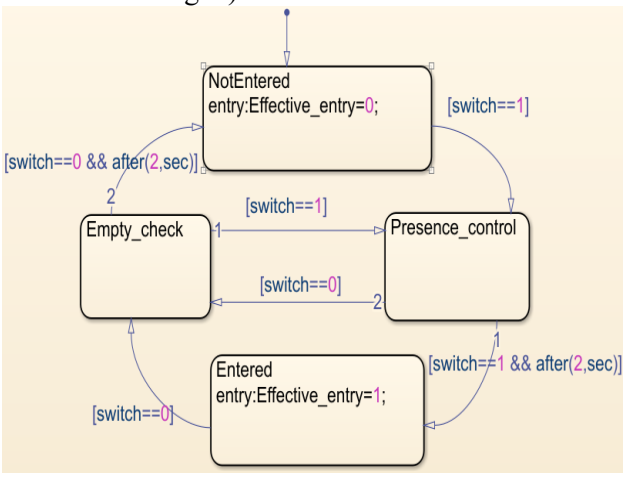

Figure 2: Mechanism of debounce avoiding accidental and sudden switching. The two mechanisms are in logical AND.

Then, it will be evaluated if activate or deactivate the light according to the result of a "Debounce" mechanism (Fig. 1.2). The power values to be assigned to the lights or air conditioning of a particular room is calculated by fuzzy logic controllers with Gaussian-type membership functions as shown in the figure 3 and 8. The optimal ranges for autonomous air conditioning (not before setting) are calculated concerning the UNI EN ISO 7730 standards (about 20° C and 40%).

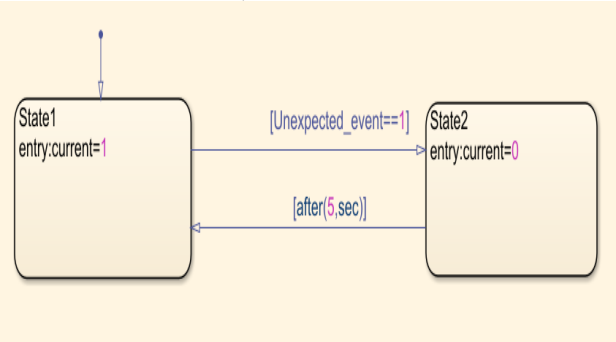

Figure 3: Diagram states of the smart differential switch.

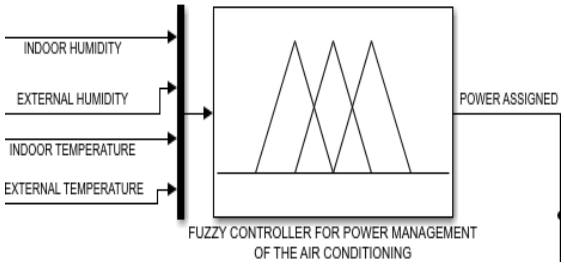

Figure 4: Fuzzy controller power calculation to attribute to the air conditioning. The evaluation is obtained taking into consideration the environment values to improve the efficiency based on the perceived thermal change.

IV. SCENARIO

The context has been simulated in Matlab/Simulink/TrueTime (a general picture is shown in the Fig. 5). The duration of the simulation is 24 long hours. It has been decided to examine the system with external temperatures that changed from 0 to 30 degrees with a Gaussian trend as that of humidity with a change from 0 to 70%.

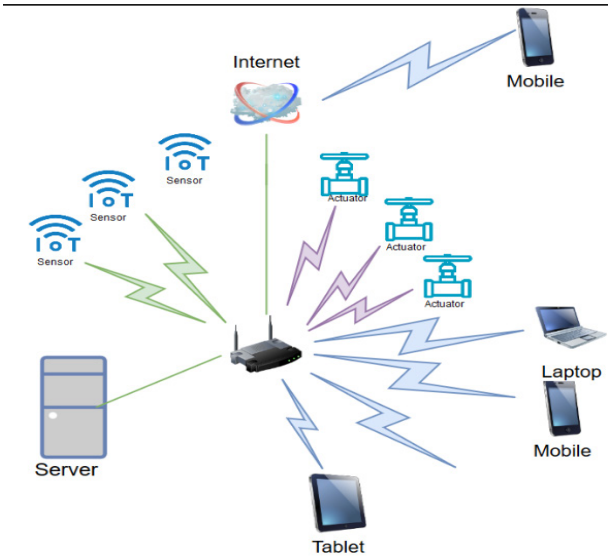

Figure 5: A general scheme of the network and communications.

All sensors dislocated in the house send the recorded values periodically to the controller and information about the position and type. The controller will evaluate the lights quality or the air conditioning, based on the previous detached values, if necessary. Each node of the wireless sensor network has allocated a specific buffer on which sending data equally to the controller to receive and identify the typology.

The server will continue, through sending of suitable commands to the smart objects, to maintain the environment climate conditions for each room, assigning proper values of power, temperature, humidity and light to each one and, if the user provides new settings, the system is adapted to new parameters.

Therefore, during all the day, the system will self-manage the resources in an independent and precise way to the user, limiting the use of the net not to stress the normal surfing, implementing the reduction policy of the throughput. An example can be that of data send by external sensors equipped with microcontroller able to store the previous values obtained, avoiding the reimport if they are equal or their difference does not exceed a specific range since such parameters do not show sudden changes in similar context. Parameters such as the external temperature/humidity are essential for a proper assignment of the exercise power since the perceived indoor/outdoor thermal change is always not constant or low, that could make the air conditioning system inefficient regarding consumption and incisiveness. It is useful to note that there are adoptable solutions on the market regarding the microcontrollers, the sensor, and the whole implementation.

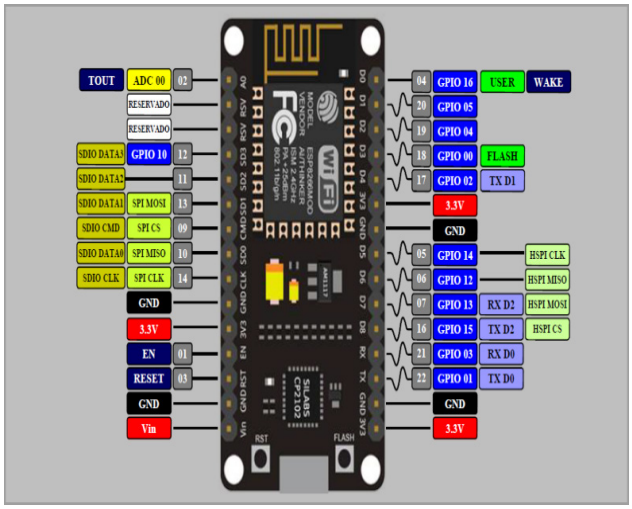

Figure 6: Schematic representation of a programmable microcontroller, NodeMCU on ESP8266 ESP-12E base, easily integrated into a circuit and complete with everything necessary.

The device must be equipped with a wireless chipset complying with the IEEE 802.11b/g/n protocol, complete support to TCP/IP and fully programmable. An example can be the NodeMCU on ESP8266 ESP-12E (Fig. 6), equipped with digital and analogical pins that are adaptable to the Internet of Things world and smart homes [5].

V. PERFORMANCE EVALUATION

During the simulation of 864 seconds (86400 s = 24h, 864 s in scale 1:100), consumptions have been measured in W of LED lamps of 30 W and the centralized air conditioner of 4 kW. An arithmetic average has been carried out. The average power required during all the day from the LED lamps is 10.27 W while that of the air conditioner is of 0.776 kW. For a good operation system, the meet of a deadline between the performance of a given task and the next one is needed. Therefore, the jitter has been measured as parameter considering a deadline of the actuators performance times of 2 seconds. Such evaluation has been carried out verifying recurrences to the end of the simulation.

A measure of the delivery times of the data packet has been carried out. Based on the given periodic nature of sensors coming data, no data packet goes beyond half a second to arrive (an example in Fig. 7).

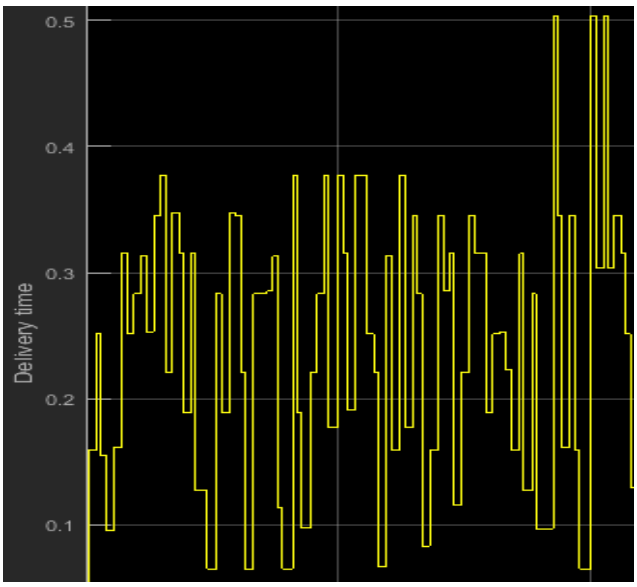

Figure 7: Commands delivery times in electro valves during all the day, not exceed the 0.5 seconds and keep themselves about the 0.3 seconds.

The throughput of the main channels has been measured to verify that data are not too many and/or too large. Considering the payload of each sensors packet, it is composed of humidity/temperature/light/movement value as a double of 64 bit.

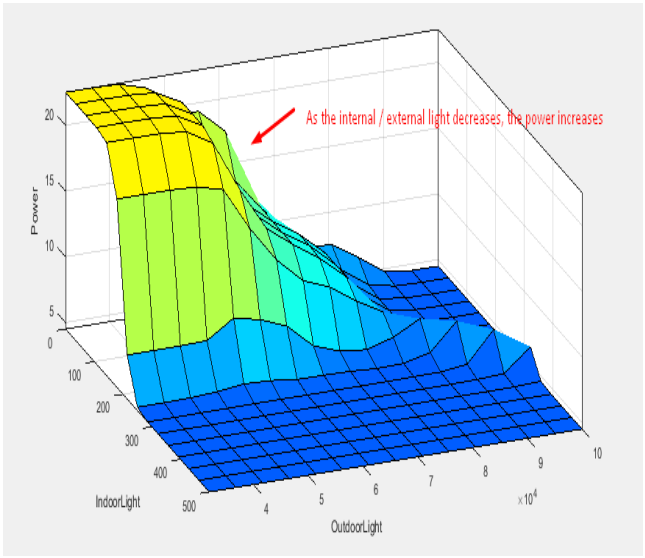

Figure 8: Obtained surface related to the fuzzy controller managing lights' power. It is useful to note the inverse proportion development power as regards the relieved light.

As a consequence, all data packet with the highest size are sent at the same time. It has been measured that the input of data in the channels by the only sensors, with sending time of 0.2 s, is 24000 bit/s. Regarding the controller (server), its performance and sending time of the data packet has been set to 3 ms and considering a payload of 128 bit a value of 42,6 kbit/s has been obtained. The data load on the channel is quite low, so in these conditions, there are no significant slowdowns.

VI. CONCLUSIONS

The goal of this paper was to develop a centralized system managed (on site) by a server to improve the quality of life for all house's occupants. It is clear that the results of this overview are quite approximate, but better research of this field could lead to the belief that such system can be developed as self-managed and autonomous. If the starting point can be the idea that a system or a house can self-manage itself and, at the same time, makes itself comfortable for a human user is, in a certain sense, the future that can be expected in this direction. If we put ourselves in the condition that the variety of parameters, habits, and lifestyles finding in the world, can be schematized and computed in a short time on any future developments with advanced algorithms, surely we could manage at best all the changes and improve the quality of life in a place where we often spend much time, i.e., our home.

REFERENCES

[1] Fredy Augusto Maciel Alves; Charles Thangaraj. "A Scalable Modular Heterogeneous System for Home and Office Automation", Year: 2016, [2016 IEEE MIT Undergraduate Research Technology Conference (URTC)] (accessed 02/03/2018).

[2] Theeramet Kaewwiset; Paitoon Yodkhad. "Automatic Temperature and Humidity Control System by Using Fuzzy Logic Algorithm for Mushroom Nursery", Year: 2017, [2017 International Conference on Digital Arts, Media and Technology (ICDAMT)] (accessed 02/03/2018).

[3] Paul Jasmin Rani, Jason Bakthakumar, B. Praveen Kumaar, U. Praveen Kumaar, Santhosh Kumar. "Voice Controlled Home Automation System Using Natural Language Processing (NLP) and Internet of Things (IoT), Year 2017, [2017 Third International Conference on Science Technology Engineering & Management (ICONSTEM)] (accessed 02/03/2018).

[4] Eshan Shailendra, Praneet Kaur Bhatia. "Analyzing Home Automation and Networking Technologies", Year 2018, [IEEE Potentials] (accessed 02/03/2018).

[5] Oran Chieochan, Anukit Saokaew, Ekkrat Boonchieng. "Internet of Things (IOT) for smart solar energy: A case study of the smart farm at Maejo University", Year 2017, [2017 International Conference on Control, Automation and Information Sciences (ICCAIS)] (accessed 02/03/2018).

SMART ENERGY HARVESTING GRID: A SMART MANAGEMENT SYSTEM FOR PRODUCTION GRIDS

Riccardo Gaetano Augello

Computer Engineering and Networks Laboratory - Kore University of Enna – Italy
Email: riccardogaetano.augello@unikorestudent.it

Abstract

The goal of this project is to empathize the importance of the network connection in those systems employed in the production of renewable energy through the analysis of data collected by wireless sensors, which become fundamental items for the maintenance, management and scalability of the system itself. This has lead to a proposal of a system that includes solar trackers and bidirectional telemetry, which together improve the efficiency of the process.

This solution can be used by companies to become more competitive and efficient in the production market.

I. INTRODUCTION

Using the Matlab software and TrueTime[1] simulator, based on Simulink, it was possible to show how to monitor and control automated systems with the wireless technologies available nowadays.

The simulation is designed with PV panels mounted on a single axis tracker have one degree of freedom and telemetry sensors that measure the produced power. Solar tracker's logic control is linked by a bus D/A to another ZigBee-type wireless device; the main Gateway is a WPAN Coordinator for the ZigBee network, saving data and displaying them to an operator or a control room via standard WiFi 802.11.

Furthermore, it is possible to give two different command to the system: the first one can send a stop command to the solar tracker if maintenance is needed, the second one can be used to activate or deactivate the forwarding of data to the operator connected with a WiFi radio device.

Several case studies propose the introduction of wireless sensor networks to collect data and analyze critical parameters.

Telemetry is an automated communications process by which measurements and other data are collected at remote or inaccessible points and transmitted to receiving equipment for monitoring [2].

Although the term commonly refers to wireless data transfer mechanisms (e.g., using radio, ultrasonic, or infrared systems), it also encompasses data transferred over other media such as a telephone or computer network, optical link or other wired communications like power line carriers.

Telemetry can be classified in two different types:

- Mono-directional, where data flow is directed towards a single direction; these systems are needed for data detection;
- Bi-directional, where data flow goes in both direction; with these systems is also possible to measure or modify a fixed parameter by remote terminal.

A solar tracker is a device that orients a payload toward the sun, increasing the amount of energy picked up by the payload and therefore his effective gain; in this case the payload is a PV panel. When it comes to solar concentration, solar trackers are useful to keep constant the focal point. The greater is the perpendicular alignment with solar beams, the greater will be the conversion efficiency and the amount of energy produced with the same surface area; the plant costs will then be reduced thanks to a smaller area needed to produce the same amount of energy.

Active trackers can be classified on the base of the electronic command that guides the movements; the one used in this project is a light-sensing tracker, where commands are generated by light sensors that detect the brightest point in the sky; this piloting grants a higher productivity when traditional cells are used, where the surface/solar radiation ratio is 1:1 and that are effective even in poor light condition, because of their sensibility to reflected or diffused light. [3]

II. RELATED WORKS

These days it is required maximum efficiency in energy production systems. A good way to be competitive is to optimize the resources, improving energy production and preventing system faults. These faults can be prevented by using a MCU on the field, that is able to measure key parameters which will be successively analysed to provide further information of the plant status.

Work done by S.S. and A.K. represents a good monitoring system that uses two kinds of devices. The first one used on field is a MCU that acts as a Client, adopted for measuring the value of brightness that impacts the solar panel and also the energy produced. The second one, a PC displaced in the control room, acts as a Server, that analyses data received from Client through two communications standards, WIFI and Ethernet.

Studying these data, it is possible to evaluate the status of solar panel even in real time. [4]

Another noteworthy work is the one conducted by A.A., M.F., F.B and T. A. A. In this paper, was developed a system able to identify and classify those faults that are statistically more frequent in solar panels. The hardware used on field for measuring and transmitting data that will be later examined is a Arduino Mega-type MCU. For data transmission, it was employed an XBee radio module that uses the IEEE 802.15.4 standard. Furthermore, it was implemented a Fuzzy Controller on the MCU to evaluate the entity of the fault. [5]

In the X. X. and Q. D.'s work, three base elements needed for the realization of a smart production grid are shown: condition monitoring, power control, and data communication to connect individual modules into a wireless sensor and actuator network.

The Server uses a neural network to calculate the maximum power production point and the best operating voltage of solar panels. There were implemented field devices to measure examined parameters, routers to extend the coverage of the network and a base station connected to the internet that acts as a coordinator. ZigBee modules were used to create the network infrastructure. Such system is able to estimate if the solar panel works in normal condition, disconnecting it from the grid in case of abnormal conditions, or else connecting it to the grid. [6]

All works examined and this paper make use of Wireless Sensor Network and various communication standards. Almost all the author mentioned above had used the IEEE 802.15.4 communication standard because of its predisposition to energy saving.

III. APPROACH

The system proposed is structured as follows:

Solar tracker's logic controller is based on analogic input and output. Using an A/D input it was possible to detect those parameters used for setting the position of the tracker itself.

Inputs description:

- Two light sensors;
- PV panels power sensor;
- Measurement of the rotation angle;
- Stop command send by the operator and received by the ZigBee node;
- Two mechanical endstop switches sensors fixed on the external sides.

Outputs description:

- Control signal connected to the motor control circuit;
- Data signal obtained by power sensor and sent to the ZigBee node.

Values measured by A/D sensors are elaborated by MBSD and Fuzzy Logic Controller in order to regulate the motor rotation speed as well as the stop when the endstop switches are triggered.

Description of the regulation of parameters based on values received from MBSD and Fuzzy Logic Controller:

Inputs directed to the Fuzzy Logic Controller are the rate of the brightness measured by sensors fixed on the external sides of the PV panel and the output is the voltage through which drive the motor. The latter rotate in the same direction of the voltage signs, at a speed that grows according to the amount of voltage applied.

The first MBSD is used to compare the brightness in a rigorous manner, while the second can control if the endstop switches are triggered. Both are equipped with a debouncing management algorithm.

Brief description of debouncing:

Debouncing is apparently a trivial problem, but it is often the cause of malfunction in micro controllers. Although they are imperceptible from humans, the mechanical bouncing of the switches can lead to impure transitions of the applied inputs, which correspond to consecutive pressure of the same button (see picture below).

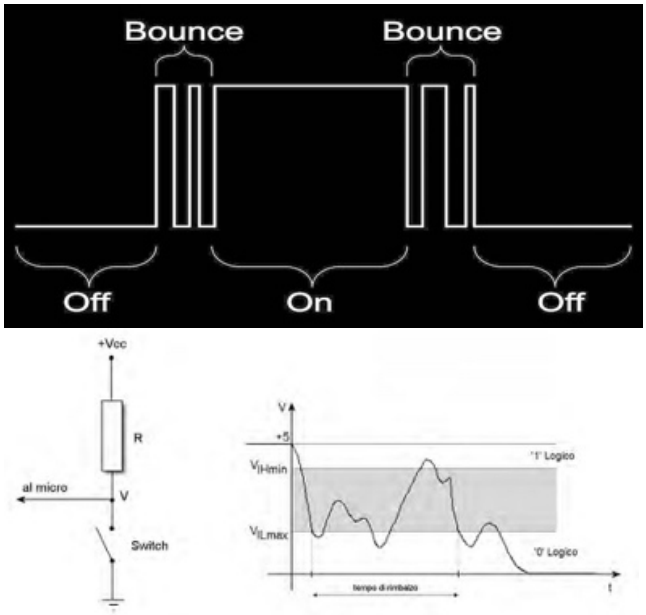

Fig. 1

"Bouncing time" it is defined as the time interval in which the signal goes through the low logic level for the first time and that where it remains in without further ambiguity and viceversa.

In order to connect the solar tracker logic control to a device with a ZigBee radio, it was emulated an analogic reading. This measured value is used for share into the network the solar panel produced power.

There are two networks in the system, the first one is a WiFi 802.11b and the second one is a ZigBee 802.15.4.

The ZigBee network was utilized for his versatility in connecting nodes between them and

therefore to promote his scalability. Using a single Coordinator and various Full Function Device it is also possible to arrange plant modules in a freer way, having the only limit in the signal range.

It was chosen to make independent the solar tracker control logic from the one into the network in order to grant right functioning if network breakdowns occur. In addition, this approach can be used in already functionally systems without network connection by making ZigBee modules working properly.

The resulting topology is a cluster type. In this kind of topology, every node has two branches, one connecting the previous and one connecting the following one. Communication between two non-consecutive nodes must go through every intermediate node and their relative branches: each step between them is called *jump* or *hop.*

The advance taken by this kind of topology lies in the easiness with which the network can be scaled, setting it in advance.

WiFi network was used to grant access to telemetry by a user with commercial devices provided with dedicated application and to implements bidirectional telemetry, allowing the possibility to give a stop command to system devices. The system has two networks, each of these relies on the Gateway that will route data traffic towards sub-network.

The Gateway has the task to act as a bridge between WiFi and ZigBee network. It sends both telemetry and user's commands that are given through the WiFi network. This node transmits the telemetry received to a device connected with an A/D bus for the storage of a log file. This procedure is repeated each time it receives a packet from ZigBee network nodes.

Brief description of the communication protocol used between both devices:

In each transaction through the bus:

- Master device take control of the bus
- It sends a request (I/O) to the second device through a signal delivered to "interrupt" slave port.
- The slave device read data from A/D ports.

The master device is the one that acts as Gateway, while the slave one is the storage device.

The main task of the Full Function Device Zig-Bee node is to send telemetry to the Gateway and give the stop command to the solar tracker control logic. Telemetry is taken from solar tracker control logic via analogic reading with an A/D port. Furthermore, this network node forward messages that are destined to next nodes. This algorithm was implemented starting from the fact that the single node is already configured to know his network id and which are previous and following nodes, this setting is done during the installation.

By using the message field sent to the Gateway, which has the destination address, a 'Handler' device, reading this field, forward this message if it is destined to other network nodes.

An exception is made for the stop message given by the operator, which doesn't have a destination field when sent by the Gateway from WiFi to ZigBee network. They are identified because opportunely marked and then read and forwarded among nodes as long as the last one is reached.

The system has a WiFi 802.11b connection. This standard was chosen because most of the available commercial devices have this kind of interface, therefore it is possible to realize dedicated application for various operating systems e.g. smartphone, tablet, pc. The user has the possibility to access to the telemetry asking for it from WiFi interface, he can also activate or deactivate the plant.

IV. SCENARIO

The simulated scenario has a series of ZigBee True Time Wireless Network nodes and the one that represents the user connected to WiFi True Time Wireless Network.

As represented in figure 1 three True Time Wireless Network blocks were utilized two configured with ZigBee standard and one configured with WiFi standard, there are also six subsystems used for the simulation of Full Function Device nodes of the ZigBee network (coloured in yellow) a Gateway (coloured in green) connected with all networks, finally the represents cyan subsystem the operator.

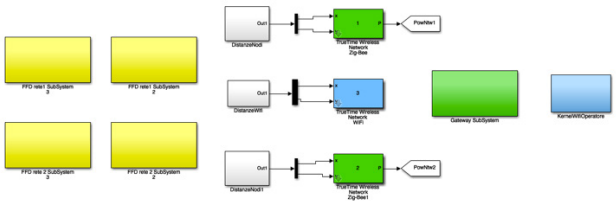

Figure 1. Snapshot of the implemented Network on Matlab

Figure 2 shows the internal snapshot that represents the network Gateway, the True Time Kernel Gateway is part of the three networks shown before and it is also connected with another True Time Kernel simulated storage device.

Description of the algorithm used for log storage:

When the Gateway receive the message that was sent by ZigBee nodes, it unboxes and transfers them to the storage device bus, activating the device with a high logic level signal on a trigger port, this signal was used to start the process scheduling, that has a task to read input data and store them in a file. The gateway acts as a bridge between ZigBee and WiFi, it forwards command given by the user to the node or the telemetry received from nodes to the user.

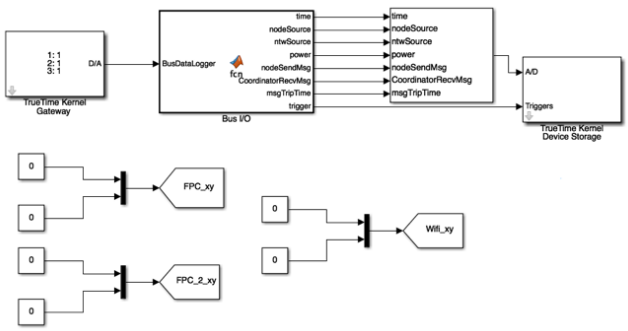

Figure 2 Snapshot inside of subsystem

The subsystem which contains the ZigBee kernel used for telemetry data transmission; it has night backup battery with a recharging circuit. It is also connected to the subsystem of the solar tracker.

Description of the subsystem:

With an A/D converter it can be measured the produced power of the solar panel and the configuration constants.

Set parameter are:

1) Node network address.
2) Next node address (if present) if not the algorithm expect point one to be set.
3) Previous node address.
4) Number of True Time Network needed parameter to send and receive the messagges with function provided by True Time.

These parameters were used to allow the message forwarding.

If the message is a stop, it is directly forwarded to next nodes and the proper task runs to stop the solar tracker.

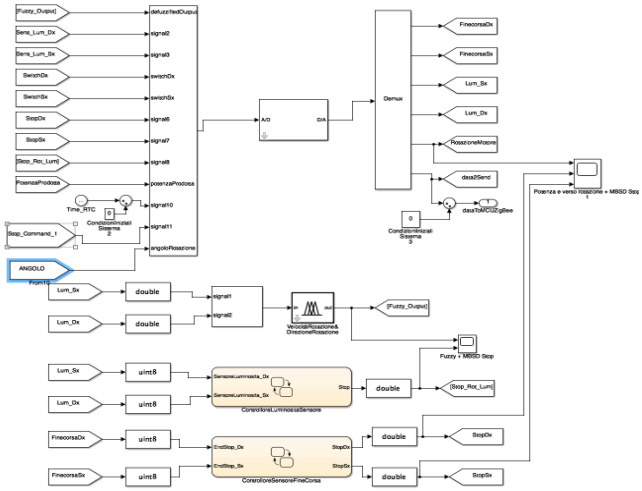

Figure 4 Snapshot of the control logic of solar tracker.

The subsystem shown in figure 4 represents solar tracker control logic. Inputs to the True Time Kernel (without considering MBSD and Fuzzy Logic Controller outputs) there are:

1) Two brightness sensors that detect the light intensity.
2) Two switches placed on the edges of the solar tracker
3) Solar panel produced power
4) Simulation time used to run night positioning procedure
5) The rotation angle of the solar tracker
6) A stop command from ZigBee node

Outputs are:

1) Analog signal for motor piloting
2) Value of the produced power to send to the ZigBee node.

Inputs and outputs not shown before are used for MBSD and Fuzzy Logic Controller.

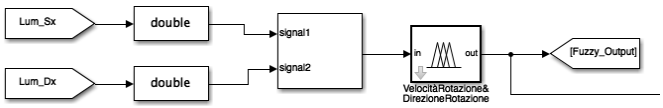

Figure 5 Snapshot of inputs and outputs connected to the Fuzzy Logic Controller block

As input to the Fuzzy Logic Controller there are the right and left brightness sensors, while as output there is an analogue signal which, after the defuzzification, is used to pilot the motor that will allow the rotation of the solar tracker.

The centroid method is used for defuzzification of the output. Having to pilot a motor where it is mounted a heavy structure it is better to use the maximum method in order to not have a peak values in output.

Description of MBSD:

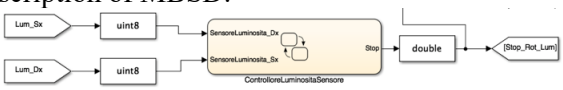

Figure 6 MBSD brightness light sensors controller

In order to straighten the control of the brightness gap between right and left sides it was used a state machine better shown below.

Such controller is used to delay the motor movement that allows the tracker rotation. When an equal value between the two sensor is reached, it stops his movements for a settable time. This system was used to avoid continuous vibrations from the tracker.

Second MBSD description:

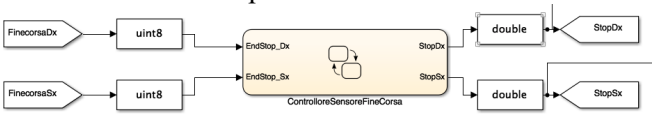

Figure 7 Inputs and outputs of 'Endstop sensor controller'

As input for the state flow (figure 7), it can be seen the endstop located at the ends of the solar tracker structure; in output, there are two variables used to stop the rotation of the motor if its maximum right or left rotation limit has been reached.

Description of the subsystem used to simulate the operator interactions.

Interactions were simulated using input signals on A/D and Trigger ports.

Input signals for the trigger port are used to detect the status variation of the commands; Such variations allow the scheduling of the proper task. If 'log signal' become one, the log function will be activated, else will be not. The same procedure was used for the stop signal.

The activation or deactivation of the function represented before is implemented thanks to messages sent by the operator to the Gateway through a WiFi device.

Brief description of modified 'True Time Battery' block.

Here a representation of an already modified block, where it is possible to connect sources of energy to recharge the battery.

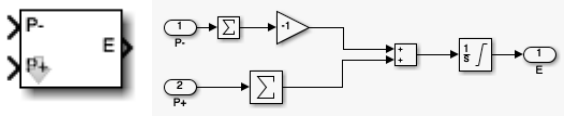

V. PERFORMANCES EVALUATION

Below it is shown the graph representing the right functioning of the Fuzzy Logic Controller and MBSD used for granting the right functioning of the motor.

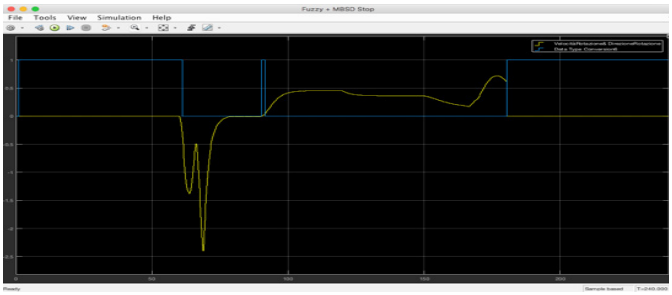

Figure 8 Overlap of the graphs showing the MBSD 'brightness controller sensors' and Fuzzy Logic Controller

Figure 8 shows the functioning of the Fuzzy Logic Controller and the MBSD descripted before as 'brightness controller sensors'. On the x axis is represented the time of simulation, on the y axis the voltage applied for the motor rotation (in yellow) and the stop signal of the rotation (in blue).

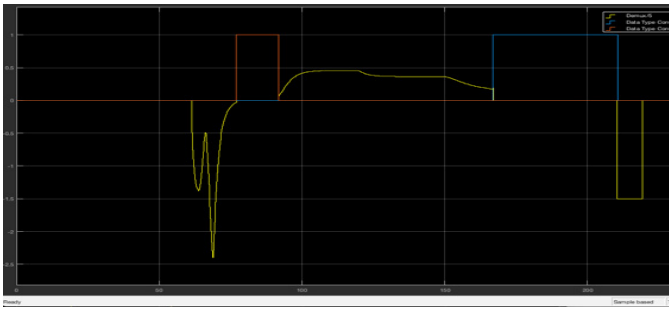

Figure 9 Real Time kernel output and 'endstop sensor controller' state flow

In this graph are represented the time of the simulation on the x axis, voltage signal (in yellow) and Boolean signal (in red and blue) on the y axis. The yellow signal describes the kernel output used for piloting the motor, red and blue signal are the Boolean output of the state flow 'controller of the endstop sensors', used to stop the motor when the switch is hit. When one of the two switches are triggered, the motor stops.

The graph represented in figure 10 has on the x axis the time of the simulations, and on the y axis the degree of the rotation of the solar tracker. The latter has a range of [-60°, 60°].

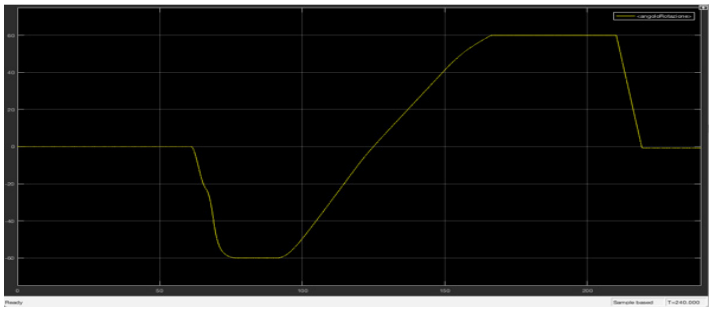

Figure 10 in the graph above, the rotation angle of the tracker is shown at each instant of the simulation

At 21 o'clock the panel is brought back to 0°, parallel to the ground. This is the result of the combination of the two MBSD and Fuzzy Logic Controller mentioned before.

- Analasys of performance metrics:

• Number of packets sent from the FFD to the Gateway.

sourceNetwork	nodeSource	power	nodeSendMsg	CoordinatorRecvMsg	msgTripTime
1	2	560.0960	8563	8561	3.4000e-04
2	2	469.6678	8563	8561	9.3400e-04
1	3	469.6678	8563	8445	0.0027
2	3	469.6678	8563	8445	0.0033

Figure 11 Samples of the content of the message exchanged between nodes

Data shown in the table were collected by using the fields included in packets sent from ZigBee nodes. Two important fields are 'nodeSendMsg' and 'coordinatorRecvMsg', rapresenting respectively messages sent from the node and received by the coordinator of the ZigBee network. Plus, there are also indicated the node number in the 'nodeSource' field and the True Time Wireless Network in the 'SourceNetwork'. As evidenced by data, there is a lack of packets either in network 1 and 2, with a considerable lack on node 3. Also, msgTripTime data is calculate as (ArrivalMsgTimeStamp – DeliveryMsgTimeStamp).

N.B. the 'TimeStamp' taken in consideration is the one given from True Time Library with the ttCurrentTime call.

• Analysis of the response time after the stop command

The response time after forwarding the stop command, measured using video printouts in Matlab's command windows, is 0.16 m[Sec].

• Analysis of the energy consumption of the

ZigBee device.

Analysis of the energy consumption of the ZigBee nodes. During the usage, the battery discharges only a little bit. The great energy saving of the ZigBee module is noteworthy. The battery is completely recharged when the solar panel begin to produce energy.

To allow better energy savings, the process planning period was changed according to the time of day. The sleep time of the process during the night was increased.

VI. CONCLUSIONS

The proposed project shows, using the modularity of the systems, that it is possible to adapt the control logic already working to the sharing of the telemetry in the network. Such functionality can be added using modules with a ZigBee radio.

The library that made it possible and simplify the realization of the code needed to complete the simulation is True Time. It allowed the simulation of cooperating devices with an integrated operating system and the management of hardware and software interrupts.

Thanks to the Matlab code generation tool it is possible to extract the algorithms implemented in the state machine and in the Fuzzy Logic Controller.

With the algorithms developed and tested in this project it is possible to create solar trackers with a degree of freedom using micro-controllers as control logic.

It is also possible to extract the modification of the True Time Battery contained in the True Time 2.0 library. This modification allows also to simulate the recharge.

A possible future development could be to experiment solar trackers with more degrees of freedom.

In the future, by studying other positioning algorithms, the project could be further developed, e.g. using the power produced by the solar panel as a reference variable.

References

[1] ″Telemetry: Summary of concept and rationale". (NASA report, 19 December 2014). *SAO/NASA ADS Physics Abstract Service*. Retrieved 19 December 2014.

[2] Dan Henriksson, Anton Cervin, Karl-Erik Årzén. “TrueTime: Real-time Control System Simulation with MATLAB/Simulink” , Year: 2003 - http://www.lunduniversity.lu.se/lup/publication/17e2d2a4-09a9-4718-92c6-6a9780e20c08 - (accessed 03/17/2017)

[3] “Inseguitore solare” , https://it.wikipedia.org/wiki/Inseguitore_solare

[4] S.Suryono e A. K Khuriati - “Wireless sensor system for photovoltaic panel efficiency monitoring using wi-fi network” (2017)

[5] Ali Al-Dahoud, Mohamed Fezari, FatmaZohra Belhouchet, Thamer A. Al-Rawashdeh – “Remote Monitoring System for Solar Power Panels using Intelligent Sensors Network” - Nov. 2016

[6] Xu Xiaoli, Qiao Daoe – “Remote Monitoring and Control of Photovoltaic System Using Wireless Sensor Network” – April 2011

STATISTICAL QUALITY CONTROL OF THE PROCESS OF LAYERED SYNTHESIS OF HULL ELEMENTS REA

Chabanenko Alexandr

Saint-Petersburg State University of Aerospace Instrumentation,
Saint-Petersburg, Russia
E-mail: Chabalexandr@gmail.com

Abstract

In recent years, the methods of layered synthesis of prototype products which is included in additive technologies have formed a fundamentally new direction in technology, where it is necessary to produce experienced, single, exclusive and unique samples of products. The fundamental difference between these methods is that the finished part is obtained not by removing the material layer from the workpiece, as it is customary in traditional methods of processing, but by layered muscle material with simultaneous receipt of the given form and Size of the product. The main peculiarity of these methods is the obligatory application of three-dimensional computer design of the product as the initial stage of the layer synthesis technology. Application of these technologies is particularly promising in the sphere of production of Hull elements REA in view of the ability to take into account the specific equipment.

For enclosures are characteristic: resistance to physical influence; Long service life; Resistance; High corrosion properties; resistance to chemical influences; Ease of movement, design principles are presented in (Fig. 1).

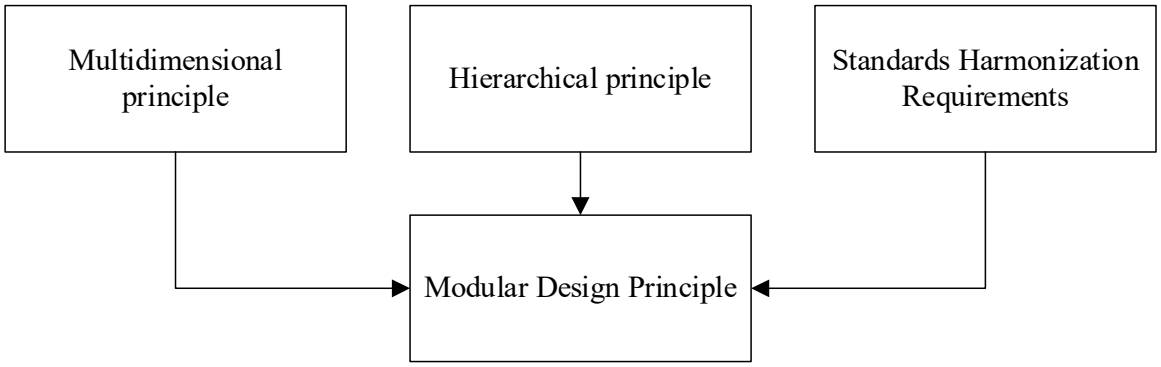

Figure 1. The principle of construction of Hull elements REA

The following works are performed during the module design:-Study of functional diagrams with the purpose of identification of the same subcircuits and unification of their structure within the specific product;

-selection of constructive;

-Design of the printed circuit board;

-selection of ways to protect the module from overheating and external influences.

At formation of a case REA it is necessary to consider those indicators which influence on manufacture of Hull elements.

On (Fig. 3) The stage of designing of a case element for the subsequent layer synthesis is presented.

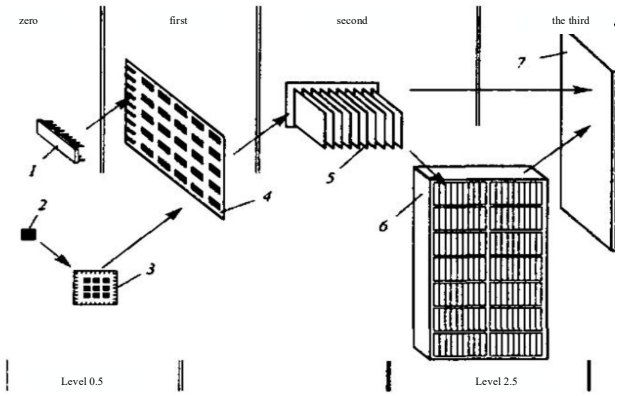

Figure 2-The constructive hierarchy and the REA of the modules the use of additive technologies allows to lay the qualitative characteristics in the design of the hull REA shielding of electromagnetic fields of electronic equipment nodes and their connections when using conductive material.

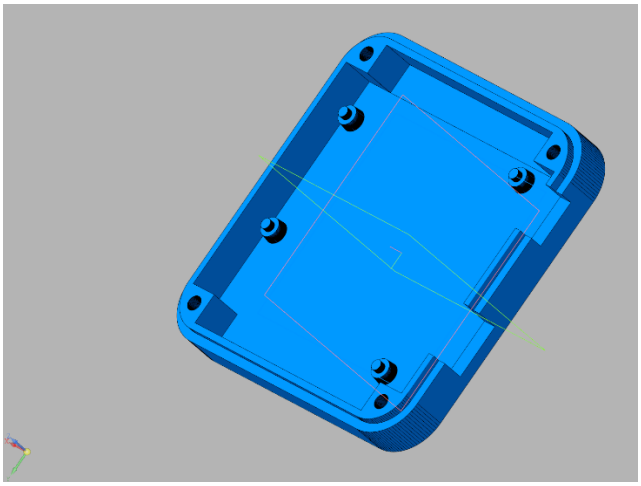

Figure 3-The stage of designing the computer model of the hull element

Ehe quality control of the process of layered synthesis of hull elements REA is based on the standards presented in (table 1).

Table 1

Quality parameters of the hull elements REA

Quality score	**Базовое значение**	**Нормируемый документ**
test for static bending: density:	117,6MPa	GOST 50598-93
density:	1,4r/cm3	GOST 9590-76
Impact viscosity by Sharpe:	8,8 kgs · cm/cm 2	GOST 50598-93
Absorption:	186mg	GOST 50598-93
Impact viscosity by Izod:	0,075J/mm	GOST 50598-93
Shear strength in the sheet plane:	250MPa	GOST 9590-76
Compression strength:	98MPa	GOST 9590-76

Compression strength: 98 MPA GOST 9590-76 Quantitative evaluation of plastic quality indicators

1. Static bending test: (SF) According to GOST 4648-71, when determining the bending voltage, it is necessary to use the following formula:

According to Gost 4648-71, when determining the bending voltage, you should use the following formula:

$$s_f = \frac{3F \cdot L_v}{2bh^2}$$

Where: F-load, n;-distance between supports, mm.-sample width, mm;-sample thickness, mm. = 204, 88h = 10mm

L_v= 60mm= 4mm

$$s_f = \frac{3 \cdot 204{,}88 \cdot 60}{2 \cdot 10 \cdot 16} = 115{,}245$$

To manage and improve the process of production of REA elements with the use of additive technologies, the chart "Pareto spreadsheet" using statistical data (table 2) and having a view (Fig. 3) is built.

Table 2

Non-conformity of additive production by layered fusion method

№	Non-compliant type
1	no extrusion at the beginning of printing
2	Распечатка не прилипает к платформе
3	Insufficient extrusion
4	Excessive extrusion
5	Cracks on the top layer
6	Hair or Web
7	Overheating
8	Layer offset or no alignment
9	Layers are separated and splited
10	Filtec Stachivaetsja
11	Clogged extruder
12	Extrusion interrupted
13	Poor filling
14	Accumulate and pimples
15	Gaps between filling and contour
16	Bend or jagged angles and edges
17	Scratches on the top plane
18	Gaps between layer angles
19	Lines on the sides of the printout
20	Vibration and "excitement"
21	Cracks between thin walls
22	Small parts do not missing
23	Uneven extrusion

To control and improve the process of production of the hull elements of REA with the use of additive technologies the chart "Pareto Spreadsheet", which has a kind (fig. 3) is constructed.

On the basis of analysis the corrective action on change of temperature mode is developed. After the introduction of the corrective action, a stable process has been set up in the middle of the tolerance field (Fig. 3.16 b), with the level of marriage 0005%. The reduction of the defect level by 60% (CP = 2.241 and IBS = 1.661) has been achieved. To prevent the TP from being re-rejected from the managed state, the snap-in is periodically checked. The result of the system operation is to reduce the defect level to 0.03% on average.

The analysis of product defects based on IPMS technology is necessary for the developed method and algorithm which have been applied for additive production. At first, the defects that lead to the greatest losses were revealed. For automation and formalization of the process of production of hull elements of REA using additive technologies, the chart "Pareto spreadsheet" was built, using statistics for 2017 according to the results of conducted Experiments in the "Laboratory of additive technologies".

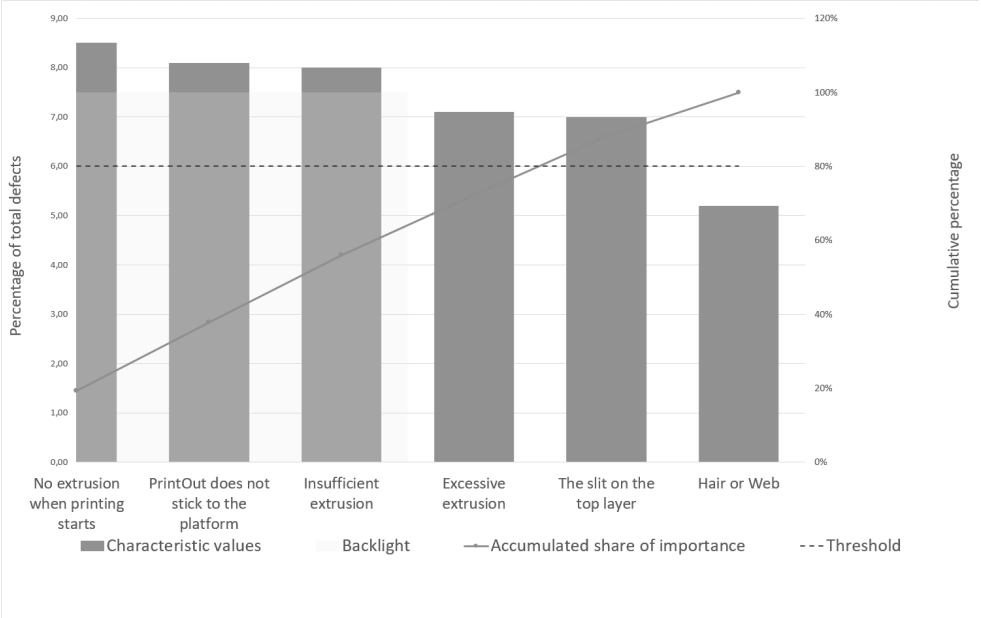

Figure 3-Distribution of types of defects in the process of printing the Lorenz curve in the diagram allowed to distinguish the most important defects from the general mass, the elimination of which contributes to a significant decrease in the level of marriage.

According to the results of the Pareto chart, the defects constituting the main share of the inadequate products are as follows:

- No extrusion at the beginning of printing.
- The printout does not stick to the platform.
- Violation of the temperature mode of the part printing.

The analysis of data on defects and reasons of their occurrence has shown, that the most part of inadequate production of 41 products because of problems connected with extrusion of polymers because of deviation from manufacturing technology, among which non-observance Temperature modes is highlighted in a special graph for a visual representation of the prevalence of this factor.

Quality management of the process of layered synthesis of hull elements of REA will improve the quality of manufactured products and reduce the costs of correcting inconsistencies in additive production.

References:

1. Разработка методов повышения качества аддитивного производства конструктивных элементов РЭА Смирнов А.О., Чабаненко А.В. Вопросы радиоэлектроники. 2018. № 1. С. 118-122.
2. ГОСТ Р 50779.11-2000 (ИСО 3534.2-93) Статистические методы. Статистическое управление качеством. Термины и определения.
3. Совершенствование производственных процессов в наукоемком производстве корпусов РЭА Чабаненко А.В., Семенова Е.Г. В сборнике: МОДЕЛИРОВАНИЕ И СИТУАЦИОННОЕ УПРАВЛЕНИЕ КАЧЕСТВОМ СЛОЖНЫХ СИСТЕМ Санкт-Петербург, 2017. С. 130-133.

AUTOMATION OF THE DECISION-MAKING PROCESS FOR ASSESSING PASSENGER TRAFFIC BASED ON SIMULATION AND EFFICIENCY OF TRANSPORT NODES

Dobrovolskaya Angelina

Saint-Petersburg State University of Aerospace Instrumentation,
Saint-Petersburg, Russia
E-mail: angd999@gmail.com

Abstract

Pulkovo airport every year increases the volume of traffic, and now by the number of served passengers per year it is the largest international airport in Russia after capital's airports[1]. Recently, there was a topical question: is there a need to build new metro station near the airport? [2] Firstly, it is necessary to evaluate the economic relevance of such investments and the prospects of its future development in the city infrastructure, as well as the efficiency of passenger flow distribution.

It should be noted that the transport availability issue of St. Petersburg airport is not new, but has a great importance. Now it is possible to get to the airport by shuttle from the metro station «Moskovskaya», but is this enough? Pulkovo - international airport, where passenger flow growing from year to year, that's why it is necessary to provide transport that allows passengers to save time and money. With the raising number of passengers, there is also a need to control passenger traffic, so the number of airport employees will increase. Although now the airport is a complex of organizations and almost 4,000 employees not all of which are get by their own transport.

From the transport development point of view, the airport may have several ways. The first way - airport modernization into a transport hub. That mean the creation of a modern interchange hub that integrates air transport with other kinds of transport. This complex can provide not only high-speed non-stop transportation of passengers to the necessary part of the city, but also connection with the nearest significant objects. Such a modern mode of transport can be a monorail following to the «Baltiyskiy» railway station or the high-speed tram «Chizhik» [3].

Figure 1. tram «Chizhik»

The second way - development of existing land transport. Now two buses follow to the airport: bus № 39 and duplicate express-route № 39E, which goes without stops from the metro station «Moskovskaya». The route operates a certain number of buses and there is a dedicated lane for them, but it does not always help to deliver passengers to the airport quickly. Passing through «Pulkovskoye» highway at certain times of the day is very difficult, which can lead to a delay of passengers on the road and late for flights. Most of the time the bus is full of passengers and the fastest transport with time spent only on the road to airport becomes unprofitable for some passengers, therefore can lead to loss of profit. It is absolutely necessary to value the need to increase the number of buses running on this route. On the one hand it will help to relieve passenger flows, and on the other hand it will not affect the time of passengers road. Maybe now the optimal number of buses with such passenger flow.

The third way – creation of a metro station in the walking distance of the airport. In other case it will be necessary to introduce a new connecting transport which will increase the cost of the project. Metro is a transport with high level reliability and since it is an underground railway allows to unload the land city traffic. If there is a metro station within walking distance from Pulkovo airport, passengers will be able to count their time, because the train runs every 3-5 minutes with rare delays for some reasons. Unwanted time loss during the stay at the airport is minimized, especially with possible option of electronic check-in for the flight. The simplicity and accessibility of this transport allows passengers to travel without unnecessary waste, so the number of trips will only grow. As well as foreign and Russian tourists will be able to reach the city without any problems. A schematic outline of the various options is shown in Fig. 2.

Figure 2. Planned ways of development routes

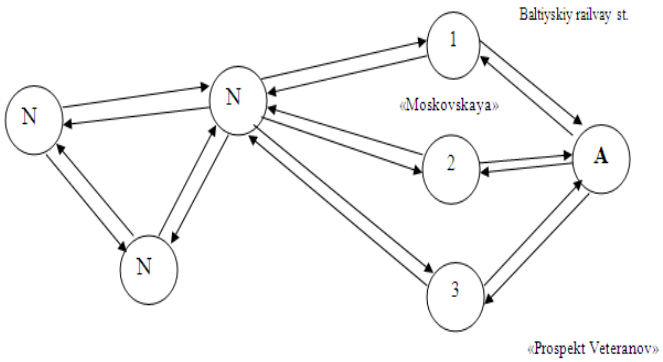

Figure 3 Scheme of distribution of passenger flows

To solve the problem of value the need to introduce a new transport line can be using different methods of forecasting the distribution of passenger flow. To calculate the efficiency of metro stations location the most widespread methods of «Correspondence matrices»[4].

The model of calculation of correspondence matrices is based on the analysis of information about the movement of passengers around the city. The micro-level of the metropolis is separated into conditional areas which the passenger moves between and base on these data it is possible to determine the intensity of movement. When building a model determined the price of the way which includes the criteria by which the passenger chooses alternative ways of travel. These criteria include:

- Travel time;
- Additional delays along the way;
- Cash costs.

Since the main factor in passengers' choice of alternative travel routes is time, all other factors are presented in minutes and added to the total price of the way:

Table 1

Matrix of passenger airport transport

	Station 1	Station 2	Station N	Airport
Station 1	0	t_{12}	t_{1N}	t_{1a}
Station 2	t_{21}	0	t_{2N}	t_{2a}
Station N	t_{N1}	t_{N2}	0	t_{Na}
Airport	t_{a1}	t_{a2}	t_{aN}	0

In this table, stations 1-N - various metro stations, between which the passenger flow is moving, t - movement time.

The scheme of distribution of alternative ways of passengers can be represented in the form of some points of movement of passengers around the city N, alternative routes of departure from the Baltiyskiy railway station, «Moskovskaya» metro station and «Prospekt Veteranov» metro station under the corresponding numbers in the figure(Fig. 3) 1, 2 and 3:

To take information about distribution of passenger flow used statistical data on the work of the metro[5]. The lobby of the station «Moskovskaya» has conceded an average of 82000 passengers per day. If assume that the majority of passengers depart from the «Moskovskaya» metro station, then is possible to calculate average number of passengers using online scoreboard Pulkovo data about one day flights.

$$\sum_{i=1}^{n} N_i * W_i = V_a - \Theta; \qquad (1)$$

where N – the number of flights; W – the capacity of the airplane; Θ – some casual error in the passengers getting on private transport.

Table 2

Calculation the number of passengers depending on the capacity of the airplane

airbus	**crj**	**e190**	**e175**	**b739**	
200	50	114	88	183	
96	8	2	1	1	
19200	400	228	88	183	
atr72	**b735**	**dh8d**	**b735h**	**b777**	**Σ**
74	118	78	215	300	
5	9	1	11	1	
370	1062	78	2365	300	24778

As a result of calculations the approximate passenger traffic of the airport was 1/3 of the total number of passengers, if you neglect some casual error Θ:

$$k = \frac{V_a}{V_m} = \frac{24778}{82000} \cong \frac{1}{3}; \qquad (2)$$

For modeling real passenger flow can be used discrete-event simulation which considers the basic sequence of events of the system; system dynamics, which provides a comparison of the causes of changes in certain factors and agent-based modeling, which allows us to consider the processes as individual

system. All of these techniques are implemented in the simulation software «Anylogic».

The real route of bus No. 39 and possible routes of monorail and subway lines were taken as a basis of modeling. The results are shown in picture 4:

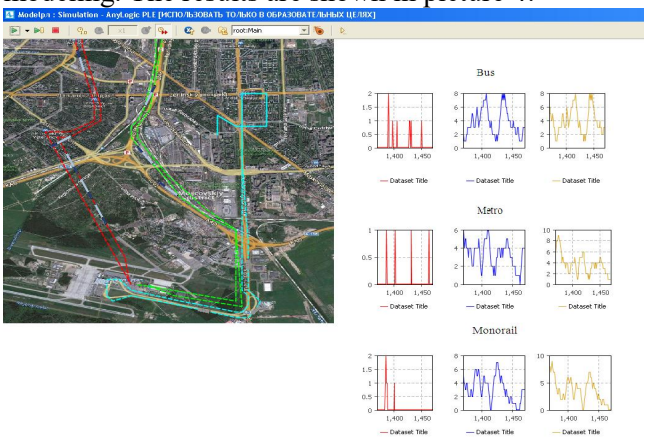

Figure 4 Modeling of passenger traffic in "AnyLogic"

Conclusion

This article discussed ways of automation the evaluation of the distribution of passenger flows. Using the creation of a mathematical model and imitation modeling it is possible to visually calculate the distribution of passengers on certain routes, in this case, on alternative routes to Pulkovo airport. It can be concluded that the introduction of additional transport to the airport absolutely necessary for our city. St. Petersburg is a significant tourist destination, which means that the passenger flow increases every year. The airport should be a modern interchange hub, which is accessible to all passengers and allows you to change transport. The development of existing land transport is not the best way, as urban road traffic is difficult at different times. Development is possible only with an increase in the number of buses running on the route, but this will not help to reduce the time of passengers. Construction of a monorail or high-speed tram is a great modern way to relieve traffic and simplify access to the airport, but the construction of roads and additional infrastructure requires large investments from the city budget. First of all, subway is a very reliable mode of transport, so it will allow each passenger to save time and money. So the metro line can be the best way for the development of the airport as a modern interchange hub, as well as the development of our city as a metropolis.

List of used literature:

1. Pulkovo airport Saint Petersburg [Electronic resource] https://www.pulkovoairport.ru/about/ (23.02.2018);
2. The St. Petersburg diary. The new station in Pulkovo and in the South-West will appreciate the experts [Electronic resource] – https://www.spbdnevnik.ru/news/2018-01-12/novoey-metro-v-pulkovo-i-na-yugo-zapade-otsenyat-eksperty/ (23.02.2018);
3. Tram "Chizhik" [Electronic resource] – http://chizhik-lrt.ru/ (23.02.2018);
4. Majorov N. N. Modeling of transport processes / N. N. Majorov, V. A. Fetisov. SPb.: Publishing house of SUAI, 2011. - 165 p.;
5. Statistics. Passenger traffic in the subway [Electronic resource] – http://www.metro-spb.ru/statisticheskie-dannye.htm (23.02.2018);
6. Fetisov V. A., Majorov N. N. Practical tasks in simulation of transport systems: proc. benefit. – SPb.: SUAI, 2012. – 185 p.

DETERMINATION OF THE SAFE ROUTE FOR SHIP DYNAMICS WITH THE USE OF ELECTRONIC CHART DISPLAY AND INFORMATION SYSTEM

Liubov Efimova

Saint-Petersburg State University of Aerospace Instrumentation,
Saint-Petersburg, Russia
E-mail: orlik96@yandex.ru

Abstract
The article describes the application of ECDIS in modern navigation and the calculation of the safe movement of the vessel according to its dimensions.
Keywords: navigation, electronic charts, course and speed vector, waypoints.
Because of the active exploration of Arctic, the problem of precise navigation is becoming more urgent.

Planning the route and mapping the coordinates on the navigational chart even today are carried out by boat masters in some cases manually, and the diagnosis of the safe vessel's movement is made visually.

The use of ECDIS (electronic chart display and information system) allows to increase the level of automation and create integrated systems for monitoring the location of the vessel. Electronic chart has accuracy and reliability in solving problems of navigation and preventing collisions of vessels due to the unceasing collection and processing information and the elimination of the subjective errors.

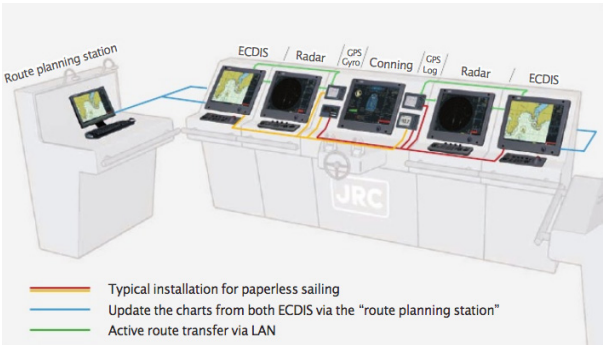

Figure 1. Example of ECDIS placement in the wheelhouse

On the display screen in dynamics and in the background of the chart can be seen at the same time:

– preliminary route;
– current vessel location;
– the track line;
– navigational waypoints and hazards;
– additional information.

In August 2017 ECDIS equipment was brought into line with the new IEC and IHO standards. Changes in standards consist mainly of new operational requirements and test methods, improvement of digital interface and data protection schemes etc.

Navigation safety is supported by complex of organizational measures undertaken on the ship and in the navigation and hydrographic support system.

On the ship navigation safety is ensured by the high organization of the navigational service and the maintenance of regulated factors affecting the safety of navigation, within the limits that guarantee the exclusion of navigation emergency cases with a given probability.

Controlled or regulated quantities of navigation, which numerical value affects the navigational safety, are called the navigation safety parameters.

These include:

– course and speed of the vessel;
– the shortest distance to the nearest navigational danger or to a colliding ship;
– deviation of the ship from the axis of the fairway (lane/sea channel);
– angles of the ship's demolition by wind and stream, etc.

Figure 2. Example of use of the electronic navigation chart

Electronic navigation charts are divided into raster and vector charts.

Raster charts are obtained by scanning paper maps with subsequent processing (adding projection, data, etc.).

Vector maps are also obtained by scanning paper maps, but with additional vectorization, i.e. with the translation of all objects into a digital code.

The main functionality of ECDIS:

– automatic replacement and loading of electronic charts;

– automatic adjustment;
– automatic change of scale;
– route planning;
– mapping vessel's coordinates;
– display of the vessel's motion vectors relative to the ground and water;
– automatic assessment of navigational safety;
– automatic maintenance of the ship's log;
– obtaining information on ports, tides, streams, etc.

The values of the parameters of navigation safety, under which the given probability of safe navigation is provided, are called admissible parameters of navigation safety.

When navigating in the recommended route along the high seas, a moderate probability of the ship out of range is assigned

(P 0,95 ... 0,99).

In many cases, the fairways and sea channels have a width commensurate with the dimensions of the ship.

The width of the safe lane of the vessel consists of two components — the geometric width of the vessel and the maneuvering strip:

$$B_{ПП} = B_Г + 2B_M, \quad (1)$$

$$B_Г = B + L\sin(C_P + \Delta C) + B\cos(c_p + \Delta C), \quad (2)$$

$$B_M = M_1 + V(t_И + t_З)\frac{\Delta C}{57,3} + \frac{V(\Delta C)^2}{57,3\omega}, \quad (3)$$

where $B_{ПП}$ — width of safe track, m; $B_Г$ — geometric width of the vessel, m; B_M — maneuvering strip, m; L, B — length and breadth of the vessel, m; ΔC — possible error in determining the drift angle, deg.; ω — angular speed of the vessel's turn during course correction, deg/min; M_1 — the apparent displacement of the vessel from the line of the given path (the limiting error in determining the position of the vessel relative to the channel axis), m; $t_И$ — discreteness of navigation definitions, sec; $t_З$ — time of delay of information from the moment of production of observations to the moment of rudder shift, sec; C_P — calculated value of the total drift due to wind and stream, deg.

$$C_P = \alpha_P + \beta_P, \quad (4)$$

where α_P, β_P — calculated value of the angle of wind and stream, deg.

The estimated margin for the width of the channel from each side:

$$H = \frac{B_{ФВК} - B_{ПЛ}}{2}, \quad (5)$$

where H — calculated safe margin of the width from each side, m; $B_{ФВК}$ — width of the channel, m.

ECDIS simplifies and automates cartographers work. On the display the operator immediately sees the possible routes of the vessel.

With the help of convenient alarm system, the operator can find out in advance about any danger.

Table 1

Speed of ECDIS information arrival during the navigation

Speed of the vessel	Information entry speed, seconds
Mooring, less than 3 knots	180
Mooring, more than 3 knots	10
0-14 knots	10
0-14 knots with course change	3,33
14-23 knots	6
14-23 knots with course change	2
More than 23 knots	2
More than 23 knots with course change	2

In addition to the alarms presented on the chart, it is possible to create one's own list by marking an additional safety contour and adding new waypoints.

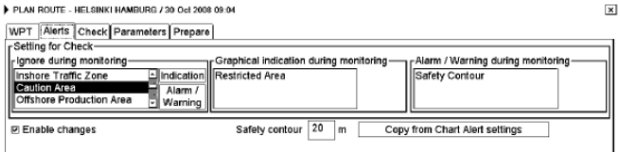

Figure 3. Choosing a caution area

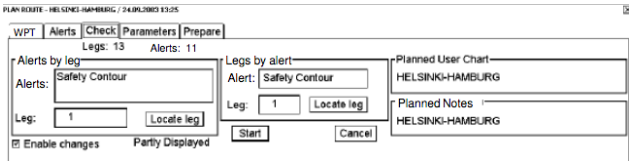

Figure 4. Choosing a safety contour

The operator adjusts the intended direction of the vessel's movement, and the system notifies him of each approaching waypoint.

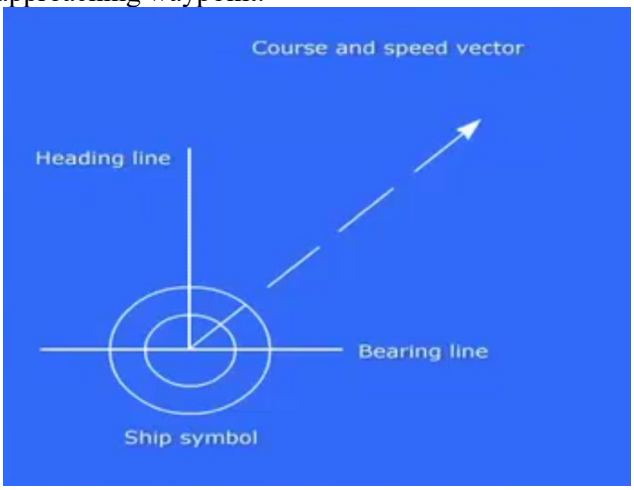

Figure 5. Ship symbol on ECDIS

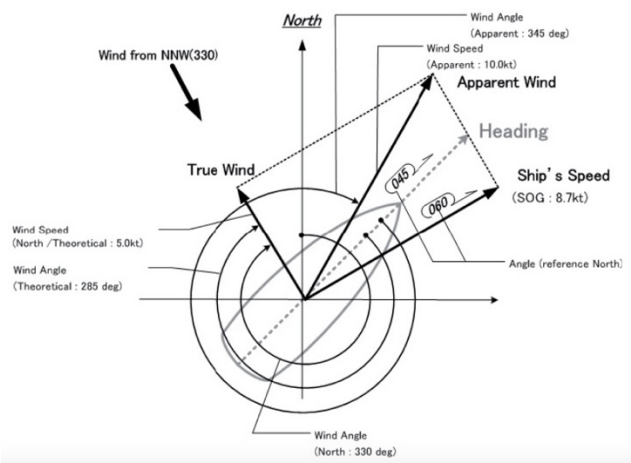

Figure 6. Schematic ship symbol, wind and speed direction

This is the standard ship symbol used on ECDIS systems. The direction of the course and speed vector is shown on figures 5, 6 as well.

The length of the vector is proportional to the speed of the ship. Each line segment represents one minute.

Own ship is by default located in the center of the display. The operator can change this position. As default the chart on the screen is oriented north up.

The navigator may find course and distance from the ship to any point in the chart or between any two points in the chart.

The navigator may display all available routs on the screen and select a suitable route for the voyage.

All data about waypoints is presented in a waypoint list. The operator can add new waypoints while sailing.

Figure 7. Adding new waypoints

When an offtrack limit is defined for the current route, an alarm will be given to the navigator whenever the ship's position is outside this limit.

Conclusion:

Being improved in 2017, the electronic navigation system greatly improves the accuracy of planning the route of the vessel, and also at the expense of a high level of automation this system solves complex shipping problems and improves the quality of navigation on the water.

References

1. Analysis of the technical level of the production capacity of the enterprise (Article) QUESTIONS OF RADIO ELECTRONICS Publishing House: Central Research Institute of Economics, Control Systems and Information Electronics (Moscow) ISSN: 2218-5453 Questions of radio electronics., 2017. № 5. P. 58-60.

2. IEC 61174 Edition 4. Performance standards for ECDIS, test methods and required test results.

3. GOST R IEC 61174-2009 Marine navigation equipment and radio communications. Electronic-cartographic navigation information system (ECDIS). Operational and technical requirements, methods and required test results.

4. Identification of key indicators of the quality of the technological process for the production of the REA hull based on FDM (Article) RADIO INDUSTRY Publishing House: Central Research Institute of Economics, Control Systems and Information Electronics (Moscow) ISSN: 2218-5453 Questions of radio electronics., 2017. № 4. P. 53-59, 53-59.

5. The electronic chart display and information system (ECDIS). Adam Weintrit, 2009.

TECHNIQUES OF IMAGE TO TEXT TRANSFORMATIONS

Emelyanov Georgij

Saint-Petersburg State University of Aerospace Instrumentation,
Saint-Petersburg, Russia
E-mail: porox9696@mail.ru

Abstract
This article explores different techniques that allow to connect the domain of images and the domain of natural language captions, enabling translation between elements of the two domains.
Keywords: images and text correlation, image to text transformation, natural language**,** likelihoods of data**,** nearest-neighbor, kernel canonical correlation analysis.

INTRODUCTION

Humans find it easy to accomplish a wide variety of tasks that involve complex visual recognition and scene understanding, tasks that involve communication in natural language and tasks that combine translation between the two modalities. For instance, a quick glance at an image is sufficient for a human to point out and describe an immense amount of details about the visual scene. Using the example in Figure 1, we can look at the image and immediately point out and describe the “red car Tesla”, the “undulating ground”, the “the car Tesla is riding on roadway”, “road marking double white lines”.

.

However, this task is more difficult for computer. In a computer, this image is represented as one large array of numbers indicating the brightness at any position. An ordinary image might have a few millions of these pixels and a computer must transform these patterns of brightness values into high-level, semantic concepts such as a “car”. A natural language description such as “the car Tesla is riding on roadway” will be represented in the computer as a sequence of integers indicating the index of each word in a vocabulary (e.g. “the car Tesla is riding on roadway” might be {823, 300, 800, 400, 731, 534, 780}).

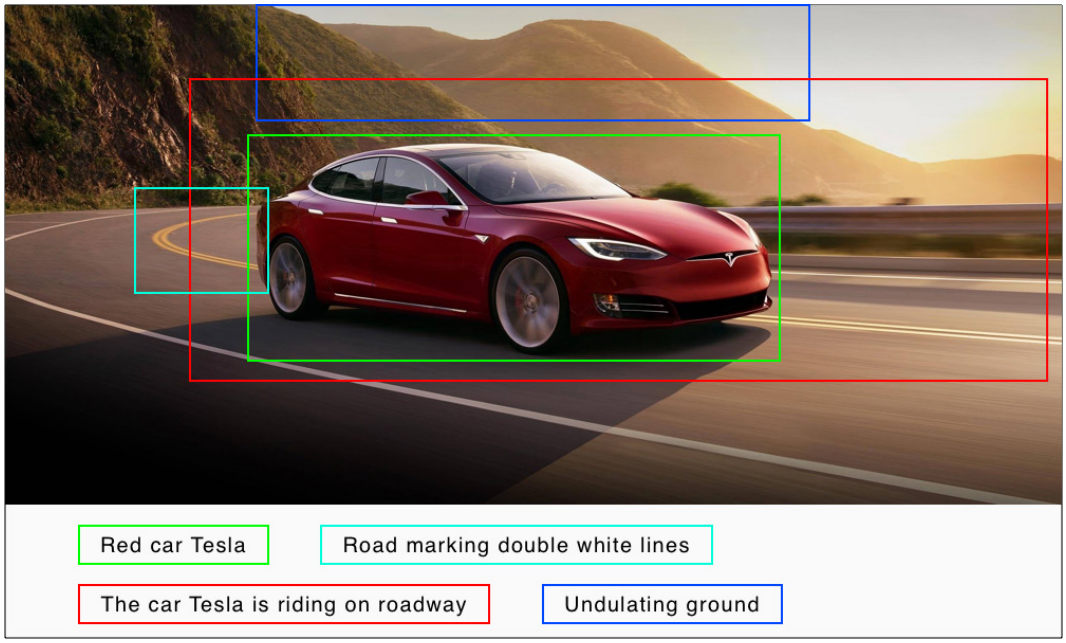

Figure 1. Example of parts descriptions of image.

Therefore, the very natural task of pointing out and naming different parts of an image in fact involves a complex pattern recognition process of identifying salient subsets of a grid of a few million brightness values and annotating them with sequences of integers. Moreover, the image captions often require detecting and describing complex high-level concepts that are not only visual but require di cult inferences.

For example, some images can be annotated by humans as “a traffic jam”, which requires the ability to detect multiple cars and analyze their quantity and spatial arrangements

EXISTING APPROACHES

ESTIMATING LIKELIHOODS OF DATA

Some of the earliest work focused on the problem of associating nouns with image region features based on statistical models that leverage co-occurrence statistics [1, 2, 3, 4].

To find detailed correlation between text and image, each portion of the image should be correlated to words instead of the whole image to words.

Assigning keywords to images portion by portion would be an ideal way to prepare learning data. However, with the exception of a very small vocabulary, such learning data cannot be found nor can be prepared. The more the size of the data increases, the more difficult assigning keywords to images portion by portion becomes. So, was developed another method to avoid this fundamental problem.

To avoid this problem, was proposed a simple method to correlate each portion of an image to keywords only using keywords for the whole image.

The procedure of the proposed method is as follows:

1) Many images with keywords are used for learning data;

2) Divide each image into parts and extract features from each part;

3) Each divided part inherits all words from its original image;

4) Make clusters from all divided images using vector quantization;

5) Accumulate the frequencies of words of all partial images in each cluster, and calculate the likelihood for every word;

6) For an unknown image, divide it into parts, extract their features, and find the nearest clusters for all divided parts. Combine the likelihoods of their clusters, and determine which words are most plausible.

The main point of this method is to reduce noise by accumulating similar partial patterns from many images with keywords. For example, suppose an image has two words, “sky” and “mountain”. After dividing the image, the part which has only the sky pattern also has “sky” and “mountain” due to the inheriting of all words. The word “mountain” is inappropriate for the part. However, if another image has two words “sky” and “river”, accumulating these to images, the sky pattern has two “sky”, one “mountain” and one “river”. In such way, can hope that the rate of inappropriate words ate gradually decreased by accumulating similar patterns.

Figure 2 shows the concept of estimating likelihoods of data.

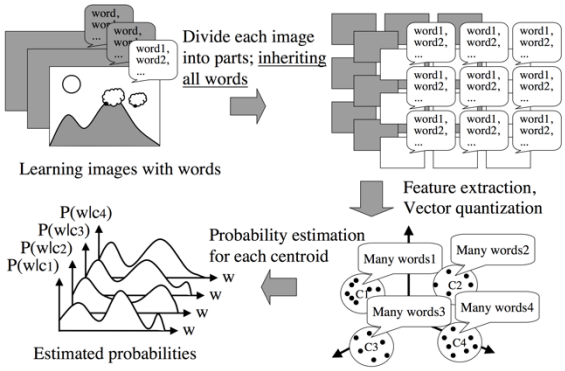

Figure 2. Concept of estimating likelihoods of data.

Some extensions of these approaches have been developed to model not just nouns but prepositions and comparative adjectives that may be used to express relationships between objects [5].

Figure 3 shows the model for image annotation with using nouns, prepositions and comparative adjectives.

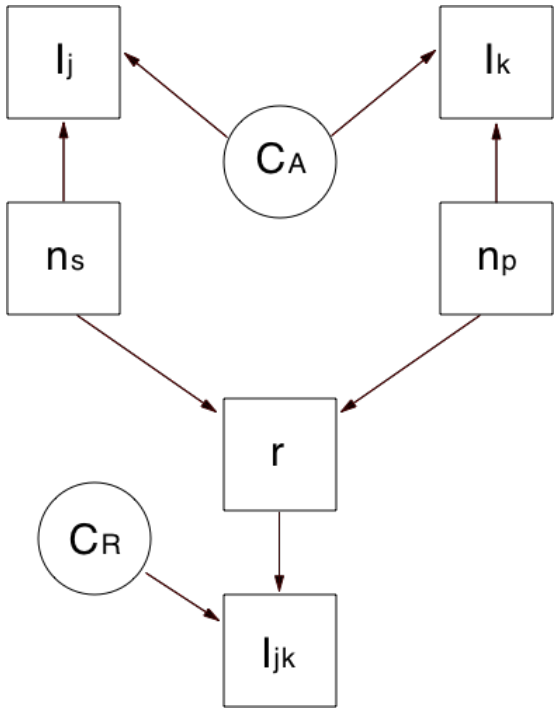

Figure 3. Graphical model with using nouns, prepositions and comparative adjectives.

Each image is represented with a set of image regions and each region is associated with an object which can be classified as belonging to a certain semantic object class. These semantic object classes are represented by nouns in the vocabulary. Assume two regions *j* and *k* are associated with objects

belonging to semantic object classes, n_s and n_p respectively. Each region is describing by a set of visual features I_j and I_k. The likelihood of image features I_j and I_k would depend on the nouns n_s and n_p and the parameters of the appearance models (C_A) of these nouns. These parameters encode visual appearance of the object classes. For every pair of image regions, there exist some relationships between them based on their locations and appearances. Relationship types are represented by a vocabulary of prepositions and comparative adjectives. Let r be a type of relationship (such as "above", "below") that holds between the objects associated with regions j and k. The nouns associated with the regions, n_s and n_p, provide priors on the types of relationships in which they might participate (for example, there is a high prior for the relationship "above" if the nouns are "sky" and "water", since in most images "sky" will occur above "water"). Every relationship is described by differential image features I_{jk}. The likelihood of the differential features depends on the type of relationship r and the parameters of relationship model C_R.

COMMON MEANING SPACE

Because this amount of data is not enough for the allocation useful information from image people have started to tackle more general language constructs and full sentences [6, 7, 8, 9].

Since image description requires the ability to associate images and sentences, all image description systems can be viewed in terms of an affinity function $f(i,s)$ which measures the degree of association between images and sentences. Given a candidate pool of sentences S_{cand}. Image annotation aims to find the sentence $s^* \in S_{cand}$ that maximizes function $f(i_q,s)$ for a query image $i_q \in I_{cand}$. In this case, $f(i,s)$ should be maximized for image-sentence pairs in which the sentence describes the image well:

$$s^* = \arg max_{s \in S_{cand}} f(i_q,s).$$

The challenge in defining f lies in the fact that images and sentences are drawn from two different spaces, I and S. There are two different kinds of defining f. One is based on Nearest-Neighbor search (NN), the other uses a technique called Kernel Canonical Correlation Analysis (KCCA).

OTHER APPROACHES

Since these ranking methods are constrained to annotating images from a finite collection of sentences, many approaches have been proposed to overcome this limitation and generate descriptions. The early work of developed an approach processed an image with a hierarchical parsing engine and then serialized to text via an intermediate process of part of speech production rules that get filled in based on the image content [10]. Unfortunately, their approach required extensive hand-coded details about the generative process. A similar approach in spirit was used earlier by Gupta who used AND-OR graphs to describe sport event videos [11]. The work of Li instead detected objects in the image and composed them into a sentence using pretrained n-grams, which act as large lookup tables of frequently-occurring short snippet phrases [12]. Kuznetsova generate captions by retrieving and then selectively combining pieces of human-written sentences [13]. Kulkarni use an approach where detections of objects, scenes, modifiers or spatial attributes are inserted into fixed sentence templates [14]. Finally, Yang et al. [15] and Mitchell et al. [16] similarly estimate likely words based on object detections and generate descriptions by growing syntactic trees with production rules.

CONCLUSION

There are a lot of different approaches that allow to transform images to texts. Some of them use the estimating likelihood of data, some use common meaning space, others try to generate full sequences. But all of them are constrained by vocabulary size and quality.

REFERENCES

[1] Yasuhide Mori. Image-to-word transformation based on dividing and vector quantizing images with words / Hironobu Takahashi, Ryuichi Oka // First International Workshop on Multimedia Intelligent Storage and Retrieval Management – 1999, pages 1–9. Citeseer,

[2] Kobus Barnard. Matching words and pictures / Pinar Duygulu, David Forsyth, Nando De Freitas, David M Blei, Michael I Jordan // The Journal of Machine Learning Research – 2003.

[3] Pinar Duygulu. Object recognition as machine translation: Learning a lexicon for a fixed image vocabulary / Kobus Barnard, Joao FG de Freitas, David A. Forsyth // In European conference on computer vision – 2002, pages 97–112. Springer.

[4] Yangqing Jia. Learning cross-modality similarity for multinomial data / Mathieu Salzmann, Trevor Darrell // In IEEE International Conference on Computer Vision – 2011.

[5] Abhinav Gupta. Beyond nouns: Exploiting prepositions and comparative adjectives for learning visual classifiers / Larry S Davis // In

European conference on computer vision – 2008. Pages 16–29. Springer.

[6] Ali Farhadi. Every picture tells a story: Generating sentences from images / Mohsen Hejrati, Mohammad Amin Sadeghi, Peter Young, Cyrus Rashtchian, Julia Hockenmaier, David Forsyth // In Proceedings of the European Conference on Computer Vision – 2010. Pages 15–29. Springer.

[7] Vicente Ordonez. Im2text: Describing images using 1 million captioned photographs / Girish Kulkarni, Tamara L Berg // Advances in Neural Information Processing Systems – 2011.

[8] Richard Socher. Connecting modalities: Semi-supervised segmentation and annotation of images using unaligned text corpora / Li Fei-Fei // In Proceedings of the IEEE conference on Computer Vision and Pattern Recognition – 2010.

[9] Micah Hodosh. Framing image description as a ranking task: data, models and evaluation metrics / Peter Young, Julia Hockenmaier // Journal of Artificial Intelligence Research – 2013.

[10] Benjamin Z Yao. I2t: Image parsing to text description / Xiong Yang, Liang Lin, Mun Wai Lee, Song-Chun Zhu –IEEE – 2010, 98(8):1485–1508.

[11] Abhinav Gupta. Understanding videos, constructing plots learning a visually grounded storyline model from annotated videos / Praveen Srinivasan, Jianbo Shi, Larry S Davis // Computer Vision and Pattern Recognition – 2009. Pages 2012–2019.

[12] Siming Li. Composing simple image descriptions using web-scale n-grams / Girish Kulkarni, Tamara L Berg, Alexander C Berg, Yejin Choi // Proceedings of the Fifteenth Conference on Computational Natural Language Learning – 2011. Pages 220–228.

[13] Polina Kuznetsova. Collective generation of natural image descriptions / Vicente Ordonez, Alexander C. Berg, Tamara L. Berg, Yejin Choi // In Association for Computational Linguistics – 2012.

[14] Girish Kulkarni. Baby talk: Understanding and generating simple image descriptions / Visruth Premraj, Sagnik Dhar, Siming Li, Yejin Choi, Alexander C Berg, Tamara L Berg // In Proceedings of the IEEE conference on Computer Vision and Pattern Recognition – 2011.

[15] Yezhou Yang. Corpus-guided sentence generation of natural images / Ching Lik Teo, Hal Daum´e III, and Yiannis Aloimonos // In Proceedings of the Conference on Empirical Methods in Natural Language Processing – 2011, Pages 444–454.

[16] Margaret Mitchell. Midge: Generating image descriptions from computer vision detections / Xufeng Han, Jesse Dodge, Alyssa Mensch, Amit Goyal, Alex Berg, Kota Yamaguchi, Tamara Berg, Karl Stratos Hal Daum´e III // Proceedings of the 13th Conference of the European Chapter of the Association for Computational Linguistics – 2012. Pages 747–756.

A SOLUTION FOR TRAFFIC MANAGEMENT IN SMART CITIES

Davide Fiorino, Angelo Marcianò

Computer Engineering and Networks Laboratory – Kore University of Enna – Italy
Email: {davide.fiorino, angelo.marciano}@unikorestudent.it

Abstract
This paper presents a solution for traffic management in various application fields of smart cities. In detail, the main aim is to achieve intelligent management of a road junction, parking, and lighting in the context of a smart city.

I. INTRODUCTION

A smart city is an urban area that uses different types of data gathered by sensors to supply information which is used to manage assets and resources efficiently [1]. The smart city concept integrates Information and Communication Technology (ICT), and various physical devices connected to the network (i.e., the Internet of Things or IoT) [2][3]. A smart city allows officials to interact directly with both community and infrastructure and to monitor what is happening and how the city is evolving.

A study by Juniper Research [4] found that measures to ease traffic will be crucial for smart cities. The key to these considerations will be the creation of a sustainable public transport network. Other measures will also be of primary importance, such as the two million intelligent parking spaces that will be installed globally by 2021. In addition, the research discovered that the smart street lighting market, which consists in LED units and micro-controlled sensors, will raise up a lot over the next five years, with over a half of the globally LED luminaires connected to the network.

A WSN (Wireless Sensor Network) could be a good starting point for a lot of IoT applications, and this is especially true for our case scenario. Furthermore, the possibility to provide connectivity to the Internet through a gateway is even more convenient to enable remote management of the smart devices and remote analysis of the environment.

The wireless protocols involved in a WSN may vary and strongly depend on the application requirements. In the scenario described in this paper, IEEE 802.11b (Wi-Fi) and IEEE 802.3 (Ethernet) standards are used. The first one to send data among the nodes of the network and the second one to establish a communication between a gateway of the WSN and an administration device. The usage of the IEEE 802.11b standard has been chosen for simulation purposes, but another wireless protocol, such as 802.11ah (HaLow) could be used as well.

II. RELATED WORKS

Traffic light control systems are widely used to monitor and control the flow of vehicles through the junction of many roads. As described in [5], the synchronization of multiple traffic light systems at adjacent intersections is a complicated problem given the various parameters involved. Conventional systems do not handle variable flows approaching the junctions. Besides, the mutual interference between adjacent traffic light systems, the disparity of cars flow with time, the accidents, the passage of emergency vehicles, and the pedestrian crossing are not implemented in the existing traffic system. As a consequence, it is possible to have traffic jams and congestions. The authors of [5] also designed a portable controller device to solve the problem of emergency vehicles stuck in the congested roads.

As pointed out in [6], it is useful to measure the traffic density by counting the number of vehicles in each lane and their weight, then park in automated parking or diverge them accordingly. It is also tricky for traffic police to monitor the whole scenario round the clock. So, the system proposed by the authors can be implemented on highways and city traffic.

In [7], it is analyzed the impact of smart traffic handling scheme in managing the radio resources among the different layers of a multimode and multiband radio network. The impact of two different traffic handling schemes on loading of GSM900/1800 layers along with Universal Mobile Telecommunications System (UMTS) 900/2100 layers was observed. Interference margin is introduced in the UMTS link budget as a system parameter that will account for systems degradation. One of the targets of this massive simulation campaign was to observe the impact of smart traffic handling scheme on interference margin.

Finally, a web-based application for vehicle drivers is proposed in [8]. The main aim is to derive the data from real-time traffic analysis to indicate the local traffic flow and to suggest the incoming vehicles

to make use of alternative routes to alleviate growth of the gridlock further.

III. THE PROPOSED APPROACH

We have chosen to implement our sistem with a star network topology with various modules that converge in a central controller that deals with the processing of data for the creation of traffic statistics. The external modules of the network take care of the management of a crossroad (with a traffic light system), a parking lot with slot control and the public lighting system of a long avenue. The transmission of data between the external modules and the hub takes place via Wi-Fi, while the internal communication in each module is wired and uses the Ethernet protocol. For the realization of this network, we have simulated several sensors to detect data, controllers, and gateways for routing, and, finally, actuators that have different functions (traffic light activation, luminary switch-on, and so on).

A first module coordinates vehicular traffic at an intersection via traffic lights. Specifically, we simulated a crossing of two orthogonal roads, with the possibility, in each lane, to continue straight or turn right. The traffic lights are not merely timed, but adjust according to the presence of vehicles, thanks to appropriate sensors.

The second module manages a controlled parking lot. Thanks to sensors, we can detect how many and which places are free and show it to the drivers on a display. The hourly car exit rate is also measured, which is used for forecasting traffic.

The third module manages the lighting of a road. It uses sensors to detect the presence of cars, as well as traffic statistics collected by the other two modules and processed by the central node. The lights will be turned off when not needed to reduce energy consumption, but always ensuring road safety.

The central node of the network consists of the module that generates the traffic forecast. In a real case, it would also be interesting to send these data on the Internet to allow users or other services to draw on them.

IV. SCENARIO

The proposed approaches have been implemented in Matlab/Simulink/TrueTime. The Crossroad module simulates the operation of a smart road junction. Inside it, we find four sensors able to detect the presence of vehicles in the four roads of the intersection. These sensors have been implemented with a Uniform Random Number block that outputs real numbers between 0 and 1. To have a Boolean output (i.e., 1: vehicle present - 0: vehicle absent), we have rounded the output value via the Matlab function block. By performing the simulation, we realized that, due to random sensors, we could verify the case in which a vehicle stopped at the traffic light disappeared. To solve this problem, we introduced an artifice, i.e., at the Matlab function blocks of the sensors, we also input the value of the respective traffic light, so that the sensors continue to give output 1 (vehicle present) if the traffic light is red. Undoubtedly, in a real context, it would not be necessary as it is rare for a vehicle to disappear from the sensor's range of action.

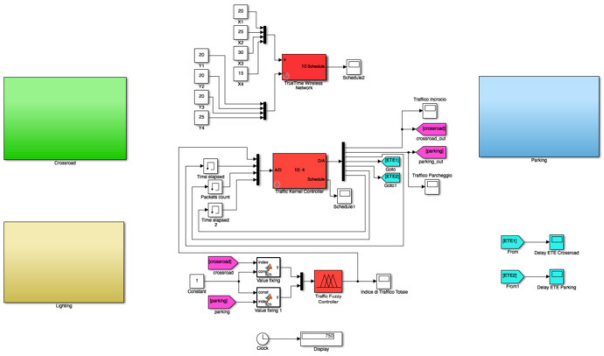

Figure 1: A schematic representation of the modules

Each sensor is connected to a TrueTime Kernel able to send the collected data to the central crossover kernel via the network. The traffic lights are implemented with TrueTime Kernel blocks connected to monitors (Scopes). The central kernel monitors the traffic lights (with MBSD approach) and calculates a traffic index for each time interval (in the 3 min simulation). Messages are forwarded through a kernel that acts as a gateway. For the calculation of this index, we use a Matlab Function block to which we input the data collected by the sensors and the maximum value of vehicles that are supposed to cross the intersection in the chosen time interval. The central kernel also takes care of sending the calculated index to the central node of the smart city via a wireless network.

In the Crossroad module, we chose to use three wired Ethernet networks: the first connects the sensors to the gateway; the second connects the gateway to the central kernel; the third connects the gateway to the traffic lights.

The Parking module simulates the operation of a smart parking space. Inside it, we have included three sensors that reveal the presence of vehicles in three parking spaces (slots). These sensors have been implemented with a Uniform Random Number block that outputs real numbers between 0 and 1. Presumably, in a real context, there will be many more slots. Each sensor is connected to a TrueTime Kernel able to send the data collected to the central parking kernel via the network. Outside the parking, there will be a monitor that will indicate the availability of seats. This monitor has been implemented with kernels and scopes. The central kernel is also responsible for calculating a traffic index for each time interval (in the 3min simulation). Messages are forwarded through a kernel that acts as a gateway. For the calculation of this

index, we use a Matlab Function block to which we input the data collected by the sensors and the maximum value of vehicles assumed to leave the parking space in the chosen time interval. The central kernel also takes care of sending the calculated index to the central node of the smart city via a wireless network. In the Parking module, we chose to use three wired Ethernet networks: the first connects the sensors to the gateway; the second connects the gateway to the central kernel; the third connects the gateway to the monitor's kernels.

The Lighting module simulates the functioning of the lighting system of an urban road. The system consists of 16 lamps divided into four sections of 4 consecutive. For each section, there is a sensor able to detect the presence of a vehicle within this sector. The lights are controlled sector by sector to give sufficient visibility to the vehicle in transit. Assuming that a vehicle is in the second section, we will turn on the previous section (I), the current section (II) and the next section (III). The sensors have been implemented with a Uniform Random Number block that outputs real numbers between 0 and 1. To have a Boolean output (i.e., 1: vehicle present - 0: vehicle absent), we have rounded the output value via the Matlab function block. Each sensor is connected to a TrueTime Kernel able to send the collected data to the central kernel of the lighting system via the network. For each sector, we have a TrueTime Kernel with four outputs corresponding to the four lights that it controls. The outputs can take Boolean values (i.e., 1: light on - 0: light off). The central kernel controls the lighting of the lights; it is based both on the data collected by the sensors and on the statistics produced by the central node and received via the wireless network. During the hours of intense traffic, a proactive approach will be adopted by switching the lights on regardless, while in the remaining time slot, they will turn on according to the presence of vehicles (reactive approach). Messages are forwarded through a kernel that acts as a gateway. In the Lighting module, we chose to use three wired networks: the first connects the sensors to the gateway; the second connects the gateway to the central kernel; the third connects the gateway to the lighting kernels.

The central node of the project consists of a TrueTime Kernel and a fuzzy logic controller. To calculate the traffic statistic, we chose to use a soft computing approach, i.e., a fuzzy controller. The central node communicates with the other three modules via a wireless network. The nodes of this network, in a real context, could be arranged at distances of the order of hundreds of meters or even of a few kilometers. Therefore, the transmission must take place at high power, which would not be a problem as the electricity grid powers the stations. The use of the star network topology was considered appropriate because, even in the event of failure of the wireless links or the central node, traffic in the smart city would be managed less optimally, but in any case, such as to guarantee correct viability.

The use of soft computing plays a central role in this project. The fuzzy logic controller is responsible for establishing the extent of traffic congestion. The total traffic index is calculated by five membership functions: very low, low, medium, high, very high. As inputs, we have two variables that are the hourly traffic indexes: one coming from the parking lot, which is based on the number of vehicles passing by, and one coming from the intersection, which is based on the number of vehicles leaving the parking lot. The indices are integer numbers from 1 to 10 (i.e., 1 little traffic, 10 much traffic). These values are sent to the fuzzy controller at the same time, once every hour. The controller will output a third hourly traffic index (integer from 1 to 10) which will take into account both the traffic in the crossroad and the parking traffic in an appropriate manner. In particular, it gives more weight to that recorded at the crossroads. The traffic statistics will be sent to the lighting system that will turn on the lights smartly (Figure 2).

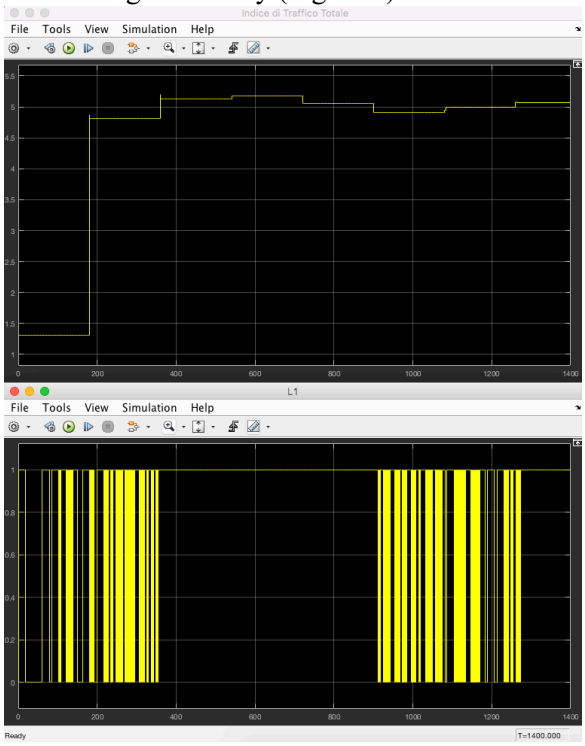

Figure 2: The traffic index and the state of a light (on-off). When the traffic index is above 5 the light is always on.

The model-based software design (MBSD) approach was used to manage the functioning of the traffic light system located at the center of a road junction. The controller of the traffic light system is configured in such a way as to allow vehicles to pass in only one direction and with a time limit. This controller receives the data from sensors that detect a car as input and drives the actuators that will change the color of the traffic light. The use of a finite-state

model for the management of a semaphore seemed perfect, as it has three states (green, yellow, red) and simple transitions. The finite-state diagram is shown in Figure 3.

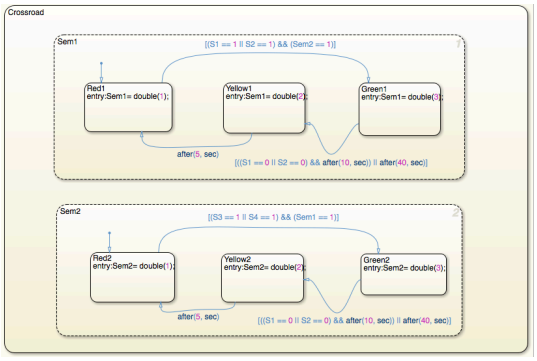

Figure 3: finite-state diagram for a semaphore

V. PERFORMANCE EVALUATION

In the context of the Crossroad and Parking modules, we chose to measure the data throughput sent by the controllers to their respective gateways. Given the slow rate of transmission, due to the nature of the context, we measured the *throughput* over a period of 180 sec. We have calculated it both as the number of packets sent in the unit of time and as the number of bits sent in the unit of time. Regarding the communication between the modules and the central node, being this wireless, we chose to monitor the *end-to-end delay* and the *reliability* (percentage of packets received compared to sent). To measure it correctly even with a non-zero error probability, we have implemented an acknowledgment mechanism (*ack*) to ensure receipt of the package containing the number of packets sent (Figure 4). The central node is the data processor for generating traffic hour statistics; this is not a real-time context so that even the presence of high delays (of the order of seconds) does not preclude the proper functioning of the system.

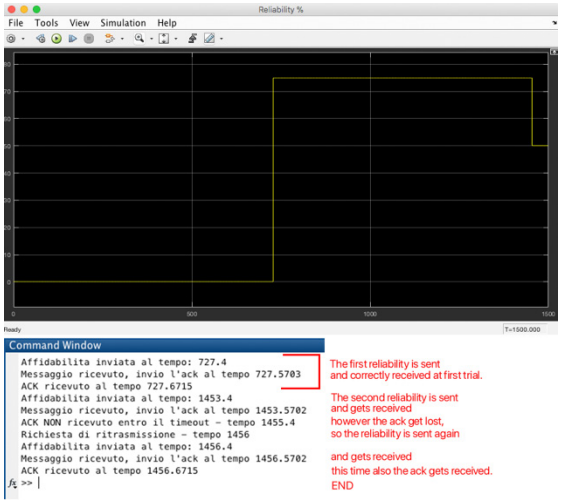

Figure 4: Example of the reliability computation

VI. CONCLUSIONS

The traffic management system proposed in this project offers the following advantages: 1) decrease of city traffic; 2) decrease of electricity consumption; 3) provide useful information to citizens. This system could be applied to a real context using many modules and dividing the city into zones. One could then calculate the traffic indices by zone and take the following actions only in that area. Finally, it could be possible to combine all traffic indexes and create a map of city traffic at various times. This map could be sent to smart cars that could recommend the most convenient route. Furthermore, by combining this system with others, such as the management of public transport, a significant improvement in mobility could be achieved. By adding sensors of environmental pollution, it could be feasible to study the correlation between traffic and pollution, as various factors vary (alternating plates, electric vehicles).

REFERENCES

[1] Matt Hamblen, Just what IS a smart city?, computerworld.com, Oct 1, 2015.

[2] Boyd Cohen, The 3 Generations Of Smart Cities, fastcompan.ycom, Oct 8, 2015

[3] Peris-Ortiz, Marta; Bennett, Dag R.; Yába, Diana Pérez-Bustamante (2016). Sustainable Smart Cities: Creating Spaces for Technological, Social and Business Development.

[4] Steffen Sorrel, Juniper Research, "SMART CITIES: Strategies & Forecasts in Energy, Transport & Lighting 2017-2022".

[5] Ghazal Bilal, Khatib Khaled, Chahine Khaled, Kherfan, Mohamad, "Smart traffic light control system", 140-145. 10.1109/EECEA.2016.7470780.

[6] Mohit Dev Srivastava, Prerna, Shubhendu Sachin, Sumedha Sharma, Utkarsh Tyagi. SMART TRAFFIC CONTROL SYSTEM USING PLC and SCADA. ISSN: 2319 - 8753.

[7] Muhammad Usman Sheikh, Department of Communication Engineering, "Assessment of smart traffic handling scheme in multimode multiband cellular network", Tampere University of Technology.

[8] Anurag Saikar, Mihir Parulekar, Aditya Badve, Sagar Thakkar, Aaradhana Deshmukh, "TrafficIntel Smart Traffic Management for Smart Cities".

MODELING OF DIGITAL METHODS OF SOUND PROCESSING IN THE MATHCAD ENVIRONMENT

Gerasimov Serafim, Vinogradov Alexander

Saint-Petersburg State University of Aerospace Instrumentation
Saint-Petersburg, Russia
E-mail: gall2000av@gmail.com, gerasimov310796@gmail.com

Abstract
The article considers the implementation of mathematical models of algorithms for processing audio signals in the Mathcad environment. As the graphic models are the structural diagrams of devices for implementing different sound effects.

INTRODUCTION

Mathematical modeling plays a significant role in the development of digital processing of sound signals.

Currently, there are a number of ready-made software products that allow implementing some or other algorithms of sound processing. This definitely is the simplest way. However, it does not allow us to disclose the mathematical essence of the algorithms underlying the signal conversion. Therefore, the idea of implementing mathematical models of digital sound processing seems to be the most attractive by instruments of computer mathematics and modeling. Such features can be provided, in particular, by the Mathcad package [2].

IMPLEMENTATION OF EFFECTS

The choice of instruments of implementing mathematical models of algorithms for processing audio signals is justified, first, by the clarity and ease of working with sound samples. Thus, load a sound signal in * .wav format, the READWAV operator is used in the matrix, and WRITEWAV is used to write the processing results [2]. The work uses single-channel audio files (mono). However, the results obtained can be extended to stereo tracks. Using the Mathcad environment also allows displaying the results of processing on the screen in the form of graphs or diagrams. This makes it possible to compare sound files with images corresponding to them. In particular, a simple one-tone sound in the time domain is a sinusoidal oscillation with a frequency corresponding to the sound height. The higher the oscillation frequency, the higher the corresponding sound.

In Fig. 1 shows a fragment of the program, which allows to illustrate how "a sine wave" sounds.

A sufficiently large number of algorithms for processing audio signals is associated with the concept of "modulation". In particular, the modulation effect can be used by modeling in the characteristic sound of individual musical instruments. The use of amplitude modulation leads to the appearance of the "tremolo" effect, which is characteristic of such an instrument as the electronic organ.

$j := 0..199999$

$S1_j := \cos(0.03 \cdot j) \cdot (2 \times 10^4)$ $S2_j := \cos(0.05 \cdot j) \cdot (2 \times 10^4)$

$WRITEWAV("C:\1\s1.wav", 4 \times 10^4, 16) := S1$

$WRITEWAV("C:\1\s2.wav", 4 \times 10^4, 16) := S2$

$S3 := \frac{S1 + S2}{2}$

$WRITEWAV("C:\1\s1-2.wav", 4 \times 10^4, 16) := S3$

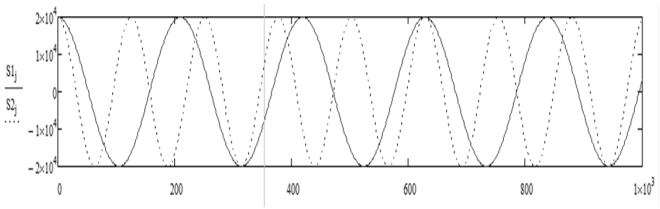

Figure 1. Sound sine wave

Below (in Fig. 2) is a block diagram of the device for implementing this effect and a mathematical description of the algorithm.

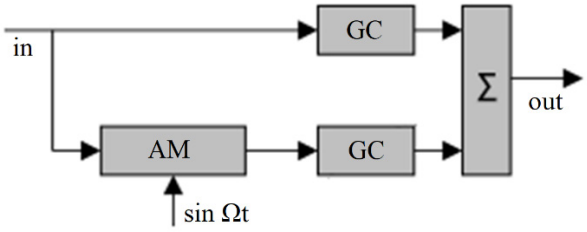

$$y(n) = \left[1 + m \cdot m(n)\right] \cdot x(n)]$$

Figure 2. Structural scheme for realizing the effect of "tremolo"

The program, which illustrates the simulation of the effect, is below in Fig. 3.

$j := 0 .. 199999$

$SM_j := \cos(0.03 \cdot j) \cdot (2 \times 10^4)(\cos(0.3 \cdot j))$

$SM1 := 0.05SM + S1$

$SA_j := (2 \times 10^4)(\cos(0.03 \cdot j))$

$WRITEWAV("C:\1\sm.wav", 4 \times 10^4, 16) := SM$

$WRITEWAV("C:\1\sm1.wav", 4 \times 10^4, 16) := SM1$

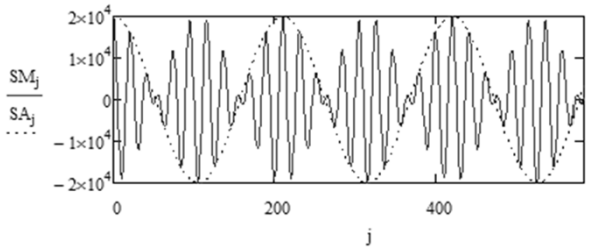

Figure 3. Modeling the effect of "tremolo"

Phase and frequency modulation is also often used to realize various sound effects. In particular, to create the timbre of the sound of the woodwinds (oboe), the "vibrato" effect based on the phase modulation effect is applied [1].

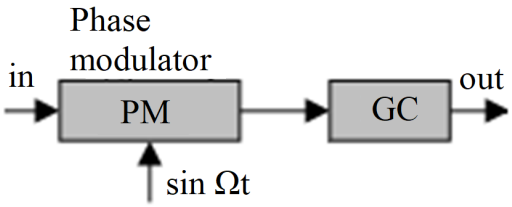

Figure 4. Structural diagram for realizing the effect of "vibrato"

In the discrete-time domain, the modulated oscillation is the expression:

$$x(n) = A_m \sin(2\pi F n + I \sin(2\pi F_{md} n))$$

The following figure can show an implementation of the effect in the Mathcad environment.

$SF_j := 0.3 \cos[0.3 \cdot j + 20 \cdot (\cos(0.03 \cdot j))] \cdot (2 \times 10^4)$

$WRITEWAV("C:\1\sf.wav", 4 \times 10^4, 16) := SF$

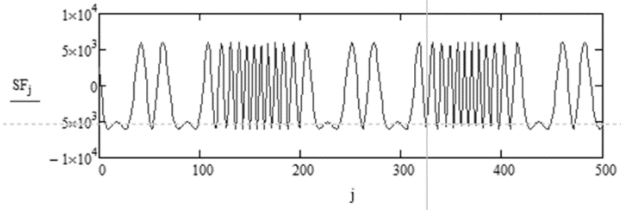

Figure 5. Modeling the "vibrato" effect

If we combine the amplitude and phase modulations together, we can obtain an effect close to the "wah-wah" effect.

$$SWOW_j := 0.3 \cos\left[0.3 \cdot \left(j - 150 \cdot \frac{j}{199999}\right) + 20 \cdot (\cos(0.03 \cdot j))\right] \cdot (2 \times 10^4)$$

$WRITEWAV("C:\1\sf1.wav", 4 \times 10^4, 16) := SWOW$

Figure 6. Modeling the "wah-wah" effect

In addition to the simple effects mentioned above, the effect of the "echo" effect is often applied to give a natural effect to the sound. To implement this effect, delay lines are usually used. The structure of the devices that realize this effect is shown in Fig. 7 [1].

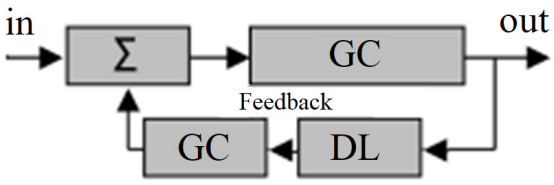

Figure 7. Structural scheme for implementing the effect of "echo"

The use of one or more delay lines in conjunction with the reverse links allows you to mix the original signal with its weakened and time-shifted copy, which creates the illusion of an echo. Feedback creates an infinite number of repetitions of sound, followed by an interval equal to the delay time. However, in reality, due to the sound attenuation effect, the number of repetitions perceived by ear is usually small. Therefore, when modeling the operation of such a device, for exemplification, you can limit yourself to three repetitions.

In Fig. 8 shows the software implementation of the "echo" effect in the Mathcad environment.

$$k := 0..199999$$

$$SEH_k := \begin{cases} S1_k & \text{if } k \le 20000 \\ \left[S1_k \cdot e^{-0.00005\cdot(k-20000)}\right] & \text{otherwise} \end{cases}$$

$$k := 0..199999$$

$$SEH1_k := \begin{cases} SEH_k & \text{if } k \le 50000 \\ SEH_{k-50000}\cdot 0.3 + SEH_k & \text{if } 50000 < k \le 100000 \\ \left(SEH_{k-100000}\cdot 0.1 + SEH_{k-50000}\cdot 0.3 + SEH_k\right) & \text{otherwise} \end{cases}$$

$$WRITEWAV\left("C:\1\seh1.wav", 4\times 10^4, 16\right) := SEH1$$

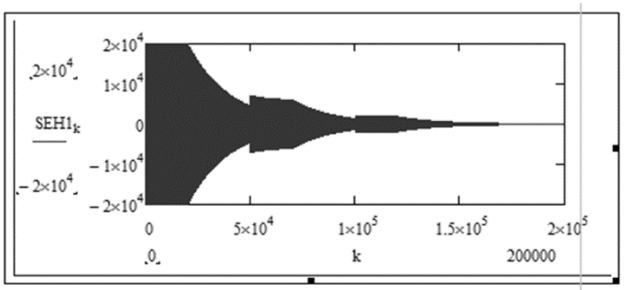

Figure 8. Modeling the "echo" effect

CONCLUSION

The possibility of signal processing in the MathCAD environment has great advantages over the available known methods. First, the most important is the ability to create any effect that can be mathematically described. Secondly, an important factor is that it is possible to adjust this or that effect to the smallest detail. When processing the sound signal, we, among other things, also get an opportunity to evaluate the received sound visually for the presence, for example, of distortions that could occur during recording. The only significant drawback is that the file being processed must have the extension ".wav", which at the moment severely limits its functionality, since this extension is not the most popular in the music environment (obviously worse, for example, to ".mp3"). Nevertheless, the program has a huge potential, and with the proper level of knowledge can be an indispensable assistant in the processing of audio signals.

REFERENCES

1. *Vologdin, E.I.* Methods and algorithms for processing audio signals / E.I. Vologdin St. Petersburg: CROWN, 2012. 96 p.
2. *Makarov, E.G.* Engineering calculations in Mathcad / E.G. Makarov St. Petersburg: Peter, 2015. 448 p.

INDUSTRIAL GREENHOUSE AUTOMATION: FROM SMART SYSTEMS IMPROVEMENT TO IOT

Marco Andrea Greco, Giuliano Torregrossa

Computer Engineering and Networks Laboratory – Kore University of Enna – Italy
Email: {marcoandrea.greco, giuliano.toregrossa}@unikorestudent.it

Abstract
This paper shows the development of an intelligent management system for an industrial greenhouse. Versatility is the primary goal of our project: managing some specific parameters our system can be adapted to the needs of any new or existing structure. In according to Internet of Things philosophy, internal microenviroinment management is performed by microsensors, which collect datas from the environment, by controllers, which analyse and create solutions, and by actuators, which drives connected devices like sprinklers or air conditioners. Our system is characterized by a smart and efficient use of resources and a good interoperability among devices, which work together and interchange informations, transforming raw datas into useful and functional informations, not only for management but also to forecast future costs and consumptions.
Keywords
Internet of Things, Wireless Sensor Network, Neural Network, ZigBee.

I. INTRODUCTION

A greenhouse is an artificial environment usually built for cultivating fruit and vegetables in places whose climate conditions would not allow to grow plants naturally. These structures protect cultivations from adverse weather conditions maintaining the same characteristics of the natural habitats required by plants and allowing the creation of artificial and more profitable seasons-related climate condition by managing several environmental factors such as air and soil humidity, temperature, exposure to light and wind speed. The increasing request for off-season products led to the more frequent use of new technologies.

The primary goal of this paper is to realize a complex system by which it would be possible to manage an industrial greenhouse by automatic monitoring of environmental conditions and by implementing devices in controlling internal greenhouse microclimate. These features would be helpful both in production maximization and in costs reduction, decreasing the human effort needed in traditional intensive agriculture.

The greenhouse concept implies the creation of an ideal environment to increase the number of different types of cultivated crops. Nevertheless, without proper control of atmospheric variables, adverse conditions may occur in the greenhouse. These variables are managed to start by their detection, using smart devices which allow the control of the heating and irrigation systems, and of the motorized mobile covers. The idea of a network made by communicating smart electromechanical systems is inspired by the SmartDust project developed in 2001 by Kristofer SJ Pister, at University of California, Berkeley. The concept of the mote, as it is often called in the literature, i.e., a sensor node of a wireless network which can manage several processes, gather sensor information and communicate with other connected nodes, is the theoretical base for this paper. A development that is not to be understood from the point of view of power, as would be expected from Moore's law. Energy saving has always been a significant feature of these units.

The proposed Smart System is composed of three macro-sections:

- Hardware components: Sensors, actuators, controllers, and networks;
- Software components: Applications in controllers which react to events and monitor costs;
- Simulation functions: Empirical physical-mathematical system which simulates reality.

II. RELATED WORKS

In the SmartDust project, Pister explains the project of a network made of a micrometrical electromechanical system capable of wireless communication for information exchange about temperature, humidity level, light exposition, and so on. [1] WSN is one of the most relevant of 21st-century technologies, especially considering the advantages on embedding costs and power consumption.[6]

Furthermore, our project tends to have more flexibility and adaptability to different kinds of input information. Costs reduction is guaranteed by the possibility of using different types of sensors; in this sense, the choice of using the ZigBee standard played a crucial role. Recently several different platforms are

working on increasing the flexibility of interconnected systems, trying to reach a new level and also preserving the capability of data injection from every kind of source, physical devices, human inputs, online data, and so on [7].

At the same time data gathering has been taken into account.[8] In this paper, both data collected by sensors and weather forecasts have been analyzed by a neural network concerning power consumption. Moreover, the use of smart devices in this field enables a reduction in resource needed [9]. It is clear, according to the cited literature, that utilizing the existing potential of both WSNs and IoT would allow researchers to offer key-findings to the agri-food industry, enabling the development of other systems similar to the one we projected and granting the chance of increasing efficiency in production and resource availability.

III. THE PROPOSED APPROACH

Choices about hardware components depended on the already available commercial devices which would guarantee reliability. Sensors belong to a Wireless Sensor Network (WSN) which ensure mobility. Microclimate corrections are made by the actuators that were led by control devices connected to each other by a wired network.

The connection between the two networks, the WSN and the wired network, which allows the communication between sensors, control devices, and actuators, is managed by a gateway, which is the center of the network (as shown in figure 1). In this way, parameters can be monitored by sensors and then processed by control devices responsible for managing actuators included in the wired network.

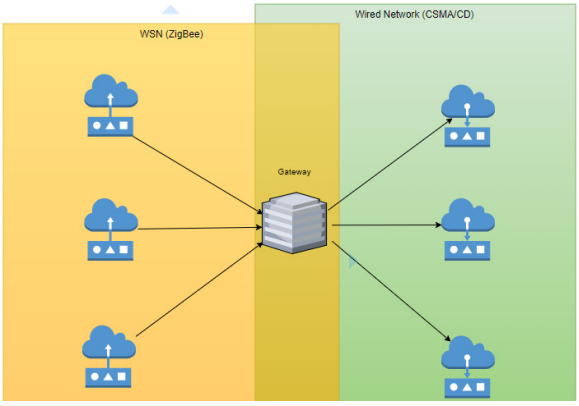

Figure 1: WSN and wired network.

WSN nodes use a technology known as Zigbee, an IEEE 802.15.4-based specification, to ensure communication. This standard specifies the application profiles based on the use, for the wireless personal area network (WPAN), of small low-consumption antennas. These WSN nodes send detected parameters to the gateway, which allows the communication with control devices connected to the wired network. The wired network, which connects actuators, was implemented with the CSMA/CD protocol (Carrier Sense Multiple Access with Collision Detection).

Control devices use soft computing techniques for the management of the actuators, specifically polyvalent logics, such as the fuzzy-logic, and a neural network. The climate control system, involved in regulating the temperature of the blown air, is managed by a Fuzzy-logic controller which checks temperature difference between the external air and the internal one. These two parameters represent the input signals of the controller. In this case, triangular waves functions - as membership functions - are the best choice in representing data. Inputs measure unit chosen is Celsius degree.

The Fuzzy-Logic controller converts inputs to linguistic variables. Then, it chooses an output based on rules described in the controller. The output is a dimensionless value which expresses blown air temperature. The Output is combined with some Matlab Function blocks as shown in figure 2, and it guarantees air flow regulation.

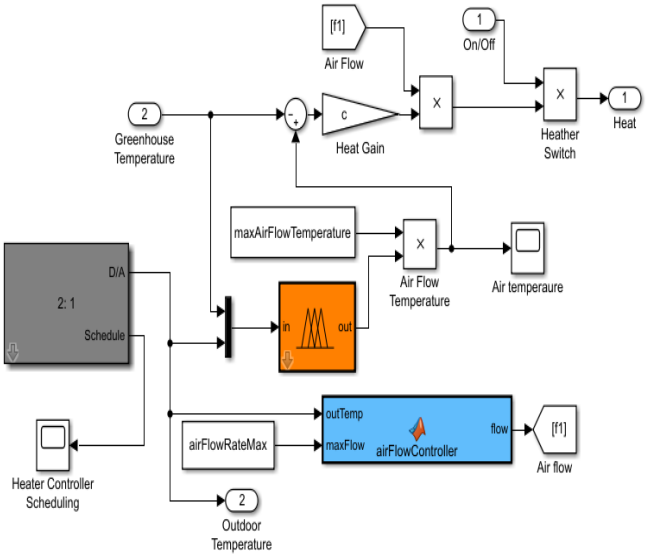

Figure 2: The climate control system.

Great importance is given to costs analysis concerning climatic cell usage. The energy cost trend is not only monitored. In fact, the system makes forecasts using a Neural Network (NN) implemented in the tool: Neural Network Toolbox. The NN training is based on results obtained during the simulation, in this way it could predict future costs of the climate control.

The irrigation system is represented by a Platform-Independent Model (PIM), a finite state machine

which describes the entire irrigation cycle analyzing actuators behavior using State flowchart. The input values are humidity and temperature level detected by the sensor network. The machine evaluates inputs detected by WSN than move through states which will turn on or turn off irrigation actuators. A debounce system has been embedded on the finite state machine, a mechanism which avoids those wrong readings of values determine passage to the next state when not needed. Also, the Greenhouse's coverage system is represented by a PIM. Input considered values refer to the external light brightness and wind speed.

IV. SCENARIO

The primary goal of this paper is to guarantee the maximum flexibility of the system previously explained, allowing changes in several parameters, such as the greenhouse size, the thermal characteristics of used materials, properties of the actuators themselves, and set up constants such as electricity costs, thanks to a configuration file included in the project without the necessity of modifying functional block.

The TrueTime Network block represents the wireless network. Inputs are the positions of the nodes belonging to the network, while outputs are the scheduling of the network and the power of the node consumption. The choice of the IEEE 802.15.4 standard simplifies the management of the devices. The wired network (Ethernet, CSMA/CD) is simulated within the same block.

Wireless sensors have been represented by subsystems made by TrueTime Kernel (which simulates the operating logic, the sensor connectivity, and an analog source which represents the environmental inputs). The Kernel schedules a timed reading task routine of the time-continuous source value and then send detected data to the gateway. Each basic unit can communicate and also to calculate and memorize.

The environmental variables control systems are represented by complex systems, constituted by TrueTime Kernels, which schedule tasks that manage the communicative aspect of these devices. As already mentioned in the second section, both soft-computing techniques and conditional controls made by Matlab functions are used mixed. A module is developed to translate physical principles and models into Matlab blocks imitating the real world and analyzing the implemented system.

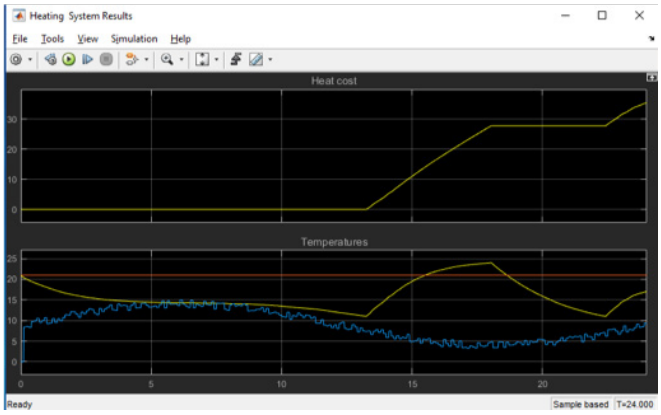

Figure 3: Simulation results: power consumption and temperatures.

V. PERFORMANCE EVALUATION

In analyzing system performances, we take into account data such as transmission capacity of the wireless channel used (Throughput), or end-to-end transmission time between terminal nodes (e.g., sensors and control devices). These measurements have been identified as critical for the system because a sensor failure or malfunctioning in detecting a parameter or in activating an actuator could compromise the entire system. An analysis was performed using the Matlab's profiler tool, as in the case of controllers consisting of Matlab Function blocks. By the simulations ran by Matlab software it could be possible to see how these parameters fit entirely within the implementation limits. The WSN throughput value stands at 4 bits/sec, representing the 0.0005% of the maximum capacity of the network. Indeed, a result of this type depends on the negligible length of the byte strings transmitted by the sensors, while the average end-to-end transmission average time is less than 0.002 sec, as shown in figure 4, ensuring the perfect functioning of the control devices.

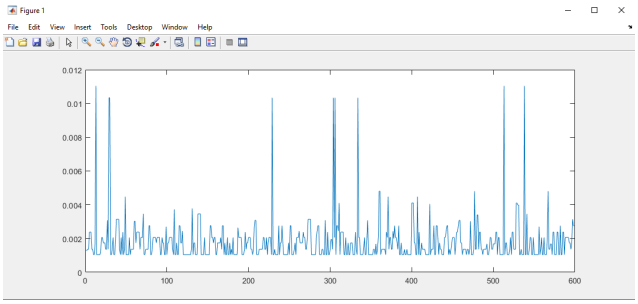

Figure 4: Performance evaluation results: Trend of the end to end delay during the simulation

VI. CONCLUSIONS

The object of this paper perfectly fits in the Simulink software, which allows us to shape and analyze complex mathematical systems such as the way heat is transferred from a greenhouse to the external envi-

ronment, an aspect analyzed and translated into a subsystem which offers consistent results. The system allows determining a result that adheres to a specific application reality, allowing a technical evaluation of a possible design. The whole system offers us the chance of both generalizing and integrating it into more complex systems, as already mentioned, maintaining a high-level of concreteness. In this sense, possible future development could be linked to the use of distributed programming techniques.

REFERENCES

[1] Smart Dust: BAA97-43 Proposal Abstract, POC: Kristofer S.J. Pister

[2] A. Cervin, D. Henriksson, J. Eker et al. "HowDoesControlTiming Affect Performance? Analysis and Simulation of Timing Using Jitterbug and TrueTime." in IEEEControl Systems Magazine,23:3, pp. 16-30, June 2003.

[3] ZigBee Specification FAQ". Zigbee Alliance. Archived from the original on 27 June 2013. Retrieved 14 June 2013.

[4] "IEEE 802.15.4". Ieee 802. Retrieved 2012-10-18.

[5] "Official IEEE 802.11 working group project timelines". January 26, 2017. Retrieved 2017-02-12.

[6] Y. Zhou, X. Yang, X. Guo, M. Zhou and L. Wang, "A Design of Greenhouse Monitoring & Control System Based on ZigBee Wireless Sensor Network," 2007 International Conference on Wireless Communications, Networking and Mobile Computing, Shanghai, 2007, pp. 2563-2567. doi: 10.1109/WICOM.2007.638

[7] Internet of Things Platform for Smart Farming: Experiences and Lessons Learnt - Prem Prakash Jayaraman 1, Ali Yavari 2,3, Dimitrios Georgakopoulos 1, Ahsan Morshed 1 and Arkady Zaslavsky

[8] M. Lee, J. Hwang and H. Yoe, "Agricultural Production System Based on IoT," 2013 IEEE 16th International Conference on Computational Science and Engineering, Sydney, NSW, 2013, pp. 833-837. doi: 10.1109/CSE.2013.126

[9] V. V. h. Ram, H. Vishal, S. Dhanalakshmi and P. M. Vidya, "Regulation of water in agriculture field using Internet Of Things," 2015 IEEE Technological Innovation in ICT for Agriculture and Rural Development (TIAR), Chennai, 2015, pp. 112-115. doi: 10.1109/TIAR.2015.7358541

[10] https://it.mathworks.com/products/fuzzy-logic.html

[11] https://www.mathworks.com/examples/

[12] https://en.wikipedia.org/wiki/Thermal_resistance

[13] https://en.wikipedia.org/wiki/Wireless_sensor_network

[14] http://ec.europa.eu/eurostat/statistics-explained/index.php/Electricity

MOVING OBJECT TRACKING SYSTEMS WITH RADAR-CAMERA FUSION

Grigoriev Evgeniy

Saint-Petersburg State University of Aerospace Instrumentation,
Saint-Petersburg,Russia
E-mail: ev.grig95@gmail.com

Abstract

The article considers the possibility of symbiosis of two fundamentally different systems for high-precision determination of the spatial coordinates of objects: an active bistatic radar system and a high-resolution optical system. The results of modeling the two-position system are presented. The limitations of each of the systems are shown separately. The structure of the radio-optical complex is proposed which allows to achieve qualitatively new results in solving problems of detection, recognition, and determination of the trajectory coordinates of objects.

INTRODUCTION

Traditionally, radar systems are used to determine the coordinates of a moving object. Because of:

- The opportunity for a short period of time to cover the vast areas of the observed space;
- the ability to inform the user about the presence of detected objects in the coverage area in real time;
- high efficiency of work in adverse weather conditions and the ability to work at any time of the day.

Radar systems have limitations. For example, the monostatic radar uses information contained in the characteristics of the electromagnetic field reflected from the object of observation. With the single-position radar it is not possible to determine the total velocity vector of the observed object, and also low azimuth resolution for these stations.

Consequently, it is profitable to use a system consisting of several stations spaced in area, where realized the algorithms of joint processing of radar information. Radar information obtained from several spaced positions allows to obtain a number of advantages in comparison with a monostatic radar, in particular: to improve the accuracy of coordinate measurements, to increase the resolution, noise immunity, etc. [1- 3].

However, even for multi-position radar systems, it is difficult to meet modern requirements for space monitoring systems, for example, it is difficult to accurately identify the boundaries of an observable object with the help of radar stations and solve the problem of object identification.

In this regard, it is proposed to use additional observation systems - visual diagnostic systems. Separately, they have a number of disadvantages indicated in table 1, but using the above described systems in symbiosis it is possible to achieve qualitatively new results in solving problems of determining the trajectory coordinates of objects, as well as their identification in difficult meteorological conditions.

RADIO-OPTICAL COMPLEX STRUCTURE

The structure of the symbiosis of the two systems is shown in Figure 1, where two transposing positions are located at a distance D from each other and perform joint monitoring of the required «Obj» object. In this case, objects can be as motionless and moving.

The second system of the radio optical complex of visual diagnostics scaning surrounding space within the monitoring zone by using the optical sensor C. After that, all information received from the two different observation systems is transferred to the control and joint processing point of information, where all information are identify, complexing and displayed in a single information field.

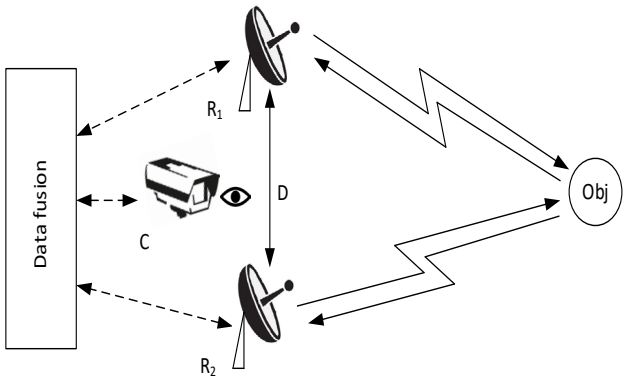

Fig 1

BISTATIC RADAR

The main advantage of multi-position radar systems is the ability to determine the coordinates of the object using distance-ranging information or goniometric [4].

So the bistatic radar system makes it possible to achieve high measurement accuracy, in comparison with a monostatic radar [5], which is relevant in modern radar systems, because it makes it possible to improve the accuracy of trajectory coordinates determination by complicating radar processing algorithms without changing existing equipment, thus saving time and financial resources.

The results of modeling the range measurements obtained separately by the single-position radar and as a result of the joint processing of the data obtained from the two-position system for various standard deviations of σ = 1, 10 and 100 meters are shown in Fig. 2. The red color indicates the measurement by one position, the blue indicates the measurement obtained by joint processing data obtained from two positions, and green the true value of the range.

SYSTEM OF VISUAL DIAGNOSTICS

The used system of visual diagnostics allows to solve problems which are difficult to solve separately by radar means, or requires large computational resources and processing time.

Table 1 shows the limitations of both systems considered and their possible solutions for radar and camera symbiosis

Table 1

	Cam	radar	two radars	radars + camera
Angle	+	±	+	+
Radial speed	-	+	+	+
Full speed vector (tangen.+ radial)	-	-	+	+
Range	±	+	+	+
Boundary detection of viewed objects	+	-	-	+
Bad weather condition working	-	+	+	+
Detec-tionof ob-jects close to each other	+	-	-	+

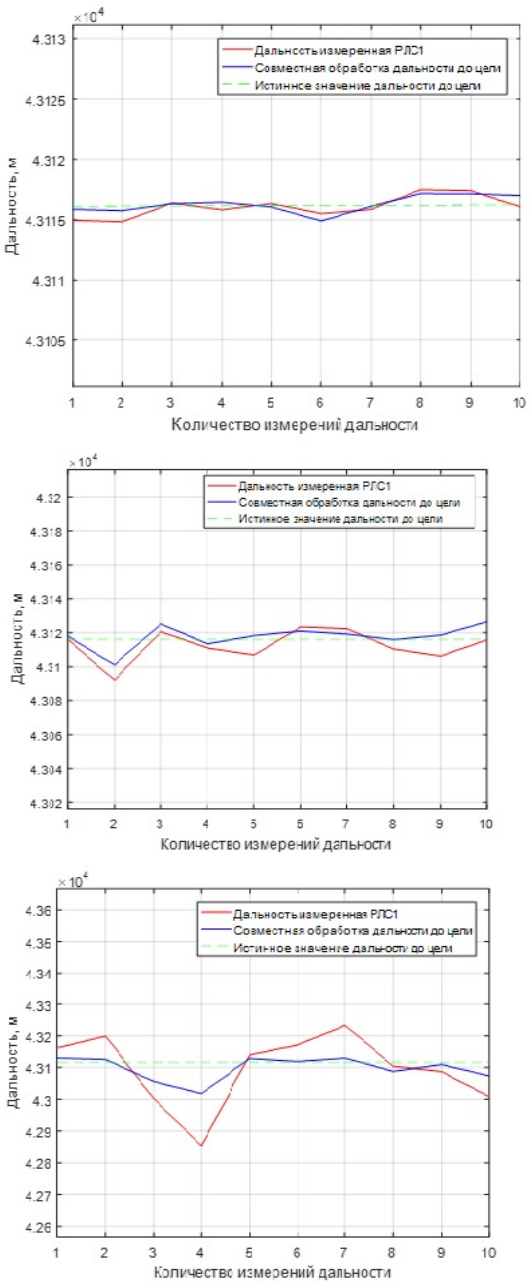

Fig. 2

CONSLUSIONS

Systems where radar and camera using together have great potential and harmoniously complement each other when solving a complex of problems

The key point in the implementation of the systems considered is the algorithms for combining the data obtained into a single information field.

With the joint use of these sensors, it is possible to achieve qualitatively new results that are not available when they are used separately.

At [6], it was proposed to use radar and camera together, but it is proposed to use one radar, the article presents the shortcomings of this approach, and also the simulation results that make it expedient to use

multi-position radar systems in symbiosis with optical sensors.

These systems can be used in various types of human activities, for example, in dealing with road safety, organizing the security of various objects or searching for and rescuing people in various disaster areas.

REFERENCES

[1] Зайцев Д.В. Многопозиционные радиолокационные системы. Методы и алгоритмы обработки информации в условиях помех. М.: Радиотехника 2007.

[2] Верба В.С. Оценивание дальности и скорости в радиолокационных системах. Часть 3. М.: Радиотехника 2010.

[3] Черняк В.С. Многопозиционная радиолокация. М.: Радио и связь 1993.

[4] Сколник М. Справочник по радиолокации. Том 4 Радиолокационные

[5] Grigoriev E. Modeling the Algorithm for Integrating the Results of Independent Measurements. Bulletin of the UNESCO department «Distance education in engineering» of SUAI, Collection of the papers issue 2.Saint-Petersburh 2017.

[6] Zhengping Ji, Danil Prokhorov. Radar-Vision Fusion for Object Classification. Information Fusion, 2008 11th Internation Conference

USE OF MECHANISMS OF AUTOMATION OF LOGISTICAL PROCESSES IN A SOCIAL INFRASTRUCTURE ON AN EXAMPLE OF ST.-PETERSBURG

Isakova Natalia

Saint-Petersburg State University of Aerospace Instrumentation
E-mail: 79117680865@yandex.ru

Annotation
The article deals with aspects related to the assessment of the possibility of switching to the full automation of the infrastructure of a large metropolis, such as the city of St. Petersburg, that can lead to the creation of a qualitative new standard of living for the population.
Key words: innovative technologies, assessment, hydropower, wind farm, smart city, smart traffic light.

The percentage of urban population in the world is growing every year. Accordingly, consumption of energy resources, water resources, equipment, communications, management resources is growing. To solve all the above needs of humanity, it was decided to create "Smart Cities", or "smart-city". At the heart of the "smart city", as a rule, there are 8 components, namely: energy, water supply, transport, security, services, integration, government, residents. [1] All these are integral parts of an intelligent city, which in turn must also be "smart", i.e. automated and integrated with each other. In this article, we will consider possible methods for implementing smart-city technologies that are relevant in the city of St. Petersburg. There is an international standard ISO 37120: 2014 "Sustainable Community Development. Indicators of the evaluation of services and urban quality of life. The application of this standard when automating the social infrastructure of St. Petersburg will ensure:

- more effective management and implementation of urban services;
- accessibility of the evaluation of results;
- reliability of estimates and validity of planned changes;

- the use of the provisions of this standard and the results for policy decisions and in daily practice by city administrators
- mutual learning between cities;
- application of this standard as a methodical and practical guide for substantiating, in understandable terms, requests for funding from various funds, including international ones;
- improvement of the investment climate;
- Planning of economic development of the city and so on. When designing the "Smart City", when calculating all its components, the most optimal solution will be the use of information modeling (BIM). However, this may cause a number of problems, since most programs are foreign, and therefore not adapted to the specifics of Russian cities. Another drawback in applying information modeling of cities in Russia is the lack of import substitution, therefore, very few standardizing documents in this area. [2]

The city is located in the northern part of the continent, and it is characterized by moist windy weather, a large amount of precipitation, and a large presence of water bodies. On average, 365 days a year, 200 days with precipitation. All these factors lead to the fact that within the "smart city" program to provide a megacity of electricity produced from the city's water sources and the region. Despite the very high costs of installing the HPP, it will pay for them completely and such energy will not be subjected to any inflation. It is also worth using the energy of tides and consider the possibility of using waves. Another equally interesting idea was proposed by the Commission on Atomic Energy in France, very suitable for the climate of St. Petersburg. The idea is to use the energy of the falling rain. Each falling drop has its effect. Getting on the piezoceramic element, it affects it physically, which leads to the appearance of an electrical potential. Further, the electric charge is modified (just as in the microphones the electrical signal is converted into oscillations). Due to the diversity of its forms, water has a truly enormous energy potential. Now, hydropower is a quarter of the world's electricity production and is a growing trend in this area. [3] The city of St. Petersburg, due to its geographical location, could be the foremost among the "smart cities" using water sources of energy. Wind power should become another branch of the development of electricity in St. Petersburg. The Leningrad region has a large number of unoccupied non-residential areas, where you can put a wind farm. An analogue of such a wind farm is already in the city of Ulyanovsk, built by the Finnish energy company OAO FORTUM and RUSNANO. Ulyanovsk wind power station has one drawback - it is low-power for a city like St. Petersburg. In order to provide the entire city for one year, about 150 Ulyanovsk wind power stations will be needed. To calculate the consumption of electricity

consumed by the city, you need to use the following formula:

$$W = P * t \cdot T, \quad (1)$$

where W - electricity consumption in kWh; P - power consumed by the city in kW; t - time of operation of the source of consumption (city) per day in hours; T - number of days of operation of the source of consumption (city).

Figure 1 shows the consumption and generation of electricity in St. Petersburg and the Leningrad Region in 2013-2017.

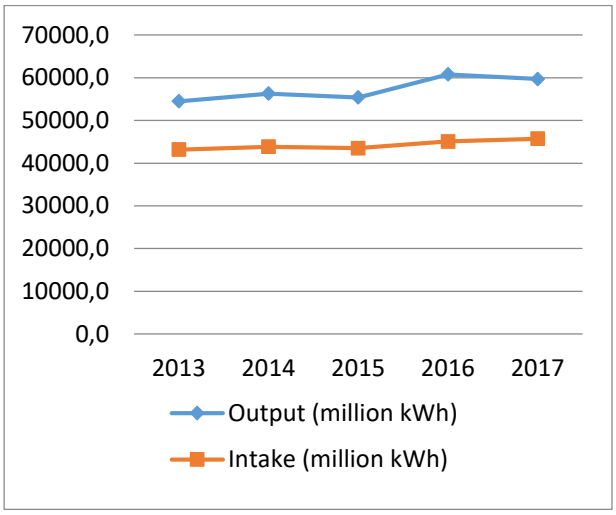

Figure 1 - Consumption and power generation in St. Petersburg and the Leningrad Region

Thus, over the past 5 years in St. Petersburg, more electricity was generated than consumed. But the existing types of power plants are not environmentally friendly and cause great damage to the environment. To reduce harmful factors, it is possible to replace part of the power plants with wind parks, which operate at the expense of an inexhaustible natural resource - wind. Despite the fact that wind power plants do much less harm to the environment, their installation for St. Petersburg is unlikely to pay off, as building a very powerful station will require very large financial investments that the city will not be able to provide. Thus, in order to provide 1/3 of St. Petersburg with such wind farms as the Ulyanovsk wind power station, it will be necessary to spend more than 150 billion rubles. Let's sum up the pros and cons of introducing wind power plants into the supply system of St. Petersburg, plus:

- an inexhaustible source of energy - significant reduction of harmful environmental impacts;

minuses:

- occupies large areas
- very high cost, unaffordable for the city budget.

The transport system of St. Petersburg within the "smart city" project needs to be modernized not only with an interactive video surveillance and monitoring system both in Moscow and further - equipping the city with "smart" traffic lights. They, collecting information on traffic congestion by traffic and pedestrian flows, could adjust the color of the signal, thus unloading the routes during peak hours and facilitating the movement of pedestrians in the daytime on multi-lane sections of roads. Such a system is used in Sydney, its use allowed to reduce traffic jams by 40%, and the amount of fuel burned in Sydney fell by 12%. Accordingly, the volume of exhaust gases decreased by 7%.

To date, in St. Petersburg, installed "smart" traffic lights, but there is one big problem: they are not synchronized with each other, and therefore they do not perform the specified functions. In the "smart city" to collect all the data requires a single center, which will integrate all the information received, on the basis of which it will be possible to make conclusions and amendments for the modernization of the system. The project of a single center is under development. For example, Barcelona is the only city where a common platform for collecting readings from all sensors is created and operates. The integrated system Sentilo combines devices for monitoring water supply, light, energy, road conditions, noise level, etc. - only about 550 sensors that collect information about the situation in the city.

The population of St. Petersburg is 3.2 times the population of Barcelona, therefore, more than 1500 similar sensors will be needed.

In July 2017, a group of companies joined forces to develop the CityNet project - the digital platform of the smart city. It is expected that the introduction of the CityNet communication platform in St. Petersburg will create the conditions for the emergence and development of a new industry - digital city services (digital smart city services). The working group of the CityNet project will create a competence center, the main task of which will be the leadership of St. Petersburg in the field of developing intelligent software and hardware solutions for smart cities. [4] Nevertheless, there are very large risks, for example, the system does not take root at the initial stages of implementation and will require large financial investments and time to eliminate errors; there may be difficulties in using the system by certain categories of citizens; reduction of workplaces in the automation of social infrastructure of the city.

One of the most interesting and promising ideas for creating a "smart city" is the introduction of "smart traffic lights." Modern "smart traffic lights" are complex devices that consist of: a controller; sensors of vehicles; directly the bodies themselves with LEDs or electric incandescent lamps; pillars or supports on which they are installed (Fig. 2).

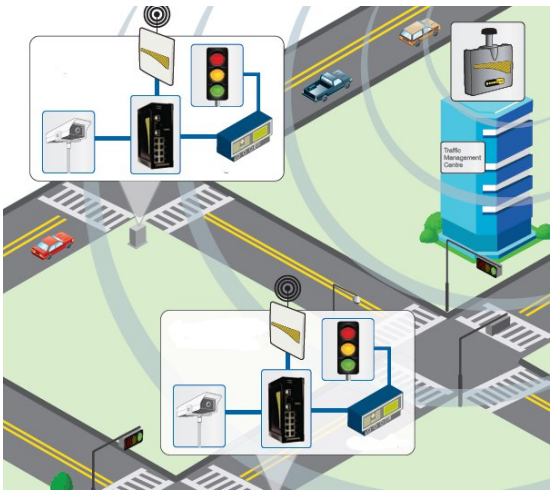

Figure 2 - The principle of the "Smart Traffic Light" system

The controller is the brain of a traffic light. It is a computer that selects the priority directions of the movement of machines and controls the distribution of flows in accordance with the readings of the sensors. The sensors scan the situation on the road every 3 seconds. Data on the transport stream is analyzed by the transport detector, this information is processed by the controller installed in a specific traffic zone. The device builds a forecast for the development of the situation and, based on this information, a control plan for traffic light objects is formed. For example, if the system records the congestion on one and the direction of the traffic, then the green light is extended to the detriment of other directions. "Smart light", guided by the readings of the sensors, regulates the traffic so that the transport is as little as possible at the crossroads, does not accumulate and does not form a stopper. According to experiments, the waiting time of the driver of the green signal when using "smart traffic lights" is reduced by 1.5-2 times compared to conventional signaling devices. In addition, "smart traffic lights" are connected to each other in a single network, they exchange data from different intersections and predict the traffic situation 10-20 minutes ahead to develop an effective mechanism for missing vehicles. In the event of a surprise, such as an accident, the system is able to promptly adjust the plan. Also, the work of "smart traffic lights" can be remotely corrected by specialists of the situation center. The systems of "smart traffic lights" are constantly being improved, and the development lies in the field of artificial intelligence. Over time, it is the traffic light that will take over the entire traffic flow adjustment, completely eliminating a person from this process. [5]

Conclusion

Implementation of the concept of automation of logistics processes in the social infrastructure of St. Petersburg is feasible in the near future. Part of the required technology in the city is already available. However, the main part - the synchronization of the entire infrastructure, has not yet been implemented and is in the project.

List of used literature:

1. Nikolaev V.A. Clever cities [Electronic resource]: Electronic magazine Jet Info 2015. №10 // URL: http://www.jetinfo.ru
2. GOST ISO 37120: 2014 Sustainable Community Development. Indicators of the evaluation of services and urban quality of life
3. Energy of water [Electronic resource] // URL: http://energy-source.ru
4. Intellectual cities [Electronic resource] // URL: http://www.tadviser.ru
5. Smart traffic lights [Electronic resource]: The electronic journal Hi-News.ru // URL: https://hi-news.ru

A SMART WASHING MACHINE

Giuseppe Messina, Francesco Raitano

Computer Engineering and Networks Laboratory – Kore University of Enna – Italy
Email: {giuseppe.messina03, francesco.raitano}@unikorestudent.it

Abstract
This paper shows the simulation of a smart washing machine. The system is composed of several steps of programming and working, and had been implemented through Matlab/Simulink/TrueTime simulation.

I. INTRODUCTION

This paper foresees the simulation of the operation of the predefined program inside a washing machine. This program is constituted by a first washing phase and a second spinning phase. The washing machine program will be started under the command given by the user through its device with the ZigBee network. This paper, is organized as follows. SECTION I describes the communication between the user and the washing machine. SECTION II describes the functioning of the MBSD and the change in the phases of the washing program. SECTION III describes the transmission of the data collected by the sensors of the values of water, detergent, and temperature. SECTION IV describes the operation of the fuzzy logic control. SECTION V describes the adjustment of the three parameters based on the received alarm values.

II. RELATED WORKS

The authors of [1] explain that with the rapid development of IoT (Internet of Things) and artificial intelligence technologies, an intelligent washing machine will be able to have a sensitive induction, an intelligent control system, and a natural interaction way. The project introduced in this paper bases its idea on the implementation through software with a programming language like MATLAB/Simulink [3] [4], of systems projects with automatic controls, which are studied in the field of mechanical engineering and automation. Following the example proposed in [2], in this project the simulated washing machine will come with a control center fuzzy logic for resource management, and following the approach of [5], was implemented the spinning phase.

III. THE PROPOSED APPROACH

SECTION I: The first part of the simulation consists in the communication of the User's choice about the start of the washing machine. Once the choice has been entered, the user's device, sends a message containing the user's choice. The message is received by a receiver, located inside the washing machine. The receiver will read the content of the message, which represents the choice to start the washing machine program. If the choice of the user is affirmative, the receiver will send a signal of "1" on the output D/A, and the manager of the program phases will later read that. Otherwise, it will send a "0" signal, where also this will be read by the manager of the program phases.

SECTION II: After that the user has confirmed the start of the program, the program's phase manager allows the passage from Phase 0, corresponding to the inactivity phase of the washing machine, to Phase 1 (washing phase). In the program phase manager, there is an MBSD block, used for synchronization and time management of the washing machine program phases. In the MBSD system, there is an input variable, an output variable, and a local one. The input variable called Activation has the task of informing the system if the start button of the washing machine has been pressed (or if the user has confirmed the start of the washing machine), and that it is, therefore, possible to start with the first phase of the program. The output variable called Program provides the rest of the washing machine architecture at which stage of the program we are at that precise moment of simulation. The local flag variable allows the phase change of the program based on the time elapsed since the start of the washing machine. The MBSD block bases its operation on two MBSD subsystems, one of which is used to receive the start signal and the subsequent time measurement, while the second one is used to sequence the phases of the washing machine program. As already mentioned before, for both MBSD subsystems, there is an idle state, which is both start and finish, in which the washing machine suspends its operation or is already suspended. The operation of the MBSD is as follows: after receiving the program start input, the second subsystem passes from the state Phase 0 to the state Phase 1, with consequent change of the value of the local variable Flag, which passes from the value 0 to the value 1. The change of the value of the Flag variable allows, in the first subsystem, the change from the Off state to the Washing state, with a consequent change of the value of the Program output variable that goes from the value 0 to the value 1. Later, precisely after 30 seconds since the start of the whole program, the second subsystem passes from the state Phase 1 to the state Phase 2, with consequent change of the value of the

local variable Flag that goes from the value 1 to the value 2. Again, the change of the value of the variable Flag allows, in the first subsystem, the change from the Washing state to the Centrifuge state, with a consequent change of the value of the Program output variable, which passes from the value 1 to the value 2. Finally, after 40 seconds from the beginning of the Washing phase, and then after 70 seconds from the beginning of the whole program, the second subsystem passes from the state Phase 2 to the state Phase 0, with consequent change of value of the local variable Flag that passes from the value 2 to the value 0. Again, the value change of the Flag variable allows, in the first subsystem, the change from the Centrifuge state to the Off state, with a consequent change in the value of the output variable Program that passes from the value 2 to the value 0. Once returned to the Off and Phase 0 status, the washing machine will not be able to reactivate until it receives new start commands.

SECTION III: The operation of the entire washing machine program starts from the reading of the levels of water, detergent, and the temperature inside the washing machine by three sensors, each one used to read one of the three variables mentioned above. Each sensor consists of a kernel and a memory block used to store the three current variables. After, the three sensors will send the data gathered of the levels of the three variables to a Gateway through a simple message containing the information. The gateway mainly carries out the task of routing the packets received from the three sensors to the fuzzy controller manager. Besides, the gateway receives from the D/A input, from the program's phase manager, the current one running. If the program is "1" or "2", the gateway performs the routing task on a regular basis. O the contrary, if the program is "0", the gateway task is canceled, definitely interrupting the entire communication and, therefore, the washing program of the washing machine, bringing it to a state of suspension or inactivity.

SECTION IV: The fuzzy control, part of the entire architecture, is divided into two functional groups. The first receives messages, the sensor data received from the gateway, and sends these values to the D/A output. It receives in the D/A input the alarm values processed by the second functional group and then sends the alarm values via messages to the final controller. The second functional group consists of four real fuzzy controllers, which process the data received from the first functional group and send the value of the alarms processed to the controller. Once the gateway has routed the various messages, the latter are received by the first functional group for fuzzy logic control, where the latter consists of a kernel block. The kernel extrapolates the values within the received messages and sends them to the D/A output, where they will arrive at the D/A input of the second functional block. In the second functional block, there are two subsystems based on the fuzzy control, where each subsystem will operate in one of the two phases of the washing machine program. The first subsystem contains two fuzzy logic controllers. The first one is used to control the water and detergent level during the washing phase. It has the water and detergent levels as input variables and the output levels as the output variables water and detergent that "should" be reached as soon as possible. Both inputs and outputs have intervals [0 - 100], which indicate the percentage of tank filling, dividing the interval into Low, Moderate and Abundant memberships, both for inputs and outputs. The second controller is used to control the temperature level during the wash. It has an input variable that indicates the current temperature level and an output variable that indicates the temperature level that "should" be reached as soon as possible. Both input and output have intervals [10 - 70], which indicate the minimum and maximum temperature supported by the washing machine, dividing in Cold, Warm and Hot. The second subsystem differs from the first exclusively from the number of outputs present in its first fuzzy controller. One is used to empty the tanks. In fact, there are the usual inputs with the same intervals and same membership to indicate the level of filling of water and detergent. However, this time, there is only one output variable that indicates the critical level of removal of both liquids, also with a range of [0 - 100] and with the same memberships. As in the first subsystem, also in the second there is a fuzzy controller for temperature regulation during the spin phase, having the same intervals and membership of the fuzzy controller of the temperature of the first subsystem. During the washing phase, the fuzzy controllers will have to try to gradually increase the values of water, detergent, and temperature according to the current value of these three variables, but without ever reaching the limit values of 100%, 100% and 80 ° C respectively. During the spin phase, vice versa, the fuzzy controllers will have to reduce/clear the current water and detergent values gradually. Once the alarms have been processed, the alarms will go into the D/A input of the first functional block. The first functional block will also have the task of reading the current phase of the program in execution that is sent to it, again in the input D/A by the operator of the phases of the program. Consequently, if the received program is equal to "1", the first functional block must take the values of the alarms processed only from the first subsystem of the second functional block, while if the received program is equal to "2", the first functional block must take the values of the alarms processed only by the second subsystem of the second functional block. Once the correct alarms are received according to the phase of the program in execution, the first functional block sends all the values acquired through messages in the network to the final regulator.

Figure 1: Internal components of the whole project. From left to right: the first block is the device of the User connected to the ZigBee network that allows the washing machine to start, the second block represents the ZigBee network itself, and the third block represents the washing machine.

SECTION V: The last point of the transmission line is regulated by the Regulator node. This node has the task of receiving all the data and alarms processed at the beginning and transferring them via D/A output to four regulators, each specific for the regulation of a parameter. The first three regulators respectively receive the current water, detergent, and temperature values, plus they receive the phase of the program currently in use and the alarm level inherent to the parameter that the regulator is processing. Besides, the presence of a fourth regulator must be detected, the latter being delegated to adjust the revolutions of the drum of the washing machine, and this is done based on the current volume of water and the phase of the program currently in use. Therefore, if the phase of the program currently in use is "1", then the regulator will maintain the number of revolutions around 5 rpm, while if the phase of the program currently in use is "2", then the regulator will increase the number of revolutions per second, around 13 rpm/sec, increasing or decreasing this value gradually if more or less water is present. The data processed by the four regulators, plus the status of the program, together represent the overall state of work of our washing machine.

IV. SCENARIO

This scenario has been simulated with Matlab / Simulink using TrueTime.

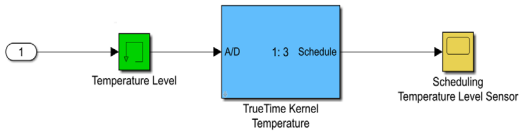

Figure 2: Internal components of Temperature Sensor.

The first part of the washing machine consists of the sensors of water, detergent, and temperature, where each inside consists of the same elements, i.e., a kernel block and a memory block for saving the current level of the variable in question (*Figure 2*). Then there is the block of the Wired Network, where inside there is the gateway for the routing of messages deriving from the three sensors and the blocking of the wired network, which represents the first network of our project. Next comes the Fuzzy Helper block, that is the one dedicated to the reception of the data of the current variables and to the transfer of these data to the real fuzzy controllers constituting a kernel that represents the fifth node of the wired network. In detail, this block represents the first fuzzy functional block. Immediately after the first functional block is the second one, the one constituted by the real fuzzy controllers, which receive the data to be processed directly from the first functional block and send to the latter the alarm levels processed. Following the two fuzzy function blocks, there is the regulation center, where the last node of the network used to receive the alarm levels, received from the first fuzzy functional block, with which it is possible to adjust the water levels, detergent, temperature and the number of turns of the basket per second. In this case, the saturators allow limiting the values of the variables above and below. For instance, water and detergent can obviously not be below 0% or higher than 100%. As the last block, but not in importance, there is the one used to manage the washing machine program phases (*Figure 3*) and the one used to receive the start message in the ZigBee network by the user.

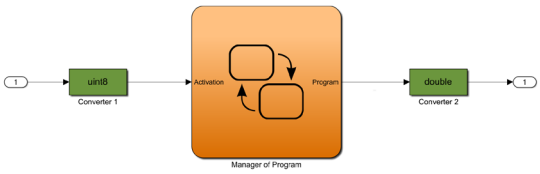

Figure 3: Internal components of manager of washing machine program.

V. PERFORMANCE EVALUATION

In this paper, it was decided to measure three performance metrics that broadly characterize the performance of the washing machine control system:

- number of processed packages (water, detergent, and temperature) from the gateway during the whole simulation period;
- delay time used by a generic packet generated by one of the three sensors to arrive from the gateway to the regulation node;
- time taken by the system to respond to the user's request to start.

To perform the first measurement, it was decided to send a unit value to the D/A output each time the gateway receives one of the three types of packets. This unit value will then be added to the partial sum of the number of previously processed packages (*Figure 4*).

To perform the second measurement, it was necessary to receive the instant of time in which the generic message is received by the gateway and the instant in which the same message is received by the node that regulates the regulation of the values. Once these two moments were obtained, it was enough to calculate the difference (*Figure 5*).

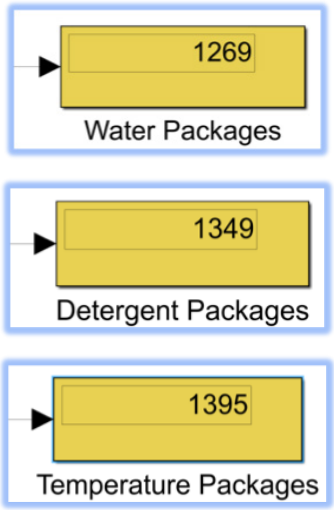

Figure 4: First measurement: number of processed packages.

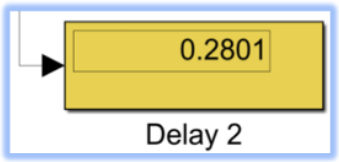

Figure 5: Third measurement: time taken by the system to respond to the user's request to start.

To perform the last measurement, it was necessary first to obtain the value of the time instant when the user confirms its choice. The first node of the ZigBee network when sends the message with content the choice of the user will also send the value of the time instant in the D/A output. After the ZigBee receiver, that is, the second node of the ZigBee network, when it receives the message sent to it by the user, it will also send in the D/A output the instant of time in which it received the message. Eventually, the difference between the two-time instants obtained will be obtained (*Figure 6*).

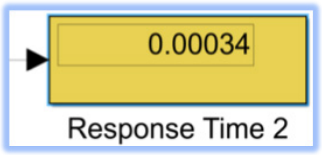

Figure 6: Second measurement: delay time used by a generic packet.

VI. CONCLUSIONS

The proposed system aimed to show how an electronic appliance, such as a washing machine, can be managed remotely from a device if the network being used and the technology of the washing machine allow it. The architecture introduced in this paper allows it without any significant change to be able to add more washing programs, with a completely transparent way for the three sensors, the gateway, and the four regulators.

REFERENCES

[1] Daoyi Wu. "Research on the micro-interactive interface design of intelligent washing machines in IOT environment"", Year: 2016, [22nd International Conference on Automation and Computing (ICAC)].

[2] Sanju Kaler, Rajeev Gupta. "The design of intelligent washing machine controller based on FIS & ANFIS", Year: 2017, [International Conference on Information, Communication, Instrumentation and Control (ICICIC)].

[3] Wang Ai-Zhen, Ren Guo-Feng. "The Design of Neural Network Fuzzy Controller in Washing Machine", Year: 2012, [International Conference on Computing, Measurement, Control and Sensor Network]

[4] Wang Gui-juan, Wang Zuo-xun, Wu Yan-rong, Xu Hong-dong. "The Application of Neuro-Fuzzy Controller in the Washing Machine Control System", Year: 2009, [Second International Conference on Intelligent Computation Technology and Automation].

[5] Ahmet Yörükoğlu, Erdinç Altuğ. "Estimation of Unbalanced Loads in Washing Machines Using Fuzzy Neural Networks", Year: 2013, [IEEE/ASME Transactions on Mechatronics].

MEDICAL ANALYSIS OF KNEE INJURIES USING KINEMATIC DESIGN WITH A MECHATRONIC APPLICATION FOR REHABILITATION

Molly Joseph

Computer and Electronic Technology - Indiana State University, Terre Haute, Indiana
Email: mjoseph22@ivytech.edu

Abstract
This paper proposes a medical analysis of knee injuries using kinematic designs with a mechatronic application for rehabilitation. The goal of the design is to enhance the recovery experience for knee injuries and help improve quality of life for person(s) with knee injuries. It has a focus on to introduce robotics into a recovery system that allows the user to still walk and function through their daily regime. The focus of the design is for the lower body, with the research being directed towards knees.

INTRODUCTION

The motivation for this exploration is to improve the life of people who have incapacities in their lower extremities by constructing therapeutic robotic innovations. Interest in lower limb orthoses started in the 1950s in various fields, such as military upgrades and restorative patient change. From that point forward, specialists have designed exoskeletons for impairments, as robot's modernism strategically assist individuals in developing their lower limbs. Today, the exoskeleton's primary function is to operate as a device for advancing patients with issues in lower limb development. The goal is to improve a patient's ability to move and to help them live a productive life (Rodriguez-Martinez, Lopez-Amaya-Urriolagiotia-Sosa, Romero-Angeles & Urriolagoitia-Calderon, 2017). In many cases, active mechanical stratagems are yet to be developed that help individuals who have impaired lower body mobility. In this approach, it is critical to strategize a restorative mechanical innovation to assist in the recovery of individuals impacted by lower limb mobility.

PROBLEM STATEMENT

Physical exercise, such as walking, running, standing, and sitting are essential in today's fast and busy world. There is also an increasing number of victims of accidents, strokes, and spinal cord injuries who are likely to become paraplegic. At the point when a substantial percentage of society cannot walk or move appropriately due to neurological or physical injury, there is an opportunity for creative solutions. This suggests that it is critical to discover substantial methods that can help provide these individuals with physical enhancements. In order to escalate the rational therapeutic approaches of knee injuries, and to help improve the personal contentment of people with lower disabilities, a unique robotic exoskeleton could be strategized. This science aspires to enable patients to improve their everyday activities and to minimize the mending process of the knee.

SCOPE

This project will analyze and design three robotic exoskeletons that accelerate the healing process of the knee. The project will investigate the methods, which include labor, parts, study, and analysis, of current rehabilitation compared to the integration of an exoskeleton with neuromuscular electrical stimulation. It will also include CAD designs of the three robotic exoskeletons and the parts needed to build them.

THEORY

Modern medicine and therapy have seen numerous advancements from generation to generation. Each one of these methods has taken steps in the right direction, but there is still room for progress. These methods can be divided into five different categories: "(1) footplate-based gait trainers, (2) treadmill gait trainers, (3) over ground gait trainers, (4) ankle rehabilitation systems, and (5) stationary gait trainers" (Diaz, Jorge & Sanchez, 2011). Each of these procedures depicts advantages and disadvantages that have been in place for a long time. With the progression of science and technology, an accumulation of these techniques might produce a more efficient outcome.

Exoskeleton technology coordinates with a human to make a mechanical-natural framework that is built out of integral subsystems. Neuromuscular diseases (NMD), focal sensory system wounds, and muscle weakness are the essential drivers of becoming handicapped or disabled. Conversely, the mechanical controllers used to perform this undertaking may require substantial power (Breen, 2015). The exoskeleton's development control calculations are not as refined as a human's capacity to coordinate. There are significant challenges to overcome before the idealistic dreams of exoskeletons can be developed. For exoskeletons to be valuable, they should supplement, rather than obstruct or compel, the human body's normal kinematics.

An exoskeleton goes through a progression of general repeating steps when it is given portability to

help the client: (1) The exoskeleton control framework utilizes sensors similar to ones that gather electromyography signals to determine the position of the client's body. (2) When the client desires to move, the exoskeleton utilizes those signals to interpret the client's planned activity. (3) The control framework chooses a pre-customized development design that modifies the client's present position with the support of the actuators. (4) After the process of expansion, the exoskeleton identifies the new position (Van Kammen, 2014).

An exoskeleton made by the Japanese organization Cyberdyne has successfully gone through the German wellbeing tests and is currently being sold in different parts of Europe (Kim & Bae, 2017). This machine is known as the Hybrid Assisted Limb, or HAL. There are two types of HAL frameworks that can help clients with performing regular living exercises. The HAL 3 offers the ability of strolling, standing, climbing, and profound knee curves, while HAL 5 is a full-body exoskeleton that incorporates arm and mid-body abilities (Kim & Bae, 2017). The HAL is a unique exoskeleton that is slender, light, and has a cutting-edge look. This research focuses on the knee joints and tendons (see Figure 1).

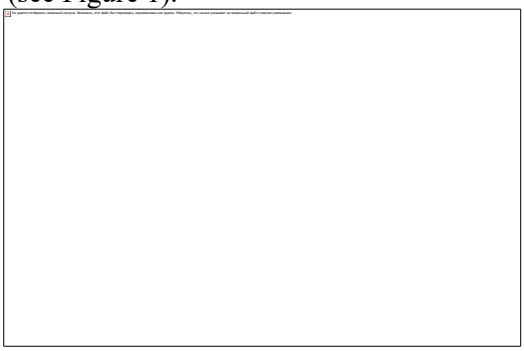

Figure 1. The anatomy of the knee (Anatomy of the Knee, 2016)

Knee joints include semitendinosus, quadriceps tendons, and various muscles. The development of the knee requires collaborations of these muscles and tendons. Consequently, the necessary application of robotic actuators for the knee joints needs a proven method of neuromuscular electrical stimulation therapy that can encourage the clients' movement and development of the knee.

RESEARCH

The very first exoskeleton venture began with the that of Yang (1890). He pitched the idea of creating an automated robotic assembly that would help individuals with strolling, running, and even hopping (Zhao, 2017).

The utilization of the automated systems of an exoskeleton should communicate an exact estimation of development flow and kinematics. Special attention should be given to an injured party to observe the healing process. Currently, the limit of the patient to ultimately regain their mobility is evaluated by continuous education and research (Diaz, Jorge & Sanchez, 2011). With the advancement of automated technologies, walking distance, acceleration, stride speed, and various ongoing efforts are there to evaluate a patient's capacity to recover the ability to walk. This makes it imperative to devise a traditional clinical technique that can enable patients to improve their walking capacity (Yua, Hanb & Choa., 2014). With that said, the three exoskeletons' mechanical devices accelerate the recovery period of the knee and measure the patient's walking capacity with the integration of neuromuscular electrical therapy.

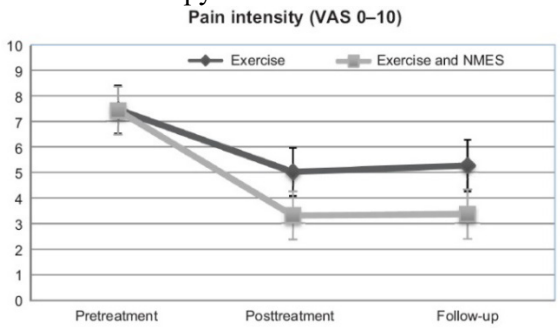

Figure 2. Knee pain intensity by group across assessments.

Figure 2 illustrates the decrease in pain levels using conventional therapy verses electrical stimulation therapy. Sixty-three patients participated in 12 bi-weekly treatments. The addition of the neuromuscular therapy shows a significant reduction in pain vs. exercise only (Laufer, Shtraker, Elbolm, 2014).

TEST AND EVALUATION

The method of designing the layout for the exoskeleton was a lengthy process. In the selection of the appropriate material, aluminum was chosen because of its weight, density, and strength. In addition, it is an anti-corrosive material and is less likely to fade because of its polished finish.

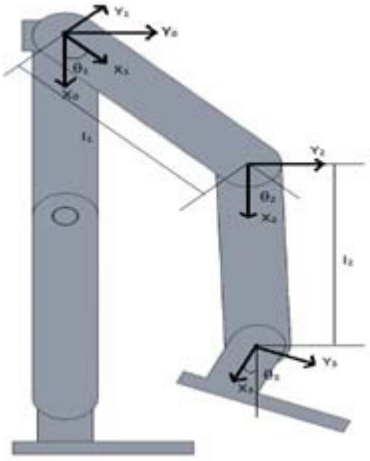

Figure 3. *Exoskeleton leg with reference frames assigned.*

Torque Calculations

Figure 3 shows the typical kinematics of walking that assisted in calculating the torque needed to

move the exoskeleton(Latif, Shaari, Ida, Isa, Jun, 2015). A male adult in the USA weighs approximately 195.7lbs, which is equivalent to 88.7 kg (Vakharia, 2016). The average male leg is then approximately 16.68% of their total

body weight, and the average foot is 1.4% (Vakharia, 2016). This data was used below to determine the torque necessary for the exoskeleton:

- The gravity constant is 9.81 m/s^2
- Leg mass = 14.7 kg
- Foot mass =1.24 kg
- The Forces calculates as follows:
- Hip (1 legs) 14.7 kg x 9.81 m/s^2 = 144 N
- Knee (1/2 leg) 7.35 kg x 9.81 m/s^2 = 72 N
- Foot 1.4 kg x 9.81 m/s^2 = 13.74 N
- Torque = F x D

The average stride for one step is 32 inches, which is 0.8128 meters. Only half of a human's stride is realized in reference to force, however. The foot would only need to be mobile for an approximate range of 10 inches, or 0.254 meters (Johnson, 2017). Considering that weight and force are distributed proportionally in the human body, the torque calculations are as follows:

- T = F x D
- Hip 144 N x .406 m = 58.46 Nm
- Knee 72 N x .406 m = 29 Nm
- Foot 13.74N x .308 m = 3.48 N

Recommended Specifications

Table 1 shows the selected motors for the exoskeletons. Given that DC motors can operate momentarily above their normally rated torque, the following gearbox specifications are selected at a 100:1 reduction ratio. Table 2 identifies the recommended gearheads needed with the motors in Table 1 for the appropriate torque. The manufacture will provide a custom coupling and adapting plate.

Table 1

Maxon motors.

Hip	Model	Maxon Motors	EC90 Flat	Continuous Torque	560mNm
Knee	Model	Maxon Motors	EC60 Flat	Continuous Torque	560mNm
Foot	Model	Maxon Motors	EC45 Flat	Continuous Torque	128mNm

Table 2

Harmonic drive gearheads

Hip	Model	Gearheads	CSD-32-50-2UH	53 Nm
Knee	Model	Gearheads	CSD-32-50-2UH	53 Nm
Foot	Model	Gearheads	CSD-14-50-2UH	3.7 Nm

DESIGN

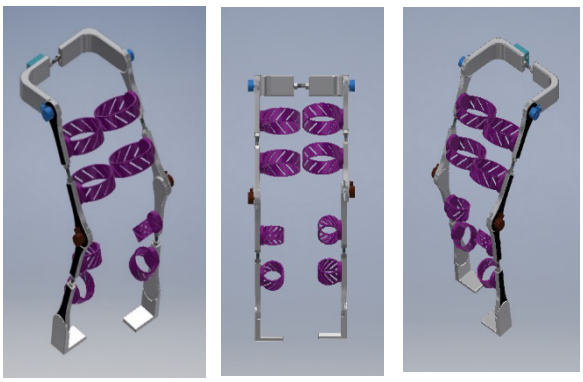

Figure 4. Model 1 exoskeleton.

Model 1

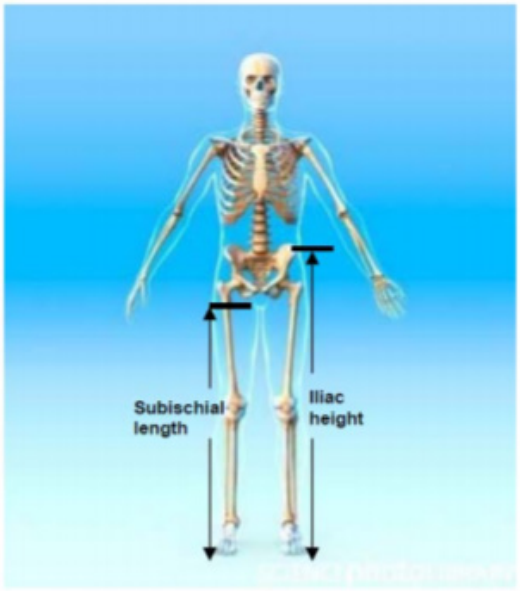

Figure 5. Iliac height and sub-ischial length. Credit: Roger Harris/SCIENCE PHOTO.

Aluminum will be the primary material in the fabrication process of the knee. With this design, there are five adjustable rods: two for the femur, two for the tibia, and one for the hip region. This will allow the exoskeleton to be adaptable. "The anatomical definition of leg length is the length of the femur + tibia. Due to the bipedal nature of the human species, "leg length" often is measured as, femur + tibia + the height of the foot, from the tibia-talus articulation to the ground" (Bogin & Silva, 2010). The measurements for the exoskeleton are for the distance between the summit of the iliac crest, the floor, and the iliac height (IH) (see Figure 5). This exoskeleton will have four DC motors to control the hip and knee joints. There is a place to rest the foot with straps along the thigh and calf region.

Model 2

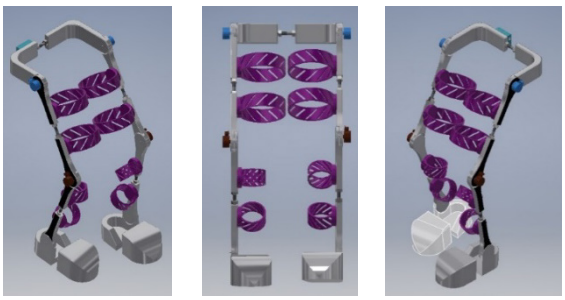

Figure 6. Model 2 exoskeleton.

As for Model 2, aluminum will again be the primary element during the fabrication process. With this design, there are five adjustable rods: two for the femur, two for the tibia, and one for the hip region. The leg length is the same as in Model 1. There is an adjustable strap on the footplate that allows it to be adjustable. This exoskeleton will have four DC motors to control the hip and knee joints.

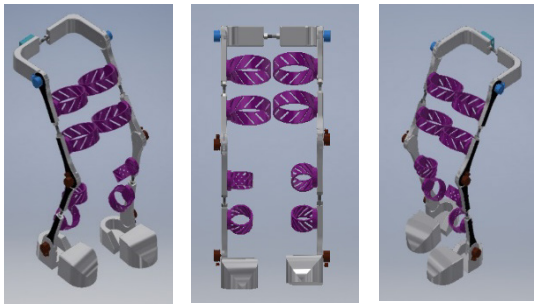

Figure 7. Model 3 exoskeleton.

Model 3

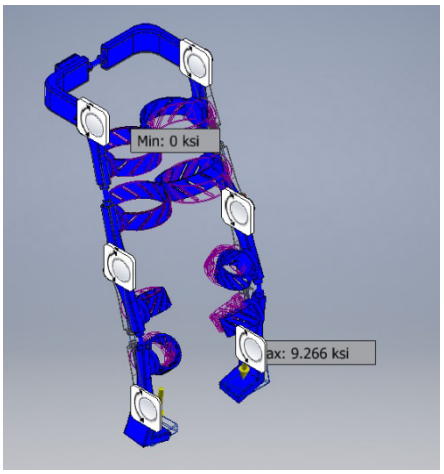

Figure 8. Von Mises stress analysis.

As for Model 3, aluminum will again be the primary material for fabrication. With this design, there are five adjustable rods: two for the femur, two for the tibia, and one for the hip region. The leg length will be the same as in Model 1. There is a strap on the footplate that allows it to be adjustable. This exoskeleton will have six DC motors to control the hip, knee, and ankle joints.

Static Analysis Results

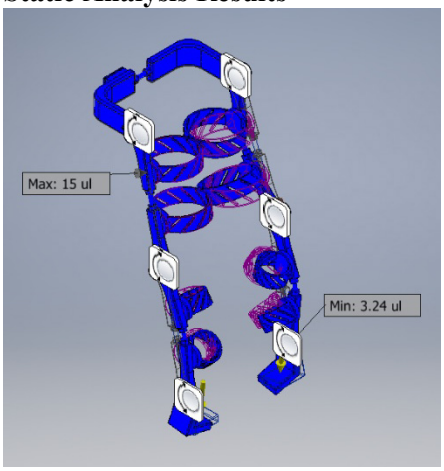

Figure 9. Safety factor analysis.

A stress analysis calculation was performed. For the evaluation, various loads and constraints were applied. The magnitude of force used was 200 lbs. The volume of the exoskeleton is 318.155in^3, and the mass is 27.6715 lbs. The Von Mises stress test produced a summary multidirectional analysis. Figures 8 and 9 provide an illustration of the analysis. The Von Mises stress test identified the exoskeleton as having a minimum of 0.00000000500831 psi and a maximum of 9.26608 psi. The results showed that the model and the material used are safe for individuals weighing up to 200lbs. The exoskeleton safety factor calculations were completed, which were determined from the ultimate tensile strength. Engineers recommend a safety factor above 1, and the safety factor of the design has a minimum of 3.24 ul to a maximum of 15 ul, verifying that the design and material used for the exoskeleton are appropriate.

COST ANALYSIS

Table 3 shows the parts needed for model 3 and identifies the total cost of the exoskeleton.

Table 3

Parts list.

Quantity	Part #	Description	Price (Unit)
4	429271	Maxon Motors EC90 Flat	$266.38
2	397172	Maxon Motors EC45 Flat	$160.50
2	CSD-17-50-2UF	Ultra Flat Gearheads	$1,121.00
2	CSD-17-100-2UF	Ultra Flat Gearheads	$1,122.00
2	CSD-20-160-2UF	Ultra Flat Gearheads	$1,292.00

Quantity	Part #	Description	Price (Unit)
6	520885	EPOS4 Compact 50/8	$499.20
6	520850	Power Cable	$16.30
6	520858	CAN-CAN Cables	$23.70
6	354045	Motor Cable	$51.60
1	NA	Arduino Uno R3 Micro Controller	$19.95
6	522-1007-ND	B B Battery BP1.2-12-T1	$16.82
1	P141-ND	BATTERY LEAD ACID 6V 4.5AH	$14.75
2	PM-081443878	Rolyan Temper Foam Splint Padding Sheets 3/8in. X 16in. X 24in.	$57.86
1	13926	Triple Axis Accelerometor	$10.49
9	S-15756	Uline Velcro Straps	$19.00
1	NA	FREEMG	$5,800.00
6	NA	Additional FREEMG Sensors	$1,000.00
1	RB-Cix-01	Jumper Wires	$3.95
2	412932	Biomedical Life Systems Bioknit Conductive Knee Brace, Universal	$111.99
1	216639	Roscoe Medical Top TENS Pain Relief System	$82.99
1	PB520B	Project Box	$8.95
1	NA	Adruino CAN bus module	$66.00
1	NA	Adruino Shield	$40.00
1	NA	3.7 Lithium Battery	$9.99
1	520857	CAN-COM Cable	$29.60
1	RB-Spa-1181	Remote Control	$4.70
1		Exoskeleton Manufacturing Cost	$ 12,275.47
1		Installation Labor Cost	$600.00

Conclusion

When an individual suffers an event that means they can no longer use their body functions properly, they will undergo a significant life change. With today's continuous failing health and tragic terrorist attacks, the need for robotic medical assistance continues to rise. The three exoskeleton innovations detailed in this report will revolutionize the therapeutic industry. The culmination of the therapeutic aid of the medical exoskeleton and the scientific method of neuromuscular electrical therapy should significantly reduce the time needed for physical recovery.

References

1. Anatomy of the Knee. (2016, May 21). Health Life Media. Retrieved Oct 26, 2017, from http://healthlifemedia.com/healthy/anatomy-of-the-knee/
2. Beyl, P. (2010, Dec). Design and control of a knee exoskeleton powered by pleated pneumatic artifical muscles for robot-assisted gait rehabilitation. Department of Mechanical Engineering. Retrieved Oct 26, 2017, from http://mech.vub.ac.be/multibody/publications/full_texts/PhD_Thesis_Pieter_Beyl.pdf
3. Bogin, B., & Varela-Silva, M. (2010). Leg Length, Body Proportion, and Health: A Review with a Note on Beauty. International Journal of Environmental Research and Public Health.
4. Center for Spinal Cord Injury. (2017). Retrieved Oct 26, 2017, from http://www.upmc.com/Services/rehab/rehab-institute/conditions/spinal-cord-injury/Pages/default.aspx
5. Diaz, I., Jorge, G., & Sanchez, E. (2011). Lower-Limb Robotic Rehabilitation: Literature Review and Challenges. (D. Jeon, Ed.) Journal of Robotics, 2011(Article ID 759764), 11. Retrieved Oct 26, 2017, from https://www.hindawi.com/journals/jr/2011/759764/
6. Rodriguez-Martinez, R., Lopez-Amaya, J., Urriolagoitia-Sosa, G., Romero-Ángeles, B., & Urriolagoitia-Calderón, G. (2017). Proposal by simple design of the lower limb exoskeleton of continuous use, provided of own mobility and body load support. Case: application due to an illness. Journal of Physics: Conference Series, 792. Retrieved Oct 26, 2017, from http://iopscience.iop.org/article/10.1088/1742-6596/792/1/012073/meta
7. Yua, S., Hanb, C., & & Choa, I. (2014). Design Consideration of a Lower Limb Exoskeleton System to Assist walking and Loan-Carrying of Infantry Soldier. . Applied Bionics and Biomechanics, 11(3), 119-134 . Retrieved Oct 26, 2017, from https://www.hindawi.com/journals/abb/2014/585837/cta/

A SMART HOME PROPOSAL FOR AUTOMATIC MANAGEMENT IN HEATING SYSTEM USING RENEWABLE ENERGY

Ludovico Paladino, Ilaria Oliva

Computer Engineering and Networks Laboratory – Kore University of Enna – Italy
Email: {ludovico.paladino, ilaria.oliva}@unikorestudent.it

Abstract
Thermoregulation systems have an essential role in building new houses for comfort management. This paper shows how the renewable energies, together with the progress in information technology and communication, can help users to increase energy saving and improve their quality of life also thanks to the ability to make a decision and automatize the best choice.
In this paper is presented a possible implementation of an active controller that operates by responding to a combination of internal set points and external signals. The optimization objective of the heating systems management is to minimize the cost of gas and electrical energy, maximizing thermal efficiency. As a result, traditional heating system and renewable energy can work together, and their benefits can be added when used in combination. The presented analysis is validated employing both simulation and experimental results, testing also the performance of the network.

I. INTRODUCTION

The renewable energies have always represented an inexhaustible resource on Earth. The necessity to reduce harmful emissions of gases and consumptions, causing climate changes, have pushed research towards a greener and more efficient products, to guarantee maximum performance with minimum consumption.

The ICT deals with management, transmission and sharing data between different devices. The protocol IEEE 802 represents a standard for communication systems, that allows independent devices to communicate each other using a physical channel at high speed and low error rate.

II. RELATED WORKS

Even if many standards exist in the world, many companies have based their approach on a proprietary bus transmission system, implicitly binding the end customer to use their own range of products, in order to guarantee compatibility between devices.

The authors of [1] have already proposed an approach with Ethernet gateway for wireless sensors to collect and share data within an existing network. This choice would also allow, as discussed in [2], connecting devices to internet natively. Obviously there is a problem concerning the power supply of wireless sensors. Some proposals in literature suggest to install batteries with a higher capacity [3] or completely shut down blocks of circuities [4].

Heat production, today, bets on renewable resources, first of all the sun, although it needs an external source. The union between the systems requires an intelligent electronic control to allow this automation. [5] One of the most efficient alternative external supplier is the heat pump, as tested in details in [6], which however has excellent performance only in positive temperatures, but it is not the most efficient choice in lower.

III. THE PROPOSED APPROACH

According to these considerations, we decided to realize the network architecture on the standards IEEE 802.3 (Ethernet) and IEEE 802.11 (WLAN), developing a hybrid domotic scenario for thermoregulation with an efficient heat pump, thermal fireplace, and solar panels, supported by the classic condensing methane gas boiler.

System, depending on room temperature and user's setting, will chose the best combination of them, preferring renewable sources. If they aren't enough, two auxiliary generators will be activated alternately or simultaneously. A thermostat, belonging to an Ethernet wired network, sends the operating modes (hot/cold) to the control unit. It will receive solar panels' and thermal fireplace's temperature from wired sensor, belonging to another network, and outdoor humidity and temperature, coming from WS. These data will be used by the control unit to choose the energy combination more convenient between the boiler and/or the heat pump.

A display will receive all of them, also with the remaining capacity of the WS battery, and estimates costs related to electricity and gas, based on consumption and values inserted by the user.

IV. SCENARIO

This scenario has been simulated through Matlab/Simulink and TrueTime software. The simulation's period is 24 seconds but reproduces 24 hours, starting from 12:00 P.M. Every parameter has been set to obtain temporally consistent results.

Solar panels and thermal fireplace have been represented through a *signal builder* that reproduce the

thermal trend in a typical day; for this reason, panels will increase temperature starting from the first lights of the sun, reaching their peak around 12:00 A.M, then decrementing until late afternoon. Thermal fireplace, instead, will simulate a daily ignition between 6:00 P.M. and 8:00 P.M. They are both connected to a single TrueTime Kernel block each, responsible for transmitting temperature data, with detection and transmission every 2 minutes, toward the control unit, through an Ethernet network with a capacity of 1 Mbits/s.

The outdoor weather sensors (temperature and humidity) have been represented by *uniform random numbers*. Thanks to a special switch, it's possible to choose which kind of day to generate (*nice*, with temperature values between 15° and 26° and humidity between 35-55% or *gloomy*, with temperature between -10° and 15° and humidity between 65-90%). In this way it's possible to check the consistency of the choices made by control unit. Both sensors are connected to a single TrueTime Kernel block that will detect and transmit the above data and the remaining capacity of the battery every 10 minutes, via a wireless network with transmit power of 20 dbm and a capacity of 0.8 Mbits/s.

Heat pump and boiler are represented by a MatLab function. They receive data on ignition, operating mode (the heat pump can also work in cooling mode) and power values, returning a ΔT output that reproduces an increase of temperature and a consumption proportional to them.

Both heat generators are connected to a single TrueTime Kernel block each, responsible for receiving and transmitting data through an Ethernet network with a capacity of 2 Mbits/s. Also, in this case, values inside MatLab functions have been adapted to ensure consistency in the results.

The thermostat has been implemented inside the user's control panel, using a MBDS for the management of system status, which, depending on the input temperature and the values set by the user, will modify his exit activating the system in cooling or heating, or turning it off completely.

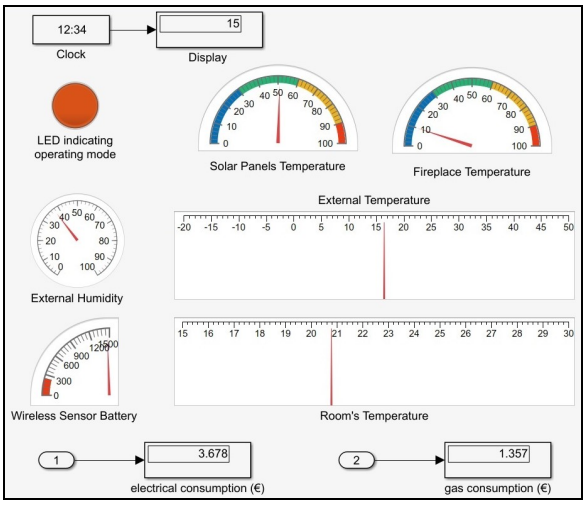

Figure 1: user's display

Through a switch, it is possible to modify the oscillations of room's temperature, simulating the operation in winter mode (20-21°) or summer mode (25-27°). These variations allow reproducing the thermal changes caused, for example, by opening a door or by the exposure of the apartment to the sun. The increases/decreases coming from the radiant floor will be added or subtracted to them. To avoid the rebound between the states, if for a few moments (less than 3 minutes) room's temperatures should fluctuate rapidly, the debounce will prevent the consequent switching on or off suddenly, which could damage the equipment. User's control panel also allows setting the current costs of electricity/gas to calculate consumptions. A TrueTime Kernel block will take in input the ON/OFF values from the thermostat, communicating directly with the control unit through an Ethernet network with a capacity of 5 Mbits/s, receiving from it all data related to the sensors to show them on the user display (Figure 1).

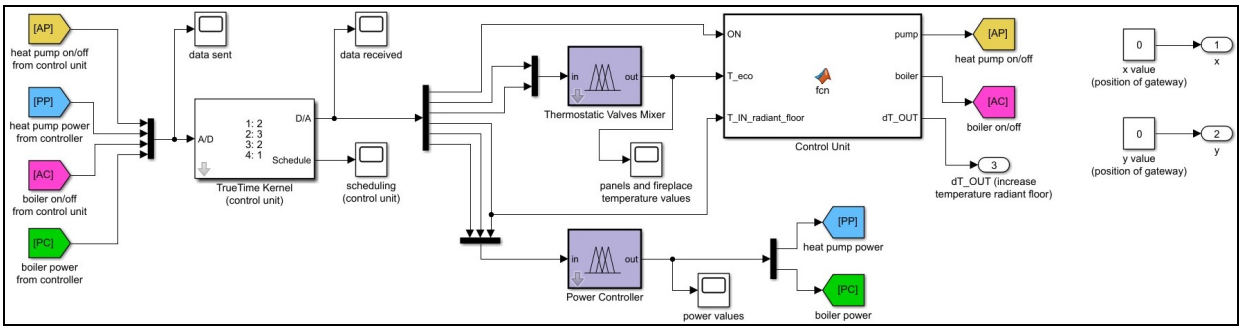

Figure 2: control unit

As mentioned in the previous paragraph, in order to make the simulation as close as possible to reality, omitting however the physical/mathematical details of thermodynamics and calorimetry, that are not relevant here, we decided to implement a MatLab function that imitate the radiant floor, increasing its temperature according to generators and/or renewable energy

sources, and at the same time giving heat to the surroundings.

The core of the system is represented by the control unit (Figure 2), which acts as a gateway between the different networks, thanks to a TrueTime Kernel block. It also contains within it a MatLab function and two fuzzy logic controllers.

The first controller acts as a thermostatic valves mixer, receiving as input the temperatures of thermal fireplace and solar panels. Its purpose is to provide a maximum temperature output that does not exceed 55° also when one of the two sources, or both, are too high (e.g.: thermal fireplace produces hot water that can exceed 80° C).

Exclude one of the two inputs, when it is not operating and falls below 30° (eg: night for solar panels or thermal fireplace turned off), or mix them both. In any case, a temperature value of between 10° and 55° will be supplied in the output. The MatLab function, after receiving the operating mode by the thermostat, will check (in winter mode) if the temperature of renewable sources is higher than radiant floor or above 45° and in positive case, it will bring its contribution to increase their temperature. Otherwise it will exclude the two sources.

The second fuzzy logic controller, depending on the outdoor temperature and humidity values, and radiant floor temperature too, will choose the least expensive energy source, switching on boiler or heat pump, or both, to integrate the production of hot water from renewable sources. Despite the coefficients of performance (COP), which measure the thermal efficiency basing of consumption, are significantly higher and economically advantageous in heat pump, compared to boiler, although the condensing technology has brought considerable improvements on it, when the temperature is too rigid and there is also a high percentage of humidity, heat pump can't work ensuring performance and energy efficiency, so it is necessary the intervention of a "traditional" heat source.

V. PERFORMANCE EVALUATION

Simulations performed have the aim to test the network and his capacity to carry out tasks for which it was designed. Traffic inside it is cyclical, because is related to periodic measurements from the sensors, and asynchronous, depending on processes that evolves over time in unpredictable ways (for example ON/OFF according to room's temperature variation).

The few data transmitted allows an easily overprovisioning of the network to ensures excellent performances without modify costs.

Results obtained on a 24-hour statistical sample show that solar panels have a delay end-to-end from the sensor to gateway of 10 ms, fireplaces 12 ms and weather sensors 5 ms.

This data will be sent individually to the control panel/display through the network 3 with the following delay: solar panels 5 ms, fireplace 4 ms, temperature 8 ms and humidity 15 ms.

Checking the time spent from each sensor to the control unit via networks 1 (WLAN, weather) and 2 (Ethernet, panels and thermal fireplace) and the time spent to complete the route from control unit to display via network 3 (Ethernet) and comparing the sum of these results with the times taken by each sensor to reach the display (panels 18 ms, thermal fireplace 18 ms, temperature 15 ms, humidity 21 ms), it is also possible to obtain the processing time of the gateway to sort the package and send it to another network: this time amounts to about 2 ms (Table 1).

The graph in *Figure 3* shows instead the response time, that is the time interval between thermostat request to switch on the system and the answer of control unit: it amounts to about 7 ms.

The count of the packets sent and received by WSN in optimal conditions, keeping within the range (Transmit power: 20.00 dbm <==> 100.00 mW - Receiver threshold: -48.00 dbm <==> 1.58e-05 mW - Maximum signal reach: 86.67 m) show that there isn't loss.

Table 1

Delay end-to-end

	from sensor to gateway	from gateway to display	from sensor to display	processing time
panels	10 ms	5 ms	18 ms	3 ms
fireplace	12 ms	4 ms	18 ms	2 ms
weather	5 ms			
temperature		8 ms	15 ms	2 ms
humdity		15 ms	21 ms	1 ms

We have also measured the delay between sending consumption data from boiler and heat pump, belonging to the network 4 (Ethernet), and their receiving by display: it's about 18 ms for both.

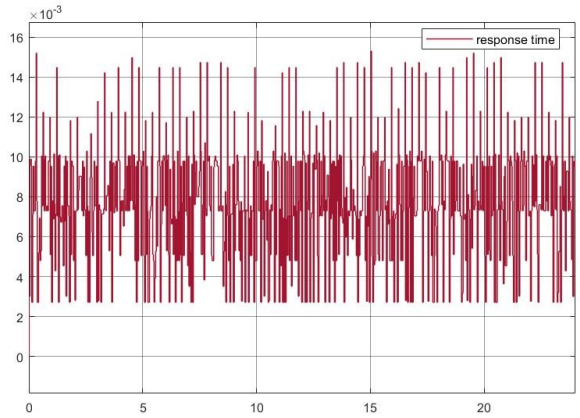

Figure 3: system response time

In order to extend battery life in the wireless sensor, after several simulations, we decided to not use a tasks that periodically calculate transmit power to

adapt it. Besides we assumed devices in a fixed installation. An additional factor used to guarantee battery lifetime duration, avoiding sensor maintenance by human intervention, is to perform a measurement and subsequent transmission every 10 minutes (6 every hour, 144 in 24 hours), trusting that daily temperature fluctuations are never so sharp in a short time.

VI. CONCLUSIONS

Introduction of Ethernet and WLAN inside home automation allows full compatibility between all devices within the network, providing the strength of a standard IEEE 802 already widespread, and it opens the doors to interesting scenarios of IoT, that allow users or programmers to connect with every system above mentioned, using a simple web browser.

It's easy, for example, monitoring the status of the system or giving user's commands from outside, also for technicians. It allows a fast advice and a rapid research of the breakdown without a real intervention on site.

People seem to be positively influenced by technology and systems' automation, increasing in the last few years their ability to use electronic devices, that ensure power saving, optimizing, reduced human intervention, even keeping the same efficiency.

REFERENCES

[1] D. Baghyalakshmi, Sukant Kothari, Jemimah Ebenezer, S.A.V. SatyaMurty, “Ethernet Gateway for Wireless Sensor Networks”, Year: 2015, IEEE Wireless and Optical Communications Networks (WOCN), 2015 Twelfth International Conference on.

[2] Ivan Ganchev, Zhanlin Ji1, M´airt´ın O’Droma, “An IoT-based Smart Electric Heating Control System: Design and Implementation”, Year 2017, Pages 760-762, Ubiquitous and Future Networks (ICUFN), 2017 Ninth International Conference on.

[3] Radouane Karli, Abdellatif Bouchalkha, Khalid Alhammadi, “Power Consumption And Battery Life Study Of A
Two-Node Wireless Sensor System System: Design and Implementation”, Year 2016, Electronic Devices, Systems and Applications (ICEDSA), 2016 5th International Conference on.

[4] G. Nikolic, T. Nikolic, M. Stojcev, B. Petrovic and G.Jovanovic, “Battery Capacity Estimation of Wireless Sensor Node”, Year 2017, Pages 279-282, Microelectronics (MIEL), 2017 IEEE 30th International Conference on.

[5] Aleksejs Jurenoks, Leonids Novickis, “Fuzzy Logic Control Method for Autonomous Heating System in Energy Efficient Homes”, Year: 2017, Pages 236-240, Integrated Circuits and Microsystems (ICICM), 2017 2nd IEEE International Conference on.

[6] Vasile S. Craciun, Viorel Trifa, Carsten Bojesen, Søren J. Andreasen, “Air Source Heat Pump a Key Role in the Development of Smart Buildings in Future Energy Systems”, Year: 2012, Pages 984-989, Electrical and Power Engineering (EPE), 2012 International Conference and Exposition on.

EARLY FIRE DETECTION USING ELECTROMOTIVE FIRE DETECTOR

Ryzhov Philip

Saint-Petersburg state University of aerospace instrumentation
E-mail: filipp777filipp@gmai.com

Annotation
This article analyzes the market of fire detectors and identified PI, which is able to operate at an early stage of pyrolysis faster than competitors.
Keywords: fire detectors, electroinduction, pyrolysis.

The most accurate device for detecting a fire is currently a fire detector. On how well selected the type of fire detector and its location, depend on the lives of people and the safety of property. Consider in more detail the types of produced fire detectors (hereinafter IP) and determine which of them is the most effective for the detection speed of the ignition process.

By referring to the monitored characteristic of the automatic fire SP are divided into [1]:

- thermal;
- smoke;
- flame's;
- gas;
- combined.

Area coverage isolated point SP, able to determine the source of fire in a small specific area, and linear, designed to control the room on fire in a linear area [1].

Smoke is considered to be the main sign of fire all over the world, since at the initial stage of the fire there is mainly melting of the material, accompanied by smoke, and only then open pockets of flame with heat are formed. So today is smoke SP are the most common.

More than 80% of smoke detectors in the world (in Russia – about 90%) are optoelectronic, which use the optical effect of scattering infrared radiation on smoke particles. Optical IP can be equipped with led or laser light emitters.

The principle of operation of the electric induction IP is to pump the studied air through the measuring line, which contains the charging and measuring chamber [2]. Then aerosol particles get an electric charge similar to their size. Charged particles direct the charge to the measuring chamber, the amount of charge depends on the size and the calculated concentration. The measuring chamber amplifies and subjects the signal to further processing.

In view of the urgent need to prevent a fire situation in the early stages of highly explosive production requires a fire detector with high sensitivity to fine particles of smoke (aerosol), which stand out during pyrolysis, which allows you to detect a fire situation long before the outbreak of the flame (Fig. 1) [2].

In addition, potentially explosive environments and buildings require highly protected, intrinsically safe and explosion-proof equipment.

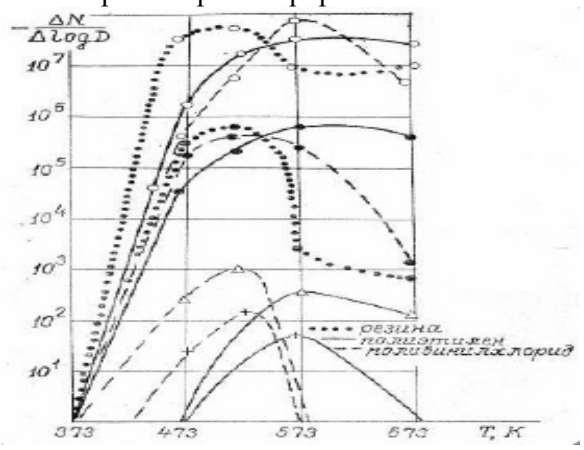

Where:
○ - 0,01 mkm; ● - 0,10 mkm; Δ - 1,00 mkm; + - 2,50 mkm.

Figure 1 - Experimental curves of the particle size differential distribution depending on the sample heating temperature

We will review point devices that combine the required qualities, and a comparative analysis of the characteristics of the detectors, which allows us to determine the most effective ones for fire prevention at an early stage.

The main representatives in a number of point smoke optical-electronic detectors are: DIP-66 (IP-212-66) Partner, DIP-41M (IP-212-41M), DIP-43M (IP-212-43M), DIP-45 (IP-212-45) Marco, DIP-141 (IP-212-141), DIP-142 (IP-212-142), DIP-3CM (IP-212-3CM), SP 212 MK To Trion, having degree of protection of housing IP 30 to 31 according to GOST 14254; IP-212-3CY, SP 212-90.Ex (home Alone-2.Ex) DIP-34ABT (IP-212-34ABT) – degree of protection IP 40-41; PI 212-52 "pulsar 53" – IP 54; SP 212 "Dimfix" 1KV, SP 212 "Dimfix" 2KV, SP 212-81 Aurora – IP 67. The fire sensitivity of an optical smoke point detectors is in the range of 0.05...0.2 DB/m, which corresponds to requirements of GOST R 533252009 [3,4].

Among fire-detectors, using electromagnetic technology, the range is much narrower. In this category, the following smoke detectors are available on the market:

- UN-DAE, the sensitivity (the mass concentration of smoke) 0.01 mg/m^3;

- IP 213-001 explosion-proof housing IP 50, responds to the aerosol concentration in the range of 0.1-30 mg/m^3;

- IP 216-001-Ex, reacts steadily to smoke of all range of the sizes of particles, irrespective of color and chemical composition (from 0,01 microns to 10 microns), aerosol concentration from 0,05 mg/m^3.

Optical smoke detectors are used in cases where it assumes the appearance of a large amount of smoke to the possible fire. The best of optical smoke detectors, including laser ones, have a lower detection limit ranging from 30 mg/m^3 [5]. Among the above models, no fire detector is able to detect a potentially fire hazard at the stage of low-temperature pyrolysis, when the concentration of gases is quite low. As shown in figure 1, the aerosol particle size 0.01-0.1 mkm reach the number density, by several orders of magnitude greater than the background, while the heating temperatures of the materials used is much lower (250-300 K) than the temperature of their ignition. High confidence identification of the fire status on the dynamics of concentration changes of aerosol particles have electromotive SP. So, the point fire detector from "RADAR" IP 216-001-EHE (Fig. 2) capable of capturing fine particles of smoke size 0.01-0.1 microns at a mass concentration ranging from 0.01 mg/m^3 [2].

Another advantage of this model is the body made in explosion-proof category 1ExdllBT6 according to GOST R 51330 and having explosion-proof shell IP 54. Provided protection to prevent the explosion of the detector due to the triggering of a detonating explosive effect on production.

Figure 2 - appearance of "RADAR" IP 216-001-EHE

The detector is designed to monitor the fire situation and issue information about the emergence of a fire situation, when used indoors in macro-climatic areas with a temperate cold climate.

Important advantages in comparison with other explosion-proof fire detectors are:

- ability to install on industrial sites in extreme conditions;

- increased probability of detection of a fire situation at the facilities;

- compatibility with modern control devices;

- over temperature detection of power electric equipment, including wiring.

Recommended installation location of the detector:

- oil and gas complexes;
- explosive industries;
- energy facilities;
- refuelling complexes;
- tunnels, mines;
- military warehouse.

Taking into account these characteristics, it can be argued that it is the electro-induction fire detectors that are preferred for installation at sites where the occurrence of a fire situation is unacceptable.

Conclusion

Summing up the results of the analysis, it should be noted that the electro-induction technology is the most advanced among competitors for fire detection at an early stage, since fire devices operating on its basis are able to identify the concentration of aerosol ranging from 0.01 mg/m3, which is not available to other similar models.

Therefore, in cases when the task of preventing fire or emergency under any circumstances (industrial and military facilities, protection of material and cultural property, life and health of people and animals, life support systems, hospitals, orphanages, sensitive facilities, etc.), it is advisable to use smoke point electromagnetic detectors.

List of references:

1. GOST R 53325-2012 fire Equipment. Technical means of fire automatics. General technical requirements and test methods [Electronic resource]. -]. 2014-01-01. - URL: https://www.gost.ru/portal/gost/home/standarts/catalognational

2. Explosion-proof smoke detector - IP 216-001-Radar-Ex [Electronic resource] / / URL: https://synt.ru/vnimanie-novinka-vzryvozashishennyi-dymovoi-pojarnyi-izveshatel-ip-216-001-radar-ex/.

3. Not bad I. Sensitivity of the smoke detector and its control [Electronic resource] / / URL: http://polyset.ru/article/st084.php

4. Not bad And. Sensitivity of the smoke detector [Electronic resource] / / security systems. No. 2. 2012. URL: http://www.secuteck.ru/articles2/firesec/chyvstvitelnost-dimovogo-izveshatelya/

5. Role A. Basic principles of particle size analysis / A. role / / Technical abstract Malverninstumentslimited. 2009. 12 c.

ANALYSIS OF EXISTING ROBOTIC SYSTEMS FOR INSPECTING TRANSMISSION LINES

Alexandra Shabanova

Saint-Petersburg State University of Aerospace Instrumentation,
Saint-Petersburg, Russia
E-mail: shabanova_ar@mail.ru

Abstract
This paper describes main robotic systems for inspecting power transmission lines. Russian and foreign (Canada, Japan and the USA) developments in this field are presented. The structure, mechanism and principle of operation of each robot are analyzed, their main advantages and disadvantages are revealed.

I. INTRODUCTION

Uninterrupted power supply to consumers is the most important task of electric power industry. The quality of energy transmission over long distances directly depends on the state of the grid elements. Overhead transmission lines are the most emergency element of the transmission grid for consumers, and therefore the creation of an inspection system for power line will solve a number of problems in this field. Today in Russia, the level of wear of power lines and used equipment reaches 70% [1], and 90% of transmission lines are not equipped with monitoring systems [2]. All this combined with a million lines, not always favorable weather conditions for work and lack of infrastructure in many areas makes the problem of creating an automated robotic system for inspecting power lines in Russia increasingly topical.

II. ROBOTIC SYSTEMS FOR INSPECTING POWER LINES IN RUSSIA

Now, the monitoring of power lines is carried out by traditional and remote methods. The traditional method includes a visual inspection without lifting and lifting to towers, and the remote method consists of satellite monitoring and aerial inspection using aircraft and helicopters. However, the use of manned aircraft is not always economically justified. As an alternative to this solution, unmanned aerial vehicles (UAV*)* are used in various regions of Russia, performed on a quadcopter scheme (quadcopter) and carrying digital photo and video equipment (Fig. 1). Based on several digital photographs that do not require the exact attachment of survey points to geographic coordinates, automated modeling and evaluation of the shape of power line towers are performed. The main disadvantage of this method of inspection is the limited scope of application of such devices, since the control of aircraft is carried out from the ground by the operator. In addition, the low carrying capacity of quadcopters does not allow the use of modern diagnostic equipment [3].

Figure 1 shows carrying out aerovisual inspection of power lines with UAV

III. FOREIGN EXPERIENCE IN THE OPERATION OF ROBOTIC SYSTEMS FOR INSPECTING TRANSMISSION LINES

In contrast to the domestic experience of operating transmission line inspection systems, foreign research institutes are actively developing robot inspectors, rolling on wires robots-RWR [4]. The first robot was LineScout (Fig. 2a), presented in 2006 by the Hydro-Québec's research institute (IREQ, Canada). It is designed to move through a single wire and is able to overcome obstacles such as warning spheres (0.76 m in diameter), corona rings, vibration dampers and a double insulator strings.

The robot mechanism consists of two parts: "extremity frames" and a "centre frame" (Fig. 2, b). "Centre frame" in its turn contains electronics and a battery, and "extremity frames" -"wheel frame" (dark frame) and an "arm frame" (light frame). The latter, in addition to the two arms and two grippers, includes two chambers on the pivoting element [5]. Overcoming barriers occurs as follows: in the immediate vicinity of the obstacle, the "arm frame "moves forward and fixes behind it to support the entire robot design, while the "wheel frame" passes under the obstacle. The implementation of this algorithm takes less than 2 minutes.

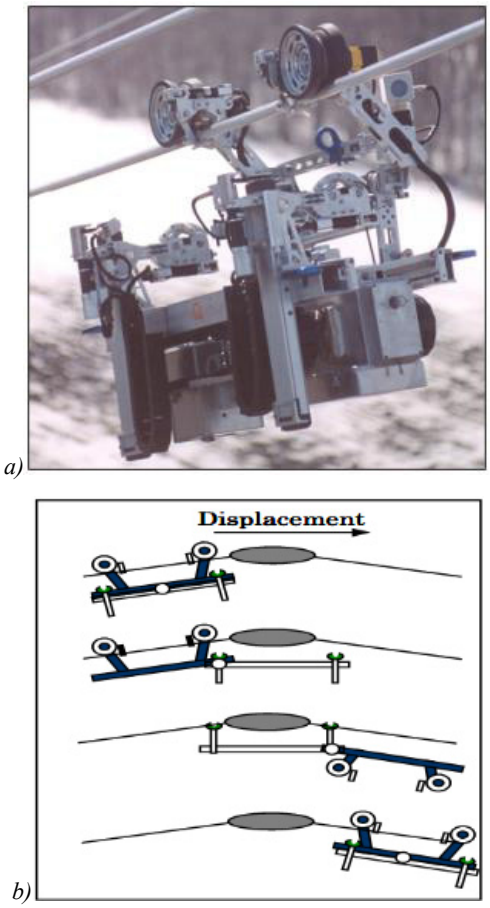

Figure 2 shows LineScout robot (a); LineScout overcomes the obstacle (b)

Diagnosis of the power line is carrying out using high-resolution cameras, a corona probe, infrared and hyperspectral sensors. On-board computer system LineScout consists of custom boards using PIC microcontroller technology that are designed to control the movement (rotation of wheels, turn and tilt the structure), DC-DC converters, protection circuits, communication systems and data acquisition.

The Japanese HiBot corp. introduced a similar robot Expliner in 2008. It is developed jointly with the Kansai Electric Power Corporation (KEPCO) and Tokyo Institute of Technology. Expliner is designed for inspection of power lines with split phases. The robot mechanism is made of carbon fiber and consists of two pulleys, a T-shaped base, a counterweight and a manipulator with two degrees of freedom (Fig. 3a).

The diagnostic system allows to inspect all the wires of the split phase simultaneously, because it consists of four sets of equipment: cameras and laser sensors to identify the change in wire diameter with a measurement accuracy of 0.5 mm and the detection of internal corrosion along the entire line [6]. Fig. 3b shows the sequence of overcoming the obstacle by Expliner. When the robot approaches the barrier, the front pulley is lifted by displacing the center of gravity and the robot travels forward, then the pulley lowers onto the wire and the obstacle is between the two pulleys, then the rear pulley rises in the same way and the Expliner moves forward bypassing the obstacle, the rear pulley lowers, and the robot continues to move in its normal state. The disadvantage of the Expliner is the impossibility of its application on the lines of the voltage class less than 330 kV, since they do not have split phases.

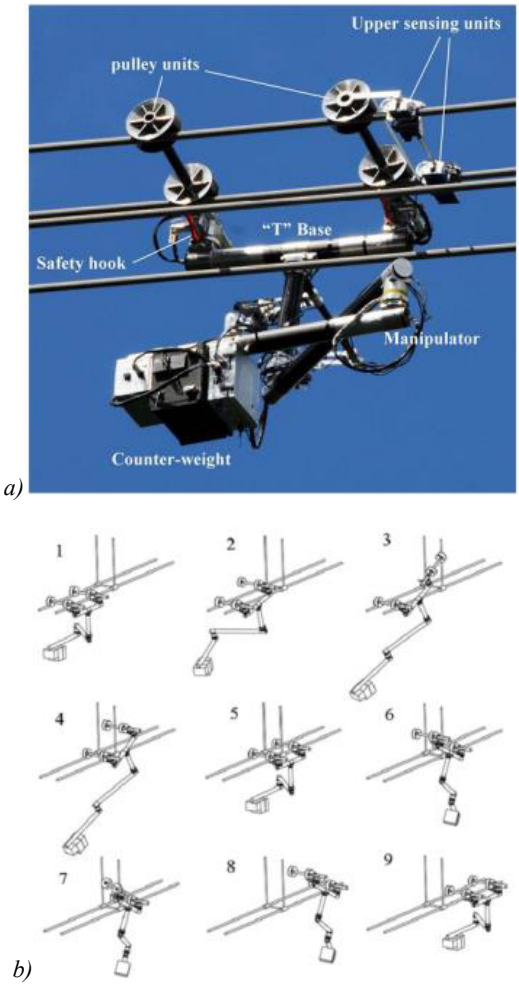

Figure 3 shows Expliner robot (a); Expliner overcomes the obstacle (b)

In the US, the development of robotic systems for the diagnosis of power lines is also underway. Scientists from the Electric Power Research Institute (EPRI) have designed a robot, that moves along the shield wire (Fig. 4).

Figure 4 shows EPRI robot

Robot is equipped with a high-resolution camera to detect obstacles such as overgrown trees. This

makes it possible to analyze the image, comparing it with the previous one. Also, the robot is equipped with sensors, which make it possible to identify electromagnetic noise [8]. The main disadvantage of this robot is its high cost.

Compared to the previous one, the SkySweeper robot, engineered at the University of California, much cheeper, since all its components are printed on a 3D printer. SkySweeper has a V-shape, on the bend of which is located the motor. This motor drives the robot's shoulders (Figure 5). The robot's shoulders are equipped at the ends with grippers, which, opening and closing, move the robot along the line [7]. The robot is equipped with a camera and an induction coils that harvest energy from the power line itself. That allows to maintain autonomous operation for an unlimited time.

Figure 5 shows SkySweeper.

In recent years, many projects are oriented not just to the creation of robotic systems for diagnosis and monitoring, but the implementation of additional functions, for example, cleaning the wires of power lines from pollution. Such development is the robot, created at the University of Georgia, the USA (Fig. 6). The robot moves with four V-wheels and four rollers, which are driven by two DC motors: one is for forward, the other is for backward. Wheels and rollers wrap the wire of the phase on both sides by means of springs with a correctly selected value of rigidity. Overcoming obstacles is carried out by compressing the springs, thereby increasing the space between the wheels, and the robot travels around the obstacle, wrapping it in the same way as the wire [9]. The system is equipped with a camera and two ultrasonic proximity sensors to detect any objects on the path of the robot. In addition, a brush rests on top of the line and, rotating, cleans the wire from debris, industrial dust and salt deposits (in coastal areas) that can accumulate on the wires and lead to corrosion. The power supply of the robot is provided by three batteries, two of which are intended for motors, and one for a brush.

Figure 6 shows University of Georgia's robot

The main disadvantages of this system include a small number of devices to diagnose the condition of power lines and low speed.

There is a comparative table of parameters of robotic systems for inspecting transmission lines below. Each of the considered robots has both advantages and disadvantages, that shows the necessity for long-term research in this field.

Table 1

Shows parameters
of the power line inspectors

robot	Line Scout	Exp-liner	EPRI	Sky-Sweeper	University of Geor-gia
speed, km/h	3,6	1,4	5	0,72	0,36
weight, kg	98	-	65	0,45	13,7
length, m	1,37	-	2	0,6	0,43
battery life, hour	5	6	-	24	24

IV. CONCLUSIONS

In this paper, the main developments in the field of power transmission line inspection were considered. The introduction of such complexes into the power system will allow to prevent emergency shutdown of consumers, and as a consequence, to reduce costs for idle production, to increase the efficiency of power transmission through conducting lines due to the use of power lines at the limit of their electrophysical capabilities. In addition, it will increase the safety of staff and in the future, when creating completely autonomous diagnostic and monitoring systems. It may completely eliminate the need for the departure of the operational team. Obviously, further research should be aimed at developing a multifunctional complex capable of not only diagnosing damage to a section of the line, but also carrying out minor repairs.

REFERENCES

[1] Website portal-energo. Энергоэффективность в электрических сетях. Провода ЛЭП пора менять. http://portal-energo.ru/articles/details/id/621.

[2] Панасенко М.В., Ахмедова О.О. Задачи мониторинга линий электропередачи в условиях метеорологических воздействий // Международный журнал прикладных и фундаментальных исследований. – 2015. – № 9-3. – с. 460-462.

[3] Попов Н.И., Емельянова О.В. Динамические особенности мониторинга воздушных линий электропередачи с помощью квадрокоптера // Современные проблемы науки и образования. – 2014. – № 2.-7 с.

[4] Pagnanoa A., Höpfa M., Tetib R. A roadmap for automated power line inspection.Maintenance and repai // 8th CIRP Conference on Intelligent Computation in Manufacturing Engineering. - 2013.-№2.- pp. 234 – 239.

[5] Montambault S., Pouliot N. Design and Validation of a Mobile Robot for Power Line Inspection and Maintenanc e// 6th International Conference on Field and Service Robotics – FSR 2007, France.- 2007. -11 p.

[6] Debenest P., Guarnieri M., TakitaK., Edwardo F.Expliner – Toward a Practical Robot for Inspection of High-Voltage Lines // Conference: Field and Service Robotics, Results of the 7th International Conference, FSR 2009, Cambridge, Massachusetts, USA.- 2009.- 10 p.

[7] Morozovsky N. Design, Dynamics, and Control of Mobile Robotic Systems // UC San Diego Electronic Theses and Dissertations.- 2014.-170 p.- p. 126-129.

ANAILYSE GAIN OF QUADRATURE AMPLITUDE MODULATION WITH EXPONENTIAL DISTRIBUTION

Rostislav Shaniyazov

Department of Information Systems Security SUAI
190000 Bolshaya Morskaya str., 67, St. Petersburg, Russia
Email: rost5000@vu.spb.ru

Abstrac

In this paper let us derive new method analyze for a general quadrature amplitude modulation(QAM), given that messages have exponential distribution the signal (symbol) to noise ratio(SNR) is $\frac{E_s}{N_0}$.

I. INTRODUCTION

In this paper, we propose a statistical QAM algorithm for the exponential distribution of messages over wireless transmission for a new coding and modulation. It is shown that the described solution has significant power consumption. The suggested solution is analyzed from the position of the Bit Error Rate, analyzing of energy signal, analyzing of noise, structure QAM constellation. All the explanations are shown for QAM system. Statistical QAM is based on the following two ideas. Firstly, the exponential distribution is used to make a distribution of the image pixels closer to the non-uniform distribution. Secondly, the resultant values of the processed symbols are mapped into the constellation point according to their frequency.

The exponential distribution is the usual situation in real life and has a lot of in common with the output of real codecs or generators of values or sensors. This distribution is well-known and easy modulating in the different types of a programming environment.

II. QAM

Due to the rapid growth of capacity demand in core networks and the advancement of digital coherent detection technology, high-order M-ary quadrature amplitude modulation (QAM) formats such as square 16QAM and 64QAM have attracted significant attention due to their potential to realize very high-speed transmission at high spectral efficiencies [4, 5].

A. Modulation

Modulation and demodulation QAM consist of the following main blocks:

1. Getting a value that is distributed according to the uniform continuous. Value are ranging from 0 to $M-1$
2. Coding by Gray code [3].
3. A matching of the points to the constellation M-QAM and giving signal x which has two carriers shifted in phase by 90 degrees are modulated and the resultant output consists of both amplitude and phase variations.
4. Transmiting signal over the communication channel and adding a noise.
5. Receiving the signal and constellation decoding with the method neighbor [1] (Using midway point between 2 symbols as the detection threshold). If the noise was a huge the value of signal could move to another nearest point.

B. Average energy of QAM

Consider a typical 16-QAM modulation scheme where the alphabets is

$$\alpha_{QAM16} = \begin{Bmatrix} \pm 1 \pm i & \pm 1 \pm 3i \\ \pm 3 \pm i & \pm 3 \pm 3i \end{Bmatrix}$$

The average energy of the 16-QAM constellation is $E_{QAM16} = 10$ [2]. The 16-QAM constellation is as shown in the figure 1.

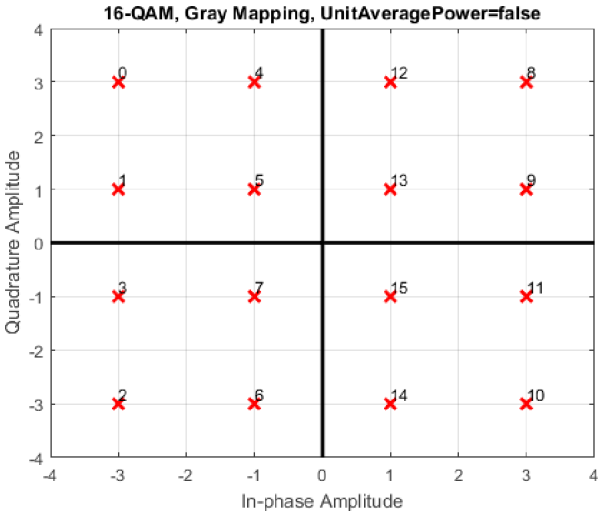

Fig. 1. Constellation QAM16

Each point in constellation is symbol. QAM16 use 16 symbols. This value will be called $M = 16$.

The average power in general standard M-QAM in which probability distribution of input values is considered to be uniform is calculated as follows [6]:

$$E_s = \sum_{i=0}^{K-1} \sum_{j=0}^{K-1} p_i((2i - K + 1)^2 + (2j - K + 1)^2)$$

p_i is probability of symbol, $K = \sqrt{M}$.

C. *Noise Model*

Let the received symbol is,

$$y = k\sqrt{E_s}s + n$$

Where $k = \sqrt{\frac{1}{\frac{2}{3}(M-1)}}$ is the normalizing factor. Value of will be used $k = \frac{1}{\sqrt{10}}$ for $M = 16$ (QAM16). s is transmit symbol at the constellation and is the noise. Assuming that the additive noise follows from the Gaussian probability distribution function,

$$p(x) = \frac{1}{\sqrt{\pi\sigma^2}} e^{\frac{-(y-\mu)}{2\sigma^2}}$$

With $\mu = 0$ and $\sigma^2 = \frac{N_0}{2}$. If has huge value, can go to another point and be decoded wrong.

The conditional probability distribution function (PDF) for given $\alpha = 1 + i$ are showing

$$p(y) = \frac{1}{\sqrt{\pi N_0}} e^{\frac{-(y-\sqrt{\frac{E_s}{10}})}{N_0}}$$

D. *Bit Error Rate(BER)*

An error is an incorrectly decoding the symbol. It happened when a point in constellation was moved to another area by noise.

The theoretical probability bit error rate(BER) function for uniform distribution QAM16 is [2]

$$P_s = \frac{3}{2\sqrt{M}} \operatorname{erfc}\left(\sqrt{\frac{\sqrt{M}E_b}{10N_0}}\right)$$

Where $\operatorname{erfc}(x) = \frac{2}{\sqrt{\pi}} \int_x^\infty e^{-r^2} dt = 1 - \operatorname{erf}(x)$, where $\operatorname{erf}(x)$ is the error function (also called Gauss error function).

III. STATISTICAL QAM

The average energy is calculated as uniform distribution. If cryptography or data compression not included in the processing of symbol, there is used an exponential distribution in real systems. Every symbol has a different probability.

A. *Main idea*

The main idea of Statistical QAM (S-QAM) for exponential distribution is to map the most frequent input values to the QAM symbols with the lowest transmission energy. As the result, the average energy consumption of the transmission system is seriously decreased because the low-energy modulation values are transmitted more common than the value with higher energy level. The typical scheme distribution is shown in the figure 2.

Compare two signals with different energy is not correct enough because they have different energy level. QAM with exponential distribution can be comparable with usual QAM if they have the same average power. The average power of QAM can be increased by increasing distance between points in the constellation.

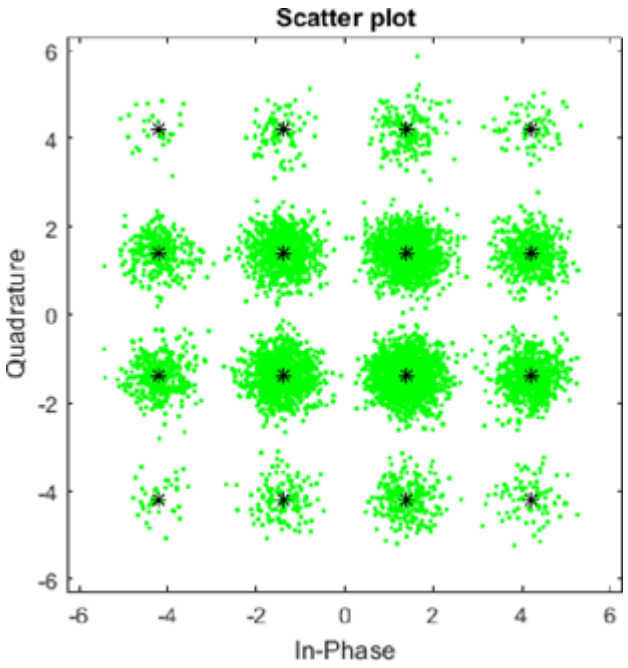

Fig. 2. Exponential distribution with SQAM16

Let use the formula from section II-B for calculating of energy for a sprawling constellation and average energy QAM16 $E_{QAM16} = 10$:

$$10 = \sum_{i=0}^{K-1}\sum_{j=0}^{K-1} p_i(A^2(2i-K+1)^2 + A^2(2j-K+1)^2) = A^2 \sum_{i=0}^{K-1}\sum_{j=0}^{K-1} p_i((2i-K+1)^2 + (2j-K+1)^2)$$

Where A is the coefficient of sprawling of the constellation. A can be gained

$$A^2 = \frac{10}{\sum_{i=0}^{K-1}\sum_{j=0}^{K-1} p_i((2i-K+1)^2 + (2j-K+1)^2)}$$

This formula depends on a probability of each symbol, but the probability of symbols depends on exponential distribution, which has the features such us mathematical expectation or intensity of input inflow. If one of this characteristics could be gained, the A coefficient would be gained for SQAM.

Compare two signals with different energy is not correct enough because they have different energy level. QAM with exponential distribution can be comparable with usual QAM if they have the same average power. The average power of QAM can be increased by increasing distance between points in the constellation.

B. *Practical results*

The Matlab code for generating signal QAM16/SQAM and transmission at a channel, pass it through additive white Gaussian noise and demodulation at the receiver will be useful for understanding the concept further. The results are shown in figure 3.

Meanwhile, if the value of the mathematical expectation is large, when the distribution resembles a uniform one, the gain from the proposed modelling scheme will be minimal.

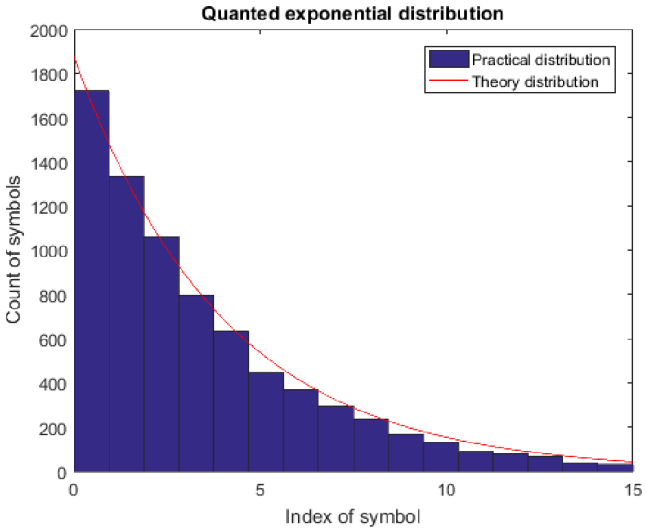

Fig. 3. The quantized symbols

The constellation for SQAM 16 is used following as shown in figure 4. The scheme of mapping symbols is a table I.

Table 1

Mapping for SQAM

Input symbols	Input binary symbols	QAM symbols		energy
		Re	Im	
0	0000	-1	1	2
1	0001	1	1	2
2	0010	-1	-1	2
3	0011	1	-1	2
4	0100	-1	3	10
5	0101	1	3	10
6	0110	-1	-3	10
7	0111	1	-3	10
8	1000	1	-3	10
9	1001	1	3	10
10	1010	-1	-3	10
11	1011	-1	3	10
12	1100	3	-3	18
13	1101	3	3	18
14	1110	-3	-3	18
15	1111	-3	3	18

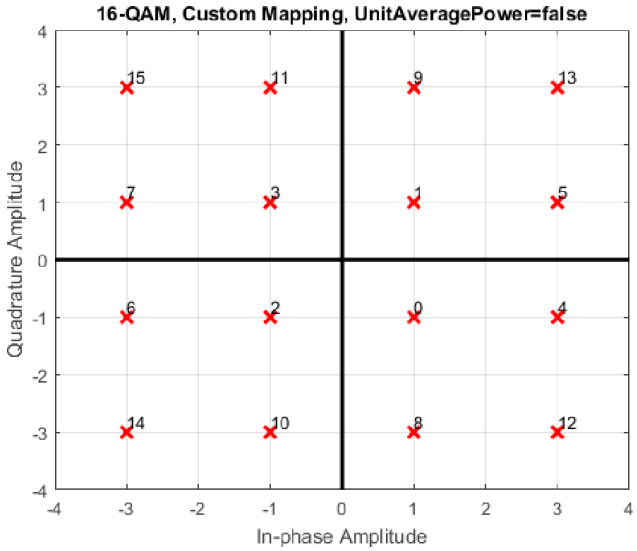

Fig. 4. Constellation Statistical QAM

The Matlab code for generating a QAM16 transmission, pass it through additive white Gaussian noise and demoduation at the receiver will be useful for understanding the concept further. The results are shown in figure 5. The symbol error rate plots obtained from simulations compare well with the theoretical formulas.

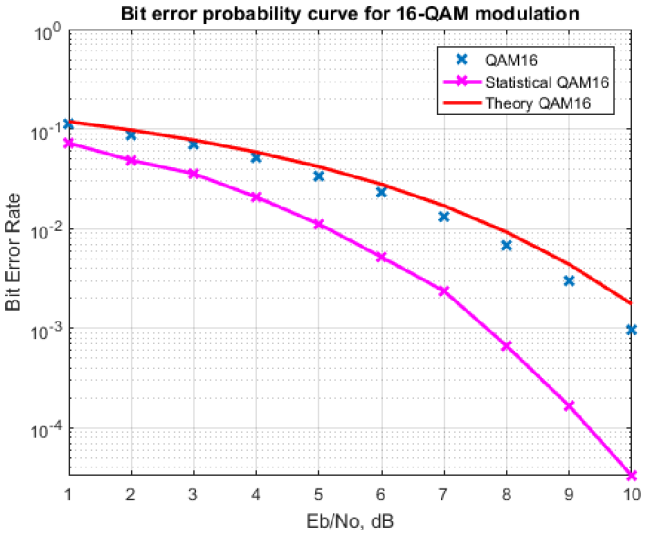

Fig. 5. BER-SNR

IV. CONCLUSION

In this paper, Statistical QAM was compared with exponential distribution scheme. It was shown that for the same average energy costs for Statistical QAM could be reduced value of bit error rate. It was shown, this system is working if the uniform distribution does not use.

REFERENCES

[1] A. Andoni and P. Indyk. Near-optimal hashing algorithms for approximate nearest neighbor in high dimensions. In *Foundations of Computer Science, 2006. FOCS'06. 47th Annual IEEE Symposium on*, pages 459–468. IEEE, 2006.

[2] J. R. Barry, E. A. Lee, and D. G. Messerschmitt. *Digital communication*. Springer Science & Business Media, 2012.

[3] A. P. Hiltgen, K. G. Paterson, and M. Brandestini. Single-track gray codes. *IEEE Transactions on information theory*, 42(5):1555–1561, 1996.

[4] J. Hongo, K. Kasai, M. Yoshida, and M. Nakazawa. 1-gsymbol/s 64-qam coherent optical transmission over 150 km. *IEEE Photonics Technology Letters*, 19(9):638–640, 2007.

[5] Y. Mori, C. Zhang, K. Igarashi, K. Katoh, and K. Kikuchi. Unrepeated 200-km transmission of 40-gbit/s 16-qam signals using digital coherent receiver. *Optics Express*, 17(3):1435–1441, 2009.

[6] A. Sergeev, A. Turlikov, and A. Veselov. Joint source coding and modulation for low-complexity video transmission.

SIMULATION MODEL OF INFORMATION SYSTEM WITH HIGH DATA INTEGRITY REQUIREMENTS

Maria Shelest

Saint-Peterburg State University of Aerospase Instrumentations,
Saint-Peterburg, Russia
mshshelest@mail.ru

Abstracts
In this paper, we describe the development of a computer model of an information system, represented as a queueing network with a specified resource reservation mechanism. The proposed computer model was developed on the basis of a method of discrete-event simulation. Model can get such parameters of the network as the number of service devices, a set of possible service request routes, a probability of selecting these routes, an intensity of requests arrival rate, the intensity of service rate in each service device and a modeling volume. This model allows calculating the following statistics: an average request sojourn time in system, an average request service time and average system load.

I. INTRODUCTION

Nowadays, the process of informatization of society actively grows. Many everyday actions are no longer possible without the use of computerized storage and processing systems (information systems, IS). An example is a library systems, reference services, subdivisions of the management structure of enterprises (bookkeeping, personnel department, etc.).

Any system which using limited means and resources and trying to satisfy a flow of incoming requirements, can be considered as a queuing network (QN) [1, 2]. The queuing network is a set of elementary queuing systems (EQS), each of which, as a rule, consists of a storage device (queue, buffer) and a server (service device, SD). The network receives requests (requirements), the process of servicing of requests can occur in a sequence from several EQS that have been assigned with predetermined probability.

The main element of most part of modern information systems are databases (DB) [3]. Special attention in such systems is paid to speed, reliability and maintaining of data integrity [4]. Therefore, in this article, queuing networks with computing resources reservation are considered. These QN represent IS with high requirements for maintaining data integrity. Reservation of resources in such QN is as follows: for the time of a request processing on a network, this request blocks a certain set of servers for other requests [5].

Since the actual task in ан analysis of information systems is a development of mathematical and simulation models that allow us to estimate the main characteristics of IS, in this paper we will estimate such characteristics of the system as: an average request service time, IS performance, a level of loading of IS modules, load of queues in a processing path, etc.

II. GENERAL ARCHITECTURE OF THE SIMULATION PROGRAM

Since a theoretical analysis of systems with resources reservation mechanisms is difficult even in a simplest cases, as a rule, a simulation method is used to estimate characteristics of IS. The most effective method of modeling queuing networks is discrete-event simulation [6, 7]. Events in the system occur at random times. The state of the system can change only at the moments when the events occur, and a complete set of system states can be obtained by moving the simulation system time from one event to another, which significantly reduces simulation time (Figure 1).

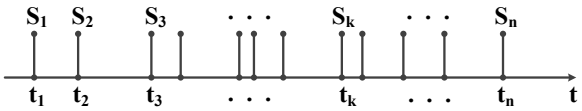

Fig. 1: Sequence of events occurrence in the system

Thus, the work of the simulation model of the system is a chronological events sequence of the system changes from one state to another (Figure 2).

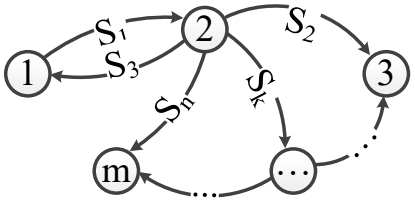

Fig. 2: Abstract machine of state changes

The purpose of this development was to create a simulation model of a system with resources reservation, working according to the principles of discrete-event simulation. The characteristics of the proposed model are given in Table 1.

Table 1

Model characteristics

Input parameters:	- a quantity of elementary QS (SD and buffer); - an intensity of a request arrival rate; - a service rate for each SD; - a set of routes; - probabilities of choosing a route;
Output parameters:	- a quantity of requests in the system; - an average service time of a request; - a sojourn time of a request in a system; - an average working time of a SD;
Reservation mechanism:	- a reservation of a SD set in a request route for a time of processing request;
Query flow:	- Poisson flow;
Order of service:	- in order of arrival (FIFO - first in, first out).

The following events are realized in the developed model:

- Arrival of a request;
- Ending of a service in SD;
- Moving of a request from a buffer to a SD;
- Moving of a request to the next SD on a route;
- Blocking a set of SD;
- Removing the block from a set of SD.

Table 2 shows the reaction of the model to the occurrence of an event.

Table 2

Connection of events

Events	Consequences of the event
Arrival of a request in free system:	- Blocking a set of SD on an entire route; - Calculation of an ending service time of request in the SD; - Calculation of an arrival time of the next request;
Arrival of a request in busy system:	- Arrival of a request into a buffer; - Calculation of an arrival time of the next request;
End of service in intermediate SD in a route:	- Moving of a request to the next SD on route;
Moving of a request to the next SD on a route:	- Calculation of an ending service time of request in a SD;
End of a service in last SD in a route:	- Removing the block from a set of SD;
Removing a block from a set of SD:	- Moving of a request from a buffer to a SD;
Moving of a request from a buffer to a SD:	- Blocking a set of SD on an entire route; - Calculation of an ending service time of request in a SD; - Calculation of an arrival time of the next request.

III. ORGANIZATION OF THE PROGRAM GENERAL CYCLE

The block diagram of the main cycle of the modeling program is shown in Figure 3.

Here K is a quantity of elementary QS in the network; μ - a service rate for each SD; λ - an intensity of a request arrival rate; *Route* - a set of routes; P - a probability of selecting one of the routes; *num* – a quantity of requests to be processed (modeling volume).

In the block *"Determining the next event"* of the block-scheme shown in Figure 3, the event closest to current system time is selected. First, the entire set of event is sorted by time, then it is rewritten in the correct order, after which the first event is selected.

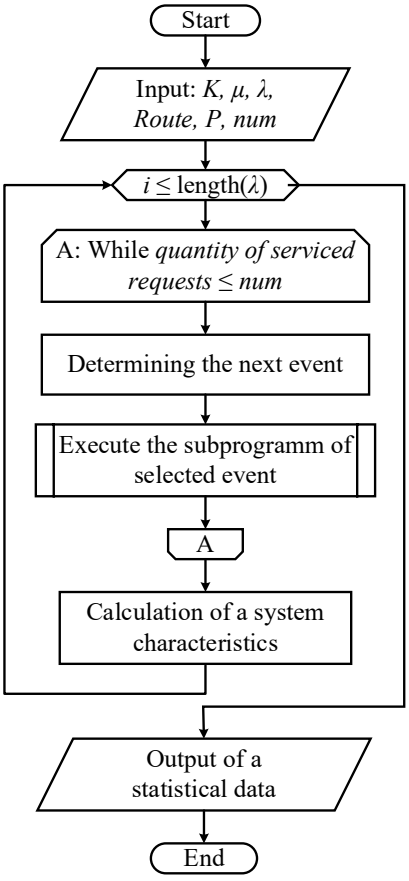

Fig. 3: Block diagram of the simulation program main cycle

In the *"Execute the subprogramm of selected event"* block, the following happens: the pointer to a function of processing the selected event is taken from the value PointerExecute variable, which subsequently runs it (see Listing 1).

Listing 1

Running the processing function of the selected event

```
func_Event =
Events_List(IndexOfNextEvent).PointerExecute;

System_table = func_Event( System_table
);
```

Consider the block *"Calculation of a system characteristics"*, presented in the block-diagram of the main modeling program, shown in Figure 3. In this block, basic calculations are performed to get statistical data on the analysis of the system functioning. The average service time of a request is estimated using the sample mean method [8]. It is known that the error of such an estimate decreases inversely proportional to the root of the modeling volume [9].

IV. SUBPROGRAMMEMS FOR EVENTS PROCESSING

A. Arrival event of request

The block-diagram of the subprogramm for processing the arrival event of request to the system is shown in Figure 4.

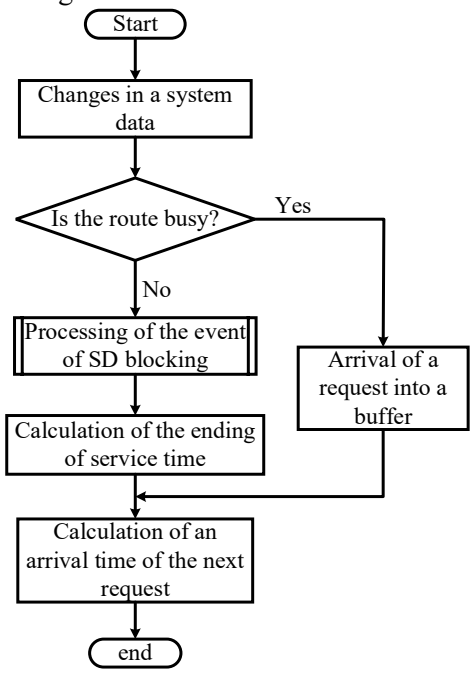

Fig. 4: Processing the arrival event of request

In the *"Changes in a system data"* block of the above block-diagram, the following actions are performed:

1) increasing of a quantity of received requests;

2) one of the routes is selected for a request. The function code for route selection is shown in Listing 2. The choice is as follows: according to the given probabilities, a random number from 1 to R, corresponding to a route number, is selected (here R is the number of routes in the network);

3) changing the current position of a request on the route. When the request is submitted to the system, its status becomes equal to 1 - this means that the request is either in a buffer, or in the first SD on its route, if it immediately accepted to the service;

4) determination of the first SD number on the request route;

5) assignmenting of the request number (the request number is given as a serial number of its arrival to the system);

6) writing the arrival time of request to the system. Sets to the current system time.

Listing 2

Route selection function

```
function Route =
generate_route(System_table)

    n = my_rand(System_table.Pr);

    switch n
      case 1
        Route = [1 2];
      case 2
        Route = [1 3 4];
end;
```

The path busyness check is performed as follows (see Listing 3): initially the path is asumed to be free (the value of the PathBlocked variable is zero), then add a variables values that specify the SD blocked (the value is zero if the SD is unblocked and one if the SD is blocked). The resulting value determines whether the path is free (PathBlocked = 0) or busy (PathBlocked > 0).

Listing 3

Path busy check

```
    PathBlocked = 0;

    for i =
1:length(Request_table(QuantityOfEnteredReque
sts).Route)

      PathBlocked = PathBlocked +
Server_table(Request_table(QuantityOfEnteredR
equests).Route(i)).ServerBlocked;

    end;
```

If the route is free, then the request goes to the service, otherwise it goes to the buffer. The following actions are performed:

1) changing in the request status;

2) writing the request arrival time to the buffer;

3) increasing of the requests number in the buffer;

4) writing of the request number to the array of requests in the buffer.

When a service request is received, the *"Processing of the event of SD blocking"* block must be executed. This block corresponds to the creation of the event of blocking a set of SD, i.e. adding a data to the structure describing the events (see Listing 4). The event time variable is assigned to the current system time, and the parameter value for the event is the request number.

Listing 4

Create of an event of SD blocking

```
Events_List(CurrentQuantityOfEvents).Na
meEvent = 'BlockOfServers';

Events_List(CurrentQuantityOfEvents).Tim
eOfStart = CurrentTime;

Events_List(CurrentQuantityOfEvents).Opti
ons = QuantityOfEnteredRequests;

Events_List(CurrentQuantityOfEvents).Poi
nterExecute = @func_BlockOfServers;
```

The next block *"Calculation of the ending of service time"* corresponds to the creation of an event of a request ending service in the first SD on its route. In this case, a value of the event occurrence time is equal to the current system time plus the request service time in the given SD, and a value of the event parameter is a number of the first SD on the request route (see Listing 5).

Listing 5

Creation of an ending service event in one SD

```
Events_List(CurrentQuantityOfEvents).Na
meEvent = 'ServiceOfRequest';

Events_List(CurrentQuantityOfEvents).Tim
eOfStart = CurrentTime + (-
1/System_table.Mu(WhichServer))*log(rand);

Events_List(CurrentQuantityOfEvents).Opti
ons = WhichServer;

Events_List(CurrentQuantityOfEvents).Poi
nterExecute = @func_ServiceOfRequest;
```

The block *"Calculation of an arrival time of the next request"* corresponds to the creation of the arrival event for the next request (see Listing 6). The time of this event will be equal to the sum of the current system time and time before the arrival of the request.

Listing 6

Creation of a request arrival event

```
Events_List(CurrentQuantityOfEvents).Na
meEvent = 'EnterOfRequest';

Events_List(CurrentQuantityOfEvents).Tim
eOfStart = CurrentTime + (-
1/System_table.Lambda)*log(rand);

Events_List(CurrentQuantityOfEvents).Opti
ons = 0;

Events_List(CurrentQuantityOfEvents).Poi
nterExecute = @func_EnterOfRequest;
```

B. Ending service event in one SD

A block-diagram of the processing subprogramm of the event of a request ending service in one SD is shown in Figure 5.

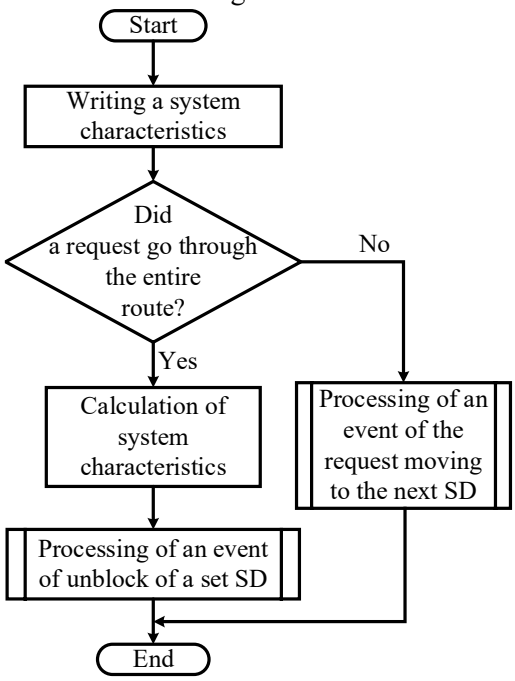

Fig. 5: Processing of the ending service event in SD

In the first block of the above block-diagram, the data of system are written, namely:

1) definition of the SD in which the service of request was finished;

2) writing the work ending time of the SD, which is equal to a current system time;

3) determination of a request number, a service of which has just been finish;

4) calculating a service time of a request in this SD;

5) changing a status of the request for "Serviced";

6) changing of a current request position on its route.

If the value of the current request position on its route is greater than the route length of this request, it means that the request has gone through the entire route, and its service in the network is completed. In this case, an SD unblock event for SD in the request rote is generated, with the start time equal to the current system time, and the parameter of the event is the number of request that was just served (see Listing 7).

Listing 7

Creation of the unblock event of SD on a route

```
Events_List(CurrentQuantityOfEvents).Na
meEvent = 'UnblockOfServers';

Events_List(CurrentQuantityOfEvents).Tim
eOfStart = CurrentTime;
```

```
Events_List(CurrentQuantityOfEvents).Opti
ons = WhichRequest;

Events_List(CurrentQuantityOfEvents).Poi
nterExecute = @func_UnblockOfServers;
```

The following parameters that related to the output of a request from the system are calculated (see Listing 8):

1)a request sojourn time in the system;

2)a number of requests that was serviced in the system.

Listing 8

Calculation after an output of a request from a system

```
Request_table(WhichRequest).TimeInSyste
m = Request_table(WhichRequest).
TimeOut(Request_table(WhichRequest).Route(en
d)) - Request_table
(WhichRequest).TimeIn(Request_table(WhichRe
quest).Route(1));
Server_table(WhichServer).QuantityOfReq
uestsServiced = Server_table
(WhichServer).QuantityOfRequestsServiced + 1;
```

If the request does not go through its entire route, an event of a moving of the request to the next SD on its route is created. The time of occurrence of this event is equal to the current system time, and the value of the event parameter is the request number to determine the next SD on its route (see Listing 9).

Listing 9

Creation an event of a request moving to the next SD

```
Events_List(CurrentQuantityOfEvents).Na
meEvent = 'FromServerInServer';

Events_List(CurrentQuantityOfEvents).Tim
eOfStart = CurrentTime;

Events_List(CurrentQuantityOfEvents).Opti
ons = WhichRequest;

Events_List(CurrentQuantityOfEvents).Poi
nterExecute = @func_FromServerInServer;
```

C. Event of a reqest moving from a buffer to an SD

The block-diagram of the subprogramm for processing the event of a moving of a request from the buffer to the SD is shown in Figure 6.

In the first block of the above block-diagram, the following calculations are performed:

1) writing a work start time of a SD;

2) writing of a request number, which passing from a buffer to a SD;

3) removing of request that has left from a buffer requests array;

4) decreasing of a quantity of request in this buffer;

5) calculating an exit time of the request from the buffer;

6) calculating a request sojourn time spent in a buffer;

7) changing a status of a request to “In processing”.

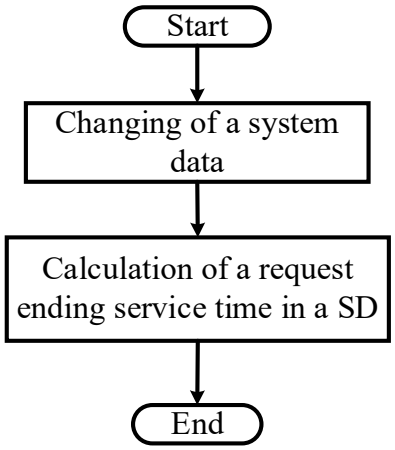

Fig. 6: Processing an event of a reqest moving from the buffer to an SD

After the changes to the system data are completed, an event of request service is created in this SD.

D. Event of request moving to the next SD on its route

A block-diagram of the procedure for processing the event of a request moving to the next SD on its route is shown in Figure 7.

In the first block of the above block-scheme the following calculations are performed (see Listing 10):

1)adetermination of the next SD on a request route;

2)writing of a request arrival time in a system.

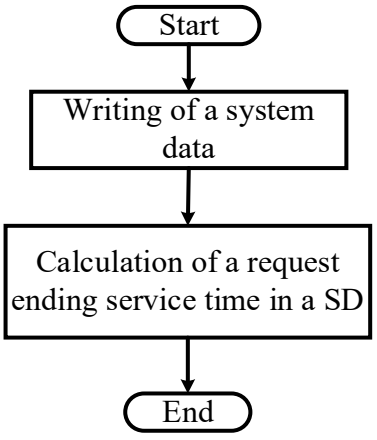

Fig. 7: Processing of a request moving event to the next SD

Listing 10

Calculations during to moving of request to the next SD on its route

```
WhichRequest = Events_List
(IndexOfNextEvent).Options;

NextServer = Request_table
(WhichRequest).Route(Request_table
(WhichRequest).CurrentStage);

Request_table(WhichRequest).TimeIn
(NextServer) = CurrentTime;
```

After the above calculations, an event of request service is created in this SD.

E. Event of blocking a set of SD

In subprogramm of processing of blocking event for a SD set, when the request is moved throught each SD on its route, the value of the variable that reflects the block of SD has becames equal to 1, i.e. each of SD has becomes blocked (see Listing 11).

Listing 11

Sequential blocking of a set SD

```
for i = 1:length(Request_table
(WhichRequest).Route)

Server_table(Request_table
(WhichRequest).Route(i)).
ServerBlocked = 1;
end;
```

F. Event of unblock of a set SD

A block-diagram of the subprogramm for processing an event of an unblock of a set SD is shown in Figure 8.

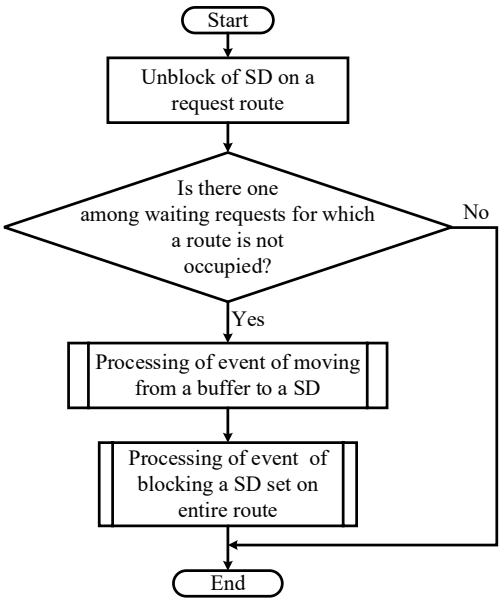

Fig. 8: Processing of an unblock event of a set SD

In the first block of the above block-csheme, the following operation is performed: when the request has moved throught entire set SD on its route, the value of the variable that reflects the block of SD is changed to 0, i.e. the SD block is removed.

After unblock of a set SD, it may happen that some of the routes have become completely free of the block, which means that requests awaiting the unblock of these routes can be received for a service. The search code for such request is shown in Listing 12.

Listing 12

Search for requests that waiting to an unblock

```
MinTime = inf;
for j = 1:System_table.
QuantityOfBuffers
if Buffer_table(j).
QuantityOfRequestsInBuffer == 0
continue;
end;
for k = 1:Buffer_table(j).
QuantityOfRequestsInBuffer
PathBlocked = 0;

for r = 1:length(Request_table
(Buffer_table(j).NumRequests(k)).
Route)
PathBlocked = PathBlocked +
Server_table( Request_table
(Buffer_table(j).NumRequests(k)).
Route(r)).ServerBlocked;
end;
if (PathBlocked == 0)&&
(Request_table(Buffer_table(j).
NumRequests(k)).TimeEnterInBuffer(j) <
MinTime)
MinTime = Request_table
(Buffer_table(j).NumRequests(k)).
TimeEnterInBuffer(j);
WhichRequest = Buffer_table
(j).NumRequests(k);
WhichBuffer = j;
end;
break;
end;
end;
```

If among the requests that waiting in buffers was found such that its route has became free, an event of the request moving from the buffer to the first SD on this request route is created , as well as the event of blocking of a set SD from the route of this request is created.

V. CONCLUSIONS

As a result of this work, a software tool was developed and debugged for the simulation of complex

information systems with high requirements to an integrity of a data.

Within the framework of a development of this work, it is planned to seach other algorithms for reserving of computing resources of information system in order to find the optimal algorithm that allows improving the performance characteristics of the system without reducing the data integrity index.

VI. REFERNCES

[1]. Osman, R., Awan, I., Woodward, M.E. Queuing networks for the performance evaluation of database designs / UKPEW. 2008. Pp.172–183.

[2]. Basharin, G.P., Tolmachev, A.L. The theory of queuing networks and its applications to the analysis of information-computing systems / Itogi Nauki i Tekhniki. Ser. Theor. probability. Mat. stat. Theor. cybernet. 1983. Vol. 21. P. 3 - 119. (In Russuan).

[3]. Golitsyna, O.A., Maksimov, N.V., Popov, I.I. Information Systems / Forum, 2009. (In Russuan).

[4]. Bernstein, P.A., Hadzilacos, V., Goodman, N. Concurrency Control and Recovery in Database Systems / Addison-Wesley, 1987.

[5]. Olifer, V.G., Olifer, N.A. Computer networks. Principles, technologies, protocols / Peter, 2010. (In Russian).

[6]. Buslenko, N. Modeling of complex systems. M .: Nauka, 1978. (In Russian).

[7]. Namestnikov, A. Development of simulation models in the MATLAB environment. UlSTU, Ulyanovsk, 2004. (In Russian).

[8]. Ventzel, E. Theory of Probability / Academy, 2003. (In Russian).

[9]. Farafonov, V., Ustimov, V. Theory of Probability and Mathematical Statistics / SUAI, 2009. (In Russian).

SYNTHESIS OF DISCRETE FILTERS BY METHOD OF INVARIANT DIFFERENTIAL EQUATIONS

Sokolova Yuliya

Student
Saint-Petersburg State University of Aerospace Instrumentation, Russia
E-mail: julia.12@mail.ru

Abstract
The technique of synthesis of various discrete linear systems is considered: low and high frequency filters, vibrational links, rejection and selective filters based on known differential equations of continuous analog filters using difference equations. To obtain difference equations describing the operation of synthesized linear systems, the derivatives of differential equations are replaced by their analogs in the form of difference equations. With the correct choice of the period of discreteness, the frequency properties of the synthesized discrete filters practically coincide with the frequency properties of the corresponding continuous filters. Specific examples of design of discrete filters of lower and upper frequencies, serial oscillatory circuit, notch selective filters by the method of invariant differential equations are given.
Keywords: filter, differential equation, difference equation, frequency transfer function.

INTRODUCTION

Currently, due to the intensive development of computer technology and the emergence of highly efficient digital devices, such as microprocessors, microcontrollers, signal processors, the most widespread digital methods of processing video signals. To improve the quality of images, suppression of noise and noise, a wide variety of low and high frequency filters, band and rejection (liters are widely used. In this case, specific requirements are imposed on the time and frequency properties of the filters, depending on the tasks being solved.

The problems of constructing discrete filters with given time and frequency characteristics in the literature have been thoroughly investigated [1, 2, 3]. To synthesize discrete filters by their continuous analogs, both frequency and time methods are used [4], The basis of frequency methods is the use of a bilinear z - transformation, which allows to develop a discrete filter with a given frequency transfer function of a continuous filter, whose frequency properties practically coincide with the frequency characteristics of a continuous analog filter.

In the case of synthesis of discrete filters in the time domain, either the invariant impulse response method or the invariant transition characteristic method [5,6] is used. Both methods are based on applying pulsed or transient characteristics of a continuous analog filter to create discrete filters.

At the same time, a method for synthesizing discrete filters is possible on the basis of differential equations describing the operation of continuous filters.

In the literature, this method is not given much attention. However, the use of differential equations allows relatively easy to obtain algorithms for virtually any discrete filters - low and high frequency filters, bandpass and notch filters.

SYNTHESIS OF DISCRETE FILTERS

The aim of the work is to create a technique for synthesizing discrete filters using differential equations of continuous analog filters.

In the most general form, a linear system (filter) of the *n*-order is described by the following linear differential equation [7]

$$a_0\frac{d^n y(t)}{dt^n}+a_1\frac{d^{n-1}y(t)}{dt^{n-1}}+\ldots+a_n y(t)=$$
$$=b_0\frac{d^m x(t)}{dt^m}+b_1\frac{d^{m-1}x(t)}{dt^{m-1}}+\ldots+b_m x(t); \qquad (1)$$
$$m\le n,$$

where $x(t), y(t)-$ input and output signals of the system; $a_i, b_i -$ are weights.

Derivatives in the relation (1) can be represented in the form

$$\frac{dy(t)}{dt}=\lim_{T\to 0}\frac{y(t)-y(t-T)}{T};$$
$$\frac{dx(t)}{dt}=\lim_{T\to 0}\frac{x(t)-x(t-T)}{T};$$
$$\frac{d^2y(t)}{dt^2}=\lim_{T\to 0}\frac{\frac{dy(t)}{dt}-\frac{dy(t-T)}{dt}}{T};$$
$$\frac{d^2x(t)}{dt^2}=\lim_{T\to 0}\frac{\frac{dx(t)}{dt}-\frac{dx(t-T)}{dt}}{T};$$
……

$$\frac{d^n y(t)}{dt^n} = \lim_{T\to 0} \frac{\frac{d^{n-1}y(t)}{dt^{n-1}} - \frac{d^{n-1}y(t-T)}{dt^{n-1}}}{T};$$

$$\frac{d^m y(t)}{dt^m} = \lim_{T\to 0} \frac{\frac{d^{m-1}x(t)}{dt^{m-1}} - \frac{d^{m-1}x(t-T)}{dt^{m-1}}}{T}. \quad (2)$$

In what follows, we assume that no significant changes occur in the time T for the functions $x(t); y(t)$, or their derivatives.

Then relations (2) can be replaced by approximate difference equations

$$\frac{dy(t)}{dt} \approx \frac{y(t)-y(t-T)}{T};$$

$$\frac{dx(t)}{dt} \approx \frac{x(t)-x(t-T)}{T};$$

$$\frac{d^2y(t)}{dt^2} \approx \frac{y(t)-2y(t-T)+y(t-2T)}{T^2};$$

$$\frac{d^2x(t)}{dt^2} \approx \frac{x(t)-2x(t-T)+x(t-2T)}{T^2}$$

……

$$\frac{d^n y(t)}{dt^n} \approx T^{-n}\sum_{i=0}^{n} c_i y(t-iT);$$

$$\frac{d^m x(t)}{dt^m} \approx T^{-m}\sum_{i=0}^{m} c_i x(t-iT). \quad (3)$$

The table 1 shows the values of the weight coefficients c_i of the difference equations corresponding to the derivatives of different orders.

Table 1

Values of weighting coefficients

n	ci									
	c_0	c_1	c_2	c_3	c_4	c_5	c_6	c_7	c_8	c_9
1	1	-1								
2	1	-2	1							
3	1	-3	3	-1						
4	1	-4	6	-4	1					
5	1	-5	10	-10	5	-1				
6	1	-6	15	-20	15	-6	1			
7	1	-7	21	-35	35	-21	7	-1		
8	1	-8	28	-56	70	-56	28	-8	1	
9	1	-9	36	-84	126	-126	84	-36	9	-1

Taking into account relations (3), the differential equation of the linear system (1) is written as finite differences

$$a_0 T^{-n}\sum_{i=0}^{n} c_i y(t-iT) + a_1 T^{-(n-1)} * \sum_{i=0}^{n-1} p_i y(t-iT) + \ldots a_n y(t) = b_0 T^{-m}\sum_{i=0}^{m} k_i x(t-iT) + b_1 T^{-(m-1)}\sum_{i=0}^{m-1} d_i x(t-iT) + \ldots b_m x(t). \quad (4)$$

In this expression, the weight coefficients c_i – correspond to the n th derivative; p_i – correspond to the $n-1$ th derivative; k_i – correspond to the m th derivative; d_i – correspond to the $m-1$ th derivative, and so on.

From the relation (4) we find the output signal of the filter

$$y(t) = a_n^{-1}[b_0 T^{-m}\sum_{i=0}^{m} k_i x(t-iT) + b_1 T^{-(m-1)}\sum_{i=0}^{m-1} d_i x(t-iT) + \ldots + b_m x(t) - a_0 T^{-n}\sum_{i=0}^{n} c_i y(t-iT) + a_1 T^{-(n-1)} * \sum_{i=0}^{n-1} p_i y(t-iT) - \ldots - a_{n-1} T^{-1}\sum_{i=0}^{1} l_i y(t-iT)\ ]. \quad (5)$$

In the discrete representation of the input and output filter signals, when $t = iT$, the operation of the discrete filter based on (5) is given by

$$y[n] = a_n^{-1}\{b_0 T^{-m}\sum_{i=0}^{m} k_i x[n-i] + b_1 T^{-(m-1)}\sum_{i=0}^{m-1} d_i x[n-i] + \ldots + b_m x[n] - a_0 T^{-n}\sum_{i=0}^{n} c_i y[n-i] + a_1 T^{-(n-1)} * \sum_{i=0}^{n-1} p_i y[n-i] - \ldots - a_{n-1} T^{-1}\sum_{i=0}^{1} l_i y[n-i]\}. \quad (6)$$

This relationship determines the algorithm of operation of a discrete filter of $n-$ order.

EXAMPLES OF SYNTHESIS OF DISCRETE FILTERS

Let us consider a number of concrete examples.

1. Low-pass filter of the third order

The frequency transfer function of a continuous filter and its differential equation have the form [7]

$$W(j\omega)=\frac{1}{\left[1+(j\omega\tau)^3\right]};\quad \tau^3\frac{d^3y(t)}{dt^3}+y(t)=x(t),$$

where $\tau-$ is the filter time constant.

After replacing the third derivative in the differential equation by its difference equivalent (the third line in the table 1), we obtain the following difference equation of the discrete low-pass filter of the third order.

$$y[n]=\frac{1}{1+a}x[n]+\frac{a}{1+a}*$$
$$*\{3y[n-1]-3y[n-2]+3y[n-3]\},\qquad(7)$$

where $a=(\tau/\mathrm{T})^3$.

Expression (7) allows us to write the amplitude-frequency response (AFC) of the filter in question in the form

$$W(\omega)=\frac{\frac{1}{1+a}}{\sqrt{\left[1-\frac{a}{1+a}(3\cos\omega T-3\cos 2\omega T+\cos 3\omega T)\right]^2+\left[\frac{a}{1+a}(3\sin\omega T-3\sin 2\omega T+\sin 3\omega T)\right]^2}}$$

The results of the calculation of the response of the continuous and discrete filters considered for the case $a=(\tau/\mathrm{T})^3=10^3$ are shown in figure 1 (1 – AFC of a continuous low-pass filter; 2 – AFC of a discrete LPF).

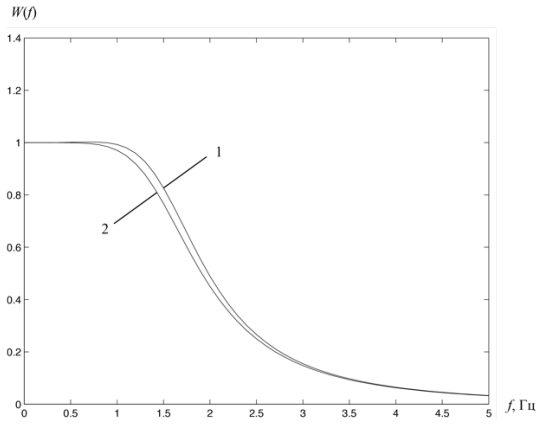

Figure 1 – AFC of a continuous and discrete LPF

From the presented AFC filters, it is seen that the deviation of the frequency response of the filters does not exceed 0,5 dB.

2. High-pass filter of the third order

In this case, the frequency transfer function and the differential equation are described by the relations [7]

$$W(j\omega)=\frac{(j\omega\tau)^3}{\left[1+(j\omega\tau)^3\right]};$$

$$\tau^3\frac{d^3y(t)}{dt^3}+y(t)=\tau^3\frac{d^3x(t)}{dt^3},$$

Applying the previously considered technique, we obtain for a discrete filter a difference equation of the form

$$y[n]=$$
$$=\frac{a}{1+a}\left\{\begin{array}{c}x[n]-3x[n-1]+3x[n-2]-\\-x[n-3]-3y[n-1]+3y[n-2]-y[n-3]\end{array}\right\}.$$

Then the response of the filter under consideration is written as follows

$$W(\omega)=$$
$$=\frac{\frac{a}{1+a}\sqrt{(1-3\cos\omega T+3\cos 2\omega T-\cos 3\omega T)^2+(3\sin\omega T-3\sin 2\omega T+\sin 3\omega T)^2}}{\sqrt{\left[1-\frac{a}{1+a}(3\cos\omega T-3\cos 2\omega T+\cos 3\omega T)\right]^2+\left[\frac{a}{1+a}(3\sin\omega T-3\sin 2\omega T+\sin 3\omega T)\right]^2}}$$

In figure 2 (1 – AFC of a continuous HPF; 2 – AFC of discrete HPF) for the case $a=(\tau/\mathrm{T})^3=10^3$ the AFC of the continuous and discrete filters under investigation is shown. In this case, the deviation of the AFC of continuous and discrete filters does not exceed 0.7 dB.

.

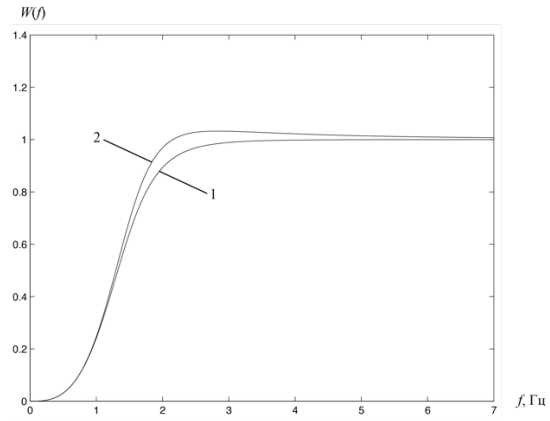

Figure 2 – AFC of a continuous and discrete HPF

Consider the synthesis of more complex linear systems by the method of invariant differential equations.

3. Sequential oscillatory circuit

For a given linear system, the frequency transfer function and the differential equation are determined by the relations [7]

$$W(j\omega)=\frac{1}{\left[(j\omega)^2 LC + j\omega rC + 1\right]};$$

$$LC\frac{d^2y(t)}{dt^2}+rC\frac{dy(t)}{dt}+y(t)=x(t),$$

where $L,C,r-$ inductance, capacity and loss resistance of the oscillatory circuit, respectively.

Replacing the second and first derivatives in the differential equation by their difference expressions (the second and first lines of the table 1), we obtain the following difference equation that determines the operation of the discrete oscillatory circuit

$$y[n]=a_0x[n]+b_1y[n-1]-b_2y[n-2],$$

where

$$a_0=\frac{1}{\left(1+\frac{LC}{T^2}+\frac{rC}{T}\right)};$$

$$b_1=\left(\frac{2LC}{T^2}+\frac{rC}{T}\right)/\left(1+\frac{LC}{T^2}+\frac{rC}{T}\right);$$

$$b_2=LCT^{-2}/\left(1+\frac{LC}{T^2}+\frac{rC}{T}\right).$$

The response of the oscillatory circuit under consideration is

$$W(\omega)=\frac{a_0}{\sqrt{\left(1-b_1\cos\omega T+b_2\cos\omega T\right)^2+\left(b_1\sin\omega T-b_2\sin\omega T\right)^2}}.$$

Frequency response of a continuous and discrete series oscillatory circuit for the case $a_0=0,009;\ b_1=1,8919$ and $b_2=0,9009$ are shown in figure 3 (1 – AFC of a continuous oscillatory circuit; 2 – AFC of a discrete oscillatory circuit). It follows from the presented data that the difference in these frequency response does not exceed 0,7 dB.

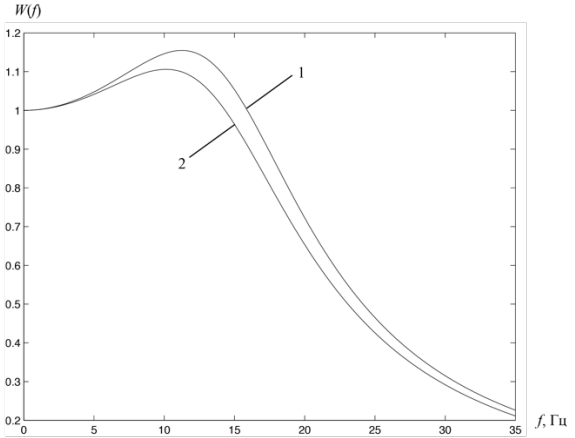

Figure 3 – AFC of a continuous and discrete oscillatory circuit

4. Notch filter

There are a large number of circuitry solutions of notch filters. Let the notch filter be built on the basis of a series oscillatory circuit. The scheme of such a filter is shown in figure 4.

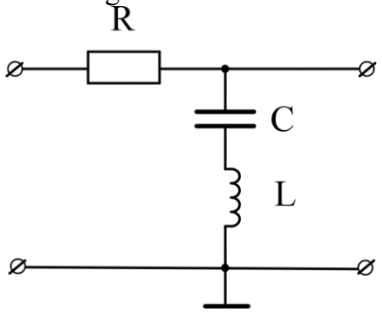

Figure 4 – Scheme of such a filter

Omitting the intermediate calculations, we will write down the frequency transfer function and the differential equation of this filter in the form

$$W(j\omega)=\frac{\left[(j\omega)^2 LC + j\omega rC + 1\right]}{\left[(j\omega)^2 LC + j\omega C(r+R) + 1\right]};$$

$$LC\frac{d^2y(t)}{dt^2}+C(R+r)\frac{dy(t)}{dt}+y(t)=$$

$$=LC\frac{d^2x(t)}{dt^2}+Cr\frac{dx(t)}{dt}+x(t),$$

where R is the resistance of the input resistor.

The difference equation and the amplitude-frequency characteristic of the notch filter are written as follows

$$y[n]=a_0x[n]+a_1x[n-1]a_2x[n-2]+$$
$$+b_1y[n-1]-b_2y[n-2];$$

$$W(\omega)=\sqrt{\frac{\left(a_0-a_1\cos\omega T+a_2\cos2\omega T\right)^2+}{+\left(a_1\sin\omega T-a_2\sin2\omega T\right)^2}\Big/\left(1-b_1\cos\omega T+b_2\cos2\omega T\right)^2+\left(b_1\sin\omega T-b_2\sin2\omega T\right)^2},$$

where

$$a_0=\left(\frac{LC}{T^2}+\frac{rC}{T}+1\right)/\left(\frac{LC}{T^2}+\frac{C(r+R)}{T}+1\right);$$

$$a_1=\left(\frac{2LC}{T^2}+\frac{RC}{T}\right)/\left(\frac{LC}{T^2}+\frac{C(r+R)}{T}+1\right);$$

$$a_2=\frac{LC}{T^2}/\left(\frac{LC(r+R)}{T}+1\right);$$

$$b_1=\left(\frac{2LC}{T^2}+\frac{C(R+r)}{T}\right)/\left(\frac{LC}{T^2}+\frac{C(R+r)}{T}+1\right);$$

$$b_2 = \frac{LC^{-1}}{T^2} / \left(\frac{LC}{T^2} + \frac{C(R+r)}{T} + 1 \right).$$

The frequency response of the notch filter for the weight coefficients $a_0 = 0,9877$, $a_1 = 1,9745$, $a_2 = 0,9873$, $b_1 = 1,9869$ and $b_2 = 0,9873$ is shown in figure 5 by a solid line. It is evident from the characteristic that at the rejection frequency the transmission coefficient is practically equal to -30 dB (1 – AFC of the notch filter; 2 – AFC of the selective filter).

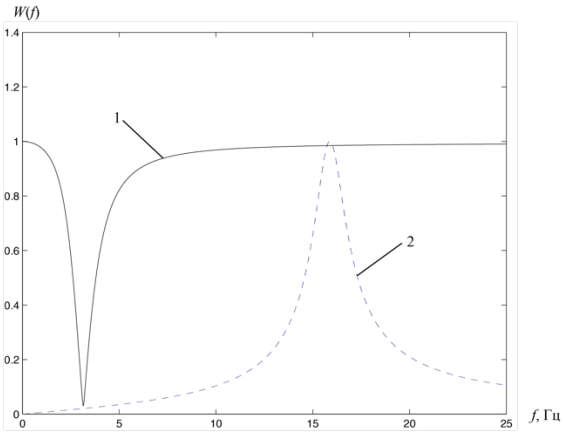

Figure 5 – AFC of the notch and selective filter

5. Selective filter

The sequential oscillatory filter is placed in the basis of the circuit-based solution of the selective filter (Figure 6).

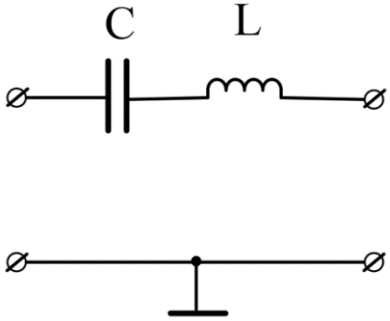

Figure 6 – Bandpass filter circuit

In the case under consideration, the frequency transfer function, the differential equation, the difference equation and the filter frequency response have the form

$$W(j\omega) = \frac{j\omega C}{\left[(j\omega)^2 LC + j\omega rC + 1 \right]};$$

$$LC\frac{d^2y(t)}{dt^2} + Cr\frac{dy(t)}{dt} + y(t) = C\frac{dx(t)}{dt};$$

$$y[n] = a\left(x[n] + x[n-1]\right) + b_1 y[n-1] - b_2 y[n-2];$$

$$W(\omega) = \sqrt{\frac{(a_0 - a\cos\omega T)^2 + (a\sin\omega T)^2}{(1 - b_1\cos\omega T + b_2\cos 2\omega T)^2 + (b_1\sin\omega T - b_2\sin 2\omega T)^2}},$$

where

$$a = \frac{C}{T};\ b_1 = \left(\frac{2LC}{T^2} + \frac{Cr}{T} \right) / \left(\frac{LC}{T^2} + \frac{rC}{T} + 1 \right);$$

$$b_2 = \frac{LC}{T^2}.$$

The frequency response of the selective filter for weight coefficients $a = 0,0099$, $b_1 = 1,9802$ and $b_2 = 0,9901$ is shown in Figure 5 by the dotted line. We can note a fairly good coincidence of the frequency response of continuous and discrete filters.

CONCLUSION

The technique of invariant differential equations considered allows one to synthesize a variety of discrete linear systems: low and high frequency filters, vibrational links, notch and selective filters based on known differential equations of continuous analog filters using difference equations. The frequency properties of synthesized discrete filters with the correct choice of the period of discreteness practically coincide with the frequency properties of the corresponding continuous filters.

REFERENCES

1 Воробьев, С. Н. Цифровая обработка сигналов / С. Н. Воробьев М.: Академия, 2013. 318 с.
2 Голд, Б. Цифровая обработка сигналов / Б. Голд, Ч. Рэйдер. М.:Сов. радио, 1973. 367 с.
3 Сергиенко, А. Б. Цифровая обработка сигналов. СПб.: БВХ-Петербург, 2015. 756 с.
4 Оппенгейм, А. Цифровая обработка сигналов / А. Оппенгейм, Р. Шафер М.: Техносфера, 2006. 855 с.
5 Зиатдинов, С.И. Анализ линейных систем на основе переходных характеристик / С. И. Зиатдинов // Информационно-управляющие системы. 2016. № 2. С. 104-106.
6 Зиатдинов, С.И. Синтез рекурсивных дискретных фильтров во временной области / С. И. Зиатдинов // Известия вузов. Радиоэлектроника. 2016. № 3. С. 3-6.
7 Гоноровский, И.С. Радиотехнические цепи и сигналы / И.С. Гоноровский М.: Радио и связь, 1986. 512 с.

SELECTION OF THE WORKING RANGE OF OPTOELECTRONIC SYSTEM FOR MONITORING THE EARTH'S ATMOSPHERE

Tarala M.

Saint-Petersburg State University of Aerospace Instrumentation,
Saint-Petersburg.
maxim-tarala@mail.ru

Abstract

To observe the object in the Earth's atmosphere by means of an optoelectronic system, an infrared optical range of 3-5 μm was chosen. Earth's atmosphere and its influence on the passage of infrared radiation was analyzed. It is revealed that in the selected operating range the greatest influence on the transmission of radiation is exerted by water vapors. The spectral transmittance coefficient of radiation for water vapors is calculated. According to the obtained data, a graph is built and conclusions are drawn.

INTRODUCTION

For the optical system works to targets in the earth's atmosphere, it is necessary to select the wavelength range at which the object of observation will be detected. To do this, it is necessary to analyze the composition of the atmosphere and its influence on the propagation of optical radiation. As the object of observation there may be meteorological formations, smoke from fires, etc.

The operating range for the optoelectronic system (OES) was chosen the average infrared range(3-5 microns).

The Earth's atmosphere consists of the following main components: nitrogen, carbon dioxide, oxygen, water vapor, methane, nitrous oxide, carbon monoxide and ozone. In addition to these gases in the atmosphere there are also many tiny particles. These particles are distributed in the atmosphere at random and have sizes in the range from 10^{-7} to 10^{-1} cm. They can be presented water drops, particles of carbon, dust, earth, smoke particles, crystals of ice, bacteria, pollen, etc.

The percentage composition of the main gases of the atmosphere remains almost constant up to heights of 25 – 30 km. But due to the presence of water vapor in the atmosphere percentage of gases may vary. Molecules of water vapor and carbon dioxide contribute to the absorption of radiation at altitudes up to 12 km. The concentration of water vapor varies from 10^{-3} to 4%, depending on the humidity and temperature. Also the water vapour concentration depends on the altitude, time of year and local weather conditions. At high altitudes, the percentage of water vapor decreases significantly due to removal from evaporating surfaces, the influence of condensation processes and low temperatures. At the height of more than 10 km water vapors are absent at all [2].

Carbon dioxide changes its concentration in the range from 0,03 to 0,05%. The smallest amount of carbon dioxide is contained above the areas, poorly populated people, the upper threshold is achieved in the atmosphere over large megacities [4].

The passage of infrared radiation (IR) in the atmosphere is seriously influenced by water vapors and carbon dioxide, which have certain absorption spectra, as well as small particles, on which the radiation scattering occurs. Water vapor selectively absorb IR radiation, the absorption bands are observed in the entire region of the IR spectrum. Carbon dioxide absorption is concentrated in the middle part of the IR spectrum. Particles also have the maximum effect in the surface layer of the atmosphere (below 150 m).

The spectral transmittance of radiation by the atmosphere, measured on a horizontal route 1,8 km above sea level, is shown in the figure 1 [3].

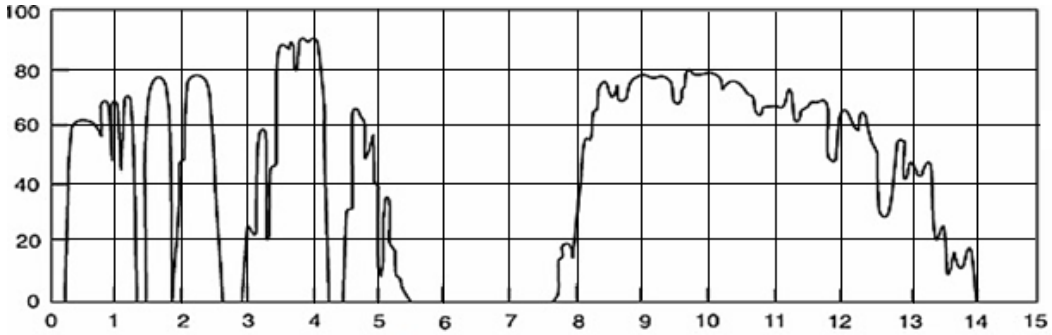

Figure 1 – Spectral transmittance of atmosphere

From figure 1 it is seen that in the atmosphere, there are Windows of transparency for the IR range. Between the transparency bands there are bands of complete absorption of IR radiation by the atmosphere, mainly carbon dioxide CO_2 (2,6–2,9 microns; 4,2–4,4 microns) and water vapor H_2O (2,5-2,8; 4,2–4,4 microns).

The IR band is often subdivided into smaller sections:

– Near-infrared, wavelength 0,7-0,9 μm;

– Short-wavelength infrared, wavelength 0,9-3,0 μm;

– Mid-wavelength infrared, wavelength 3-5 μm;

– Long-wavelength infrared, wavelength 8-14 μm.

The near-infrared is characterized by the use of natural or artificial radiation. Reflected from the observed objects, the radiation passes through an uncooled photodetector based on relatively cheap charge coupled devices or complementary structures of metal-oxide semiconductor, which has good spatial resolution. At the heart of the work with the short-wave IR range is the use of illumination generated by the glow of the night sky, which is formed due to the photochemical reaction of hydroxyl in the upper atmosphere at altitudes of about 85 km. This illumination is several times higher than the light from the starry sky, which allows the OES to operate in moonless nights. This system is based on a non-cooled photodetector capable of operating at ambient temperature using a relatively simple thermal stabilization system. This range is good because compared to the visible, the passing radiation is less attenuated due to haze, dust and fog. In the short-wave IR range, as well as in the near IR, reflected radiation from objects generated by third-party sources is used.

Mid-wavelength IR band is usually well suited for systems designed to detect rocket engines, small arms, artillery ammunition outbreaks, fire outbreaks, food, etc. For most sensors this range do not require cooling to cryogenic temperatures, which significantly reduces size, energy consumption, mass, cost, and time of entering the operating mode after switching on.

Long-wave IR band is designed to operate on their own radiation of objects of observation. To detect radiation, both uncooled photodetectors and cooled to cryogenic temperatures are used. Long-wave IR systems operate at a relatively high range of target detection and recognition. The recognition work is based on the contrast between the target and the background. Such systems are used in industrial control, medical thermography, as well as in military equipment [3].

1. MATH MODEL

The main component absorbing infrared radiation in the atmosphere is water vapor. To calculate the absorption coefficient of water vapor introduced the concept of effective absorbing mass measured in the amount of deposited water – ω.

For a horizontal track, the effective absorbing mass is calculated using the formula [4]: $\omega = \omega_0 L$, где L – track length in km, ω_0 – absorbing mass of gas in the surface layer on the track 1 km. In case of observation of the air object from the ground, the route will be inclined. To calculate the effective absorbing mass on such a track, it is necessary to resort to another formula [5]:

$$\omega = \int_{H_1}^{H_2} \omega_0 \left(\frac{P(h)}{P_0} \right)^{1,75} \frac{T_0}{T(h)} \frac{dh}{\sin\alpha}, \qquad (1)$$

where P_0 = 1013 mbar; T_0 = 273 K, α – the slope angle of the track, the count is from the horizon; altitude profile of temperature and pressure are calculated according to GOST 4401:

$$T(h) = T_0 - 0,0065h, \qquad (2)$$

$$P(h) = P_0 \left(1 - \frac{h}{44308} \right)^{5,255}, \qquad (3)$$

where *h*– height in meters (<11 km).

When finding the effective absorbing mass of water vapors, it is necessary to calculate the vertical profile of the humidity distribution. According to the sources [6, 7, 8] to altitudes of 10 km the change of absolute humidity with height sufficient for engineering calculations it is possible to accurately describe by the function:

$$a(h) = e(0)\exp(-0,5h). \qquad (4)$$

The elasticity of water vapors can be found by the formula [6]:

$$e(0) = 6,107 \cdot 10^{\frac{7,665t}{243,33+t}} \frac{f}{100}, \qquad (5)$$

where f – the relative humidity of air in %, t – the temperature in ºC.

Substituting expressions (2-5) in formula (1), we obtain:

$$\omega_{H2O} = \int_{H_1}^{H_2} \frac{21,7}{T_0} \cdot 6.107 \cdot 10^{\frac{7,665t}{243,33+t}} \times \times \frac{f}{100} \left(1 - \frac{h}{44308} \right)^{0.9} \exp(-0,5h) \frac{dh}{\sin\alpha}. \qquad (6)$$

Formula (6) is the required formula for finding the effective absorption of the mass of water vapour on an inclined track.

2. RESULTS OF RESEARCHS

Take the following conditions to calculate: the slope of the track length of 10 km (L), height 9 km (h), the air temperature at the ground 10 °C (t), air humidity 70% (f), the angle of inclination of 8 degrees (α). Substituting the data into the formula, it is easy to calculate that we obtain an effective absorbing mass of water vapor equal to 9,8 mm. Using the tables from the source [3], we calculate the transmission coefficients of water vapor for the selected range of 3-5 microns (table 1).

Table 1

The spectral transmittance of radiation by water vapor.

The wavelength, μm	The spectral transmittance
3	0,065
3,2	0,353
3,4	0,738
3,6	0,947
3,8	0,98
4	0,97
4,2	0,947
4,4	0,804
4,6	0,621
4,8	0,458
5	0,293

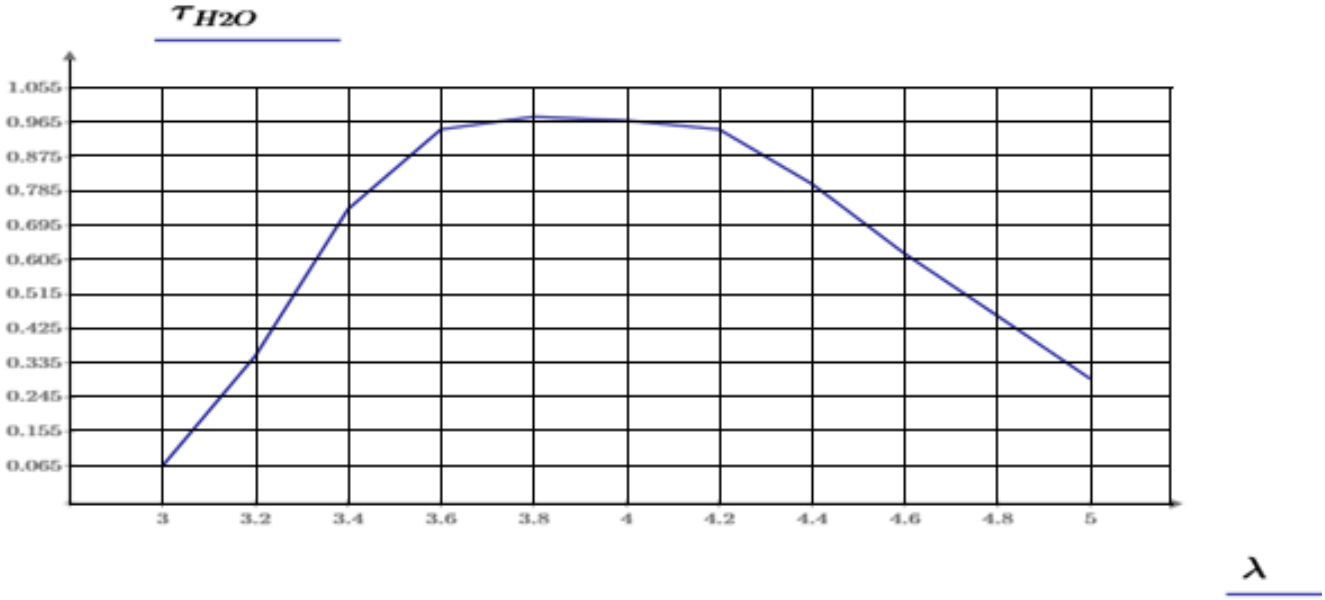

Figure 2 – Graph of spectral transmittance of infrared radiation by water vapor in the range of 3-5 μm.

According to the obtained coefficients, it is possible to build a graph (figure 2).

CONCLUSION

Comparing the graphs shown in figure 1 and 2 it can be concluded that the coefficients are calculated correctly. The spectral transmission coefficient of water vapor calculated according to the formula (6), presented in table 1, indicates that the operation of the OES in the 3-5 μm range is possible, especially if the receiver is adjusted to the wavelengths of 3,5-4,3 μm.

REFERENCES

[1] Mikryukov V.E. Kurs termodinamiki; Moskva, GUPIMP RSFSR, 3-e izd. 1960 - 236 s.

[2] Shripad P. Mahulikar Infrared signature studies of aerospace vehicles / P. Mahulikar Shripad, Hemant R. Sonawane, G. Arvind Rao; Progress in Aerospace Sciences; Volume 43, Issues 7–8, October–November 2007, Pages 218-24

[3] Kriksunov, L. Z. Spravochnik po osnovam infrakrasnoj tekhniki; Moskva, Sovetskoe radio, 1978 g. - 400 s.

[4] Wei Huang Impact pf background radiation on the long wave infrared radiation characteristics of

aircraft at high altitude / Wei Huang, Hong-hu Ji; Defence Science Journal; Volume 66, № 1, January 2016, Pages 51-56

[5] Romanov K.YU. Programmy rascheta spektral'nyh funkcij propuskaniya atmosfery v diapazone ot 0,3 do 14 mkm dlya gorizontal'nyh i naklonnyh trass [Electronic resource]/ K. YU. Romanov, A. N. Starchenko, V. G. Filippov, N.I. SHCHerbakova; NII kom-pleksnyh ispytanij optiko-ehlektronnyh priborov i si-stem, g. Sosnovyj Bor, Leningradskaya oblast'; 2006 – 5 p. URL: http://docplayer.ru/34223155-Programmy-rascheta-spectralnyh-funkciy-propuskaniya-atmosfery-v-diapazone-ot-0-3-do-14-mkm-dlya-gorizontalnyh-i-naklonnyh-trass.html (date of request 14.03.2018)

[6] McClachey R.A. Optical Properties of the Atmosphere / R.A. McClachey, R.W. Fenn, J.E.A. Selby, J.S. Garing, F.E. Volz; Air Force Cambridge Res. Lab, Bedford, 1970

[7] Zuev V.E. Rasprostranenie vidimyh i infrakrasnyh voln v atmosfere. Moskva, Sovetskoe radio, 1970 – 496 s.

[8] Atmosfera. Spravochnik. Leningrad, Gidrometeoizdat, 1991-508s

DEVELOPMENT OF NEW MICROWAVE ELECTRON BEAM DIAGNOSTICS AND MULTISTAGE DEPRESSED COLLECTOR SYSTEM FOR GYROTRONS

Pavel Trofimov

Postgraduate student
Peter the Great Saint-Petersburg Polytechnic University,
Saint-Petersburg, Russia
trofpa@yandex.ru

I. INTRODUCTION

A gyrotron is a high-power microwave radiation generator that can create record amount of output power in the range from a few kilowatts to several megawatts in millimeter and submillimeter frequency ranges, substantially exceeding capability of conventional vacuum microwave devices, such as traveling-wave tubes (TWT), magnetrons, klystrons and so on [1]. Gyrotrons have already become highly required tools for electron current drive and plasma heating in controlled fusion experiments, such as International Thermonuclear Experimental Reactor (ITER) [2] and Demonstration Power Station (DEMO) power plant. Gyrotrons are also used for particle acceleration, high resolution spectroscopy, material processing and other applications.

The efficiency of gyrotrons strongly depends on the quality of the helical electron beam (HEB) being formed. Such parameters as mean values of transverse and longitudinal velocities of the beam electrons and the spread in their values highly influence gyrotron efficiency. To attain high efficiencies, it is necessary to increase the working value of the pitch factor (the ratio between velocities that characterizes the amount of electron energy associated with their transverse motion) because the transverse energy of electrons is converted to the microwave field energy in gyrotrons.

Theoretical analysis of three-dimensional nonuniform HEBs encounters serious problems, which makes attainment of experimental data on the velocity characteristics of such beams very desirable. Knowledge of these parameters is desirable both for the beam upstream from the cavity entrance and for the spent beam deposited onto the collector [3,4]. The task of diagnostics of dense magnetized electron beams of gyrotrons assumes the application of special experimental techniques that should combine high reliability, sensitivity with low beam disturbance, and sufficient spatial and temporal resolution. Previously, modifications of two basic methods — the method of retarding field and the method of a diaphragm and a collector screen — were used for definition of average spreads and mean values of longitudinal and transverse components of electron velocity in gyrodevices [5,6]. The major drawback of these methods is the disturbance in the self-field of electron space charge in the case of introduction of additional electrodes in the beam tunnel [17]. Weakly disturbing diagnostic techniques had also been used for measuring electron velocities in gyrotrons, but they showed to be inefficient because of the large uncertainty of information on the space charge field distribution [8].

However, the efficiency of gyrotron with high quality HEB still does not usually exceed 35–40 % [9]. The overall efficiency can be increased by recuperation in which the spent beam is decelerated by the electric field in the collector region, transferring part of electron energy remained after gyrotron generation back to the electric circuit. Presently, high power gyrotrons are usually implemented with one stage depressed collector systems that allow to raise the total efficiency up to 50–55 %. The implementation of multistage recuperation systems will allow to achieve even higher efficiency. Such systems split the HEB on fractions with different electron energies and provide its deposition on collector sections with different potentials ([9–12]). However, previously developed techniques did not provide sufficient spatial separation or collector systems based on these techniques were too complicated for realization in gyrodevices.

In this work we demonstrate the concept and design of the new weakly disturbing velocity diagnostics and continue the development of the multistage recuperation system for the SPbPU's experimental gyrotron [13] that was started earlier in the recent work of authors [14]. The development of the design of these elements of the device and three-dimensional numerical calculations of their operation were held using program package CST Studio Suite of 3D simulation.

II. MICROWAVE DIAGNOSTICS

The mechanism of new diagnostics is similar to the operation of traveling wave tubes. The idea of microwave diagnostics lies in amplification of electromagnetic wave, which propagates along the gyrotron tube with phase velocity equal or close to the longitudinal velocity of electrons. As a result, electrons transfer part of its kinetic energy to the electromagnetic wave. For the varying frequency of the input signal

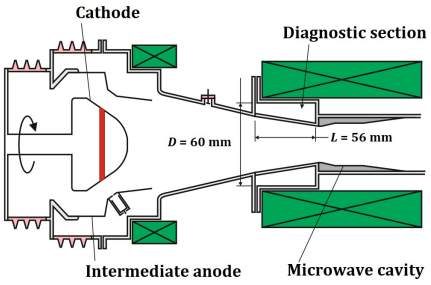

Fig. 1. Schematic picture of the cross section of experimental gyrotron

and in the presence of the dispersion electron-optical system, an electromagnetic wave interacts with several fractions of the electron beam that have different longitudinal velocities. The experimental information on the longitudinal velocity of electrons can be obtained analyzing the dependence of the amplification factor on the frequency of the input signal. We also can estimate the transverse velocity and the pitch factor assuming that the beam is monoenergetic.

Various types of slow-wave systems (SWSs) are used to reduce the phase velocity of the wave and by that achieve its approximate equality with velocity of electrons. In case of the gyrotron beam propagation, information on electrons' velocity characteristics in the area between cathode and interaction region represents a special interest. In this area electrons propagate in adiabatically increasing magnetic field and the longitudinal velocity of electrons changes along the way. Thus, for implementation of microwave diagnostics in these conditions we need to design the conical dispersive slow-wave system, which can change the phase velocity of electromagnetic wave through it. In addition, for sufficient amplification of the electromagnetic wave we need to keep the constant distance between the surface of the electron beam and conducting wall of the diagnostics to ensure the admissible coupling between the wave and the electrons.

Obviously, the implementation of the proposed diagnostics depends to a considerable extent on the design of the specific experimental setup because it presumes the installation of an additional section in the region of magnetic compression of the beam at the

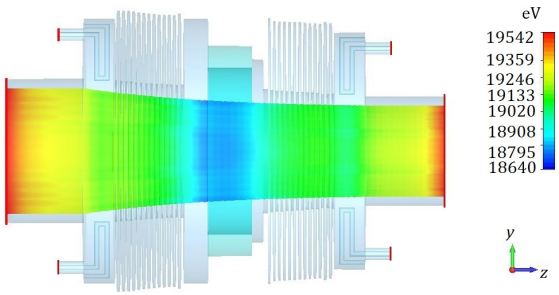

Fig. 2. Model of conical diagnostic section for the experimental gyrotron

cavity entrance. In this study, we determine the possibility of applying these diagnostics in the experimental gyrotron of the St. Petersburg Polytechnic University [13] with output power around 100 kW and operational frequency of 74.2 GHz. Figure 1 shows the scheme of the cross section and main elements of this gyrotron. In this experimental gyrotron, there is a special cavity where the diagnostic section can be installed. With given geometric parameters of this special cavity, longitudinal size L of the section should not exceed 56 mm and its maximal diameter D must be 60 mm.

Taking into account all mentioned factors, the SWS of the type of cylindrical diaphragmatic waveguide was chosen for the design of microwave diagnostics as most appropriate slow-wave structure in such conditions. The simulation of this system with electron beam is shown in Fig. 2. In the central part of the SWS an absorber with parameters $\varepsilon = 30$, $\tan(\delta) = 0.5$ was introduced to prevent the self-excitation of the system and to reduce the effect of re-reflections. The length of the entire system is 55.7 mm. The return loss level was not worse than –15 dB, and the level of introduced losses was –10 dB.

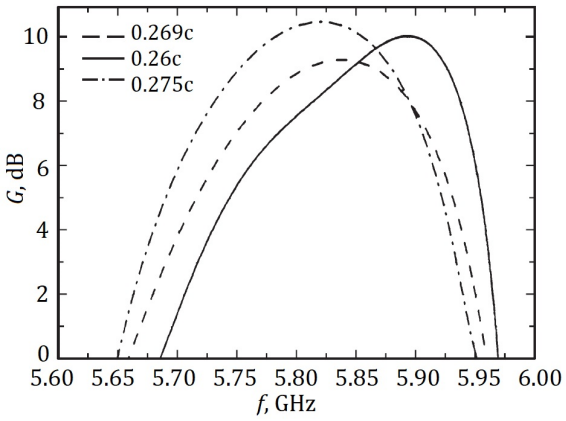

Fig. 3. Dependence of gain on frequency for different initial electron velocities

Fig. 3 shows the frequency dependences of the amplitude gain for an input signal of power 1 W for different values of the mean longitudinal velocity of electrons at the entrance of the diagnostic section. The observed shift in the gain peak to the long-wavelength region upon an increase in the velocity indicates that the developed technique can be used in gyrotrons for determining the mean longitudinal velocity of electrons, as well as the mean transverse velocity and the pitch factor under the assumption that HEBs are monoenergetic. The procedure of applying the given diagnostics requires preliminary calculations and optimizing the diagnostic section for each individual gyrotron. The set of the frequency dependences of the gain obtained in numerical simulation serves as the basis for comparison with the corresponding experimental

dependences and for determining the mean values of electron velocities and the pitch factor on this basis.

III. MULTISTAGE RECUPERATION SYSTEM

The design of multistage recuperation system is based on the method of separation of electrons with different energies. The concept of this separation lies in the radial shift of electron trajectories in the presence of crossed electric magnetic fields. The similar approach was used in the previous theoretical and experimental studies [11, 12, 15] in which the authors analyzed electron trajectories of gyrotron HEBs in the presence of azimuthal electric and axial magnetic fields. These fields were used to suppress low-frequency oscillations in a gyrotron electron-optical system by separation of primary and trapped electrons in the region between the cathode and the cavity [15] and to design a collector assembly of a high-power gyrotron [11, 12].

In the collector region of a gyrotron, the spent HEB propagates in a weak magnetic field. Therefore, the transverse velocity of an electron is negligible in comparison with its longitudinal (along a magnetic field line) velocity. In the proposed method, it is assumed to add the azimuthal component of magnetic field B_θ and the axial retarding electric field E_z in addition to already existing axial component of magnetic field B_z. As a result, electrons are decelerated and simultaneously drift in the radial direction with the velocity $v_{dr} = \frac{E_z}{B_\theta}$. The radial shift is obviously determined by the time of motion of electrons in the crossed fields, which depends on the electron initial energy. Thus, this method provides the separation of the electrons with different energies in the r–z plane. With appropriate selection of shape and voltage of the collector sections, this method can provide effective operation of a Nstag recuperation scheme in which the beam electrons with the energy from $\sim e\varphi_i$ to $\sim e\varphi_{i+1}$ are collected by the section with the depressed potential φ_i (here $i = 1, 2,...N$, $\varphi_i < 0$, $|\varphi_{i+1}| > |\varphi_i|$, the body potential $\varphi_b = 0$).

The 4-stage depressed collector that based on this method of separation was designed using the CST Particle Studio software. The most important element of this depressed collector is the magnetic system providing both axial and azimuthal components of magnetic field. An electromagnet with toroidal-type winding was designed previously to provide azimuthal magnetic field (Fig. 4). The axial magnetic field was generated by the gyrotron main solenoid and by the set of Helmholtz-like coils to create uniform axial magnetic field in the recuperation region. The drawback of this system is limited access for electrons to the area of separation. A part of the electron beam inevitably deposits on the collector tube in the transition region of wiring strands where external winding of the toroidal-type magnet connects with the internal winding. One of the most important design objectives is to decrease the losses of electrons deposited on the collector tube in this region.

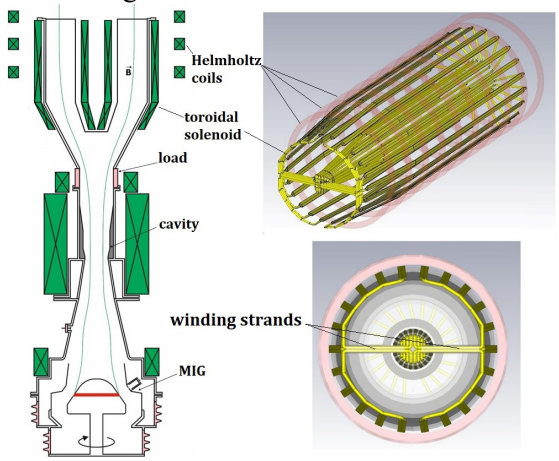

Fig. 4. The model of electromagnet with toroidal-type winding

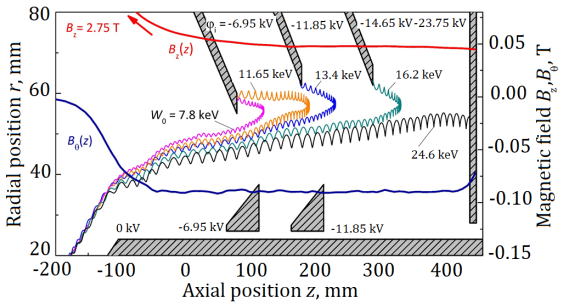

Fig. 5. Magnetic field profiles $B_z(z)$ and $B_\theta(z)$ at r = 50 mm, collector sections at different potentials φ_i and trajectories of electrons with different initial energies W_0.

The calculated distributions of the axial B_z and azimuthal B_θ components of magnetic field at r = 50 mm are shown in Fig. 5. Electrodes at different potentials are placed in the separation region ($z > 0$) for deceleration of electrons. The magnitude of magnetic field in the recuperation area is approximately constant. Fig. 5 also illustrates the schematic layout of the collector sections and electron trajectories for the initial coordinates z_0 = –340 mm (the center of the resonator) and r_0 = 8.26 mm, the initial pitch-factor α_0 = 1.28, and the initial energies W_0 = 7.8, 11.65, 13.4, 16.2, 24.6 keV. The trajectory analysis also covered electrons with other initial parameters (837 trajectories in total). Figure 5 shows that all electrons are collected by electrodes with potential corresponding to its initial

energies. The energy of electrons remained in the rotational motion determines the slight difference between the potential ϕ_i of collector section and the magnitude of W_0 / e for electrons collected by this section. This difference depends on pitch factor and velocity distribution of the spent beam in the collector region. The radial shift of electrons in the crossed electric and magnetic field is big enough to separate electrons with different energies even in the presence of a typical spread of the guiding center radial position. For the optimized version of the magnet, the previously mentioned losses of electrons are ~ 10 % of the whole electron beam. It should be noted that the negative effect from these losses can be reduced if the collector tube has the same potential as the first collector section (ϕ_1 = –6.95 kV).

Estimation of the gyrotron efficiency was made based on new experimental data of energy spectra of electrons in the spent HEB. These data were obtained with the unique retarding field spherical energy analyzer of the SPbPU's gyrotron. Optimum potentials of the collector sections providing maximum recuperation efficiency were defined. The overall efficiency of the gyrotron with the designed 4-stage depressed collector is estimated to be over 70 %.

IV. CONCLUSION

In this work, we tested a new method of microwave diagnostics for determining of electron velocities and showed the possibilities of its implementation in experimental gyrotron of 4-mm wavelength. The information that was obtained through calculations was used to select the type and parameters of designed diagnostic section. 3D simulation of electron beam and wave interaction showed that this method can be used for determining of mean values of electron velocities. It should be noted that pre-cavity beam drift channels in most modern high power gyrotrons are manufactured in a form of a structure similar to our designed diagnostic section. It is made to suppress the excitation of parasitic oscillations of electron space charge at frequencies close to operational [16]. After the appropriate modification of the electron-optical system for matching the beam with the wave, this part of the device can be used as a slow-wave structure for implementation of described method.

The 4-stage depressed collector system based on applying crossed azimuthal magnetic and axial electric fields has been designed for the experimental 74.2 GHz, 100 kW gyrotron. The calculations of electron trajectories showed a possibility to achieve effective separation of electrons with different energies in the presence of typical radial coordinate and velocity spreads of electrons. The estimation of efficiency of the gyrotron with 4-stage depressed collector based on experimentally obtained energy spectra showed the possibility to achieve overall efficiency up to 70 %.

V. ACKNOWLEDGMENT

The study was supported by the Russian Science Foundation (project no. 16-12-10010).

References

[1] Nusinovich G.S. Introduction to the Physics of Gyrotrons / G.S. Nusinovich // Baltimore, MD, USA: The Johns Hopkins Univ. Press. – 2004. – P. 352.

[2] Gantenbein G. 140 GHz, 1 MW CW gyrotron development for fusion applications – Progress and Recent Results / G. Gantenbein [et. al.] // Journal of Infrared, Millimeter and Terahertz Waves. – 2011. – Vol. 32 N 3. – P. 320-328.

[3] Guss C.W. Velocity ratio measurements of a gyrotron electron beam / W.C. Guss, T.L. Grimm, K.E. Kreischer, J.T. Polevoy, R.J. Temkin // Journal of Applied Physics. – 1991. – Vol. 69 N. 7. – P. 3789-3795.

[4] Glyavin M.Y. Experimental studies of gyrotron electron beam systems / M.Y. Glyavin, A.L. Goldenberg, A.N. Kuftin, V.K. Lygin, A.S. Postnikova, V.E. Zapevalov // IEEE Transactions on Plasma Science. – 1999. – Vol. 27 N. 2. – P. 474-483.

[5] Avdoshin E.G. Experimental investigation of the velocity spread in helical electron beams / E.G. Avdoshin, L.V. Nikolaev, I.N. Platonov, S.E. Tsimiring // Radiophysics.and Quantum Electronics. – 1973. – Vol. 16 N. 4. – P. 461-466.

[6] Antakov I.I. Experimental investigation of electron-velocity distribution in a helical electron beam / I.I. Antakov, V.A. Gintsburg, E.V. Zasypkin, E.V. Sokolov // Radiophysics and Quantum Electronics. – 1975. – Vol. 18 N. 8. – P. 884-887.

[7] Kuftin A.N. Advanced numerical and experimental investigation for gyrotrons' helical electron beams / A.N. Kuftin, V.K. Lygin, V.N. Manuilov, A.S. Postnikova, V.E. Zapevalov // International Journal of Infrared and Millimeter Waves. – 1999. – Vol. 20 N. 3. – P. 361-382.

[8] Calame J.P. Measurements of velocity ratio in a 90 MW gyroklystron electron beam / J.P. Calame [et. al.] // IEEE Transactions on Plasma Science. – 1994. – Vol. N. 4. – P. 476-485.

[9] Goldenberg A.L. Energy spectra of electrons and depressed potential collector in gyrotrons / A.L. Goldenberg, V.N. Manuilov, M.A. Moiseev, N.A. Zavolsky // International Journal of Infrared and Millimeter Waves. – 1996. – Vol. 18. – P. 3-55.

[10] Singh A. Design of a multistage depressed collector system for 1-MW CW gyrotrons–Part I: Tra-

jectory control of primary and secondary electrons in a two-stage depressed collector / A. Singh, S. Rajapatirana, Y. Men, V.L. Granatstein, R.L. Ives, A.J. Antolak // IEEE Transactions on Plasma Science. – 1999. – Vol. 27. – P. 490-502.

[11] Pagonakis I. Gr. A new concept for the collection of an electron beam configured by an externally applied axial magnetic field / I.Gr. Pagonakis, J.-P. Hogge, S. Alberti, K.A. Avramides, J.L. Vomvoridis // IEEE Transactions on Plasma Science. – 2008. – Vol. 36. – P. 469-480.

[12] Pagonakis I. Gr. Multistage depressed collector conceptual design for thin magnetically confined electron beams / I. Gr. Pagonakis, C. Wu, S. Illy, J. Jelonnek // Physics of Plasmas. – 2016. – Vol. 23. – 043114.

[13] Louksha O.I. Dynamic processes in helical electron beams in gyrotrons / O.I. Louksha, D.B. Samsonov, G.G. Sominskii, S.V. Semin // Technical Physics Journal. – 2013. – Vol. 58. – P. 751-759.

[14] Louksha O.I. A multistage depressed collector with azimuthal magnetic field for gyrotrons / O.I. Louksha, P.A. Trofimov // Technical Physics Letters. – 2015. – Vol. 41. – P. 884-886.

[15] Louksha O.I. Experimental study and numerical modeling of the electron beam formed in the electron-optical system of a gyrotron / O.I. Louksha, G.G. Sominskii, D.V. Kas'yanenko // Journal of Communications Technology and Electronics. – 2000. – Vol. 45. – P. 71-76.

[16] Gantenbein G. Experimental investigation and analysis of parasitic RF oscillations in high-power gyrotrons / G. Gantenbein [et. al.] // IEEE Transactions on Plasma Science. – 2010. – Vol. 38 N. 6. – P. 1168-1177.

CONTENTS

The scientific edition

BULLETIN OF THE UNESCO DEPARTMENT
«DISTANCE EDUCATION IN ENGINEERING» OF THE SUAI

2018

Collection of the papers
Issue 3

Computer imposition

Papers are publish in author's edition

Подписано в печать 15.03.2018. Формат 60x84 1\8.
Бумага офсетная. Тираж 150 экз. Заказ № 149.

Редакционно-издательский центр ГУАП
190000, Санкт-Петербург, Б. Морская ул., 67

Department of operative polygraphy
SUAI
190000, St. Petersburg, st. B. Morskaya, 67